

Reference

NBS
Publi-
cations

NBSIR 82-2555

NAT'L INST. OF STAND & TECH



A11106 259429

1 Annual Report: Technical Assistance for Future Insulation Systems Research

November 1982

Sponsored by:

Office of Electric Energy Systems

Department of Energy

Washington, DC 20585

QC
100
.U56

82-2555

1982



DEC 6 1982
not acc. - Ref
GC 100
1456
82-2555
1082

NBSIR 82-2555

1981 ANNUAL REPORT: TECHNICAL ASSISTANCE FOR FUTURE INSULATION SYSTEMS RESEARCH

R. J. Van Brunt, M. Misakian, and D. A. Leep

U.S. DEPARTMENT OF COMMERCE
National Bureau of Standards
National Engineering Laboratory
Center for Electronics and Electrical Engineering
Electrosystems Division
Washington, DC 20234

E. C. Beaty

U.S. DEPARTMENT OF COMMERCE
National Bureau of Standards
Quantum Physics Division
Boulder, CO 80303

J. W. Gallagher

Joint Institute for Laboratory Astrophysics
University of Colorado
Boulder, CO 80309

C. M. Cooke, K. Wyatt, and R. G. Gels

High Voltage Research Laboratory
Massachusetts Institute of Technology
Cambridge, MA 02139

November 1982

Sponsored by:
Office of Electric Energy Systems
Department of Energy
Washington, DC 20585



U.S. DEPARTMENT OF COMMERCE, Malcolm Baldrige, *Secretary*
NATIONAL BUREAU OF STANDARDS, Ernest Ambler, *Director*

TABLE OF CONTENTS

	Page
LIST OF FIGURES	vi
LIST OF TABLES.	xii
Abstract.	1
I. INTRODUCTION	3
II. TECHNICAL PROGRESS	6
II.A. Characteristics of Corona Pulses in SF ₆	6
II.A.1 Motivation.	6
II.A.2 Instrument Development.	6
II.A.3 Corona Pulse Characteristics for SF ₆	11
II.B. Modeling of Discharge Inception and Electron Avalanche Growth in SF ₆	19
II.B.1 Motivation.	19
II.B.2 Theory.	20
II.B.2.1 Introduction.	20
II.B.2.2 Basic Discharge Processes	21
II.B.2.3 Deterministic Model of Avalanche Growth	25
II.B.2.4 Effect of Space Charge on Avalanche Growth.	27
II.B.2.5 Stochastic Model of Avalanches.	35
II.B.3 Measurement of Electron Avalanche Distributions	38
II.B.4 Remaining Problems.	44

TABLE OF CONTENTS (cont.)

	Page
II. TECHNICAL PROGRESS	
II.C. Basic Mechanisms for Corona Inception in SF ₆	45
II.C.1 Motivation and Introduction	45
II.C.2 Definition of Corona Inception.	46
II.C.3 Calculation of Corona Inception	51
II.C.4 Discharge Initiation Mechanisms	60
II.C.5 DC Polarity Effect.	60
II.C.6 Geometrical Effects	66
II.D. Electron Swarm Data for Electronegative Gases.	70
II.D.1 Motivation.	70
II.D.2 Definitions and Method of Data Handling	70
II.D.3 Experimental Techniques	72
II.D.3.1 Spatial Current Growth.	72
II.D.3.2 Transverse Diffusion Coefficient.	75
II.D.3.3 Temporal Current Growth.	75
II.D.3.4 Sampling Techniques.	75
II.D.3.5 Errors	76
II.D.3.6 Computations Using the Boltzmann Equation.	76
II.D.4 Data for Sulfur Hexafluoride	78
II.D.4.1 Drift Velocity	79
II.D.4.2 Ratio of Diffusion-to-Mobility and the Diffusion Coefficients	79
II.D.4.3 Electron Gain and Loss Processes	82

TABLE OF CONTENTS (cont.)

	Page
II. TECHNICAL PROGRESS	
II.E. Chemical Diagnostics Development.	89
II.E.1 Motivation	89
II.E.2 Effects of Polar Contaminants on the SF ₆ Dielectric Constant.	89
II.E.3 Production of Oxyfluorides and Water Vapor From Corona Discharges in SF ₆	93
II.F. Optical Diagnostics of Discharges	97
II.F.1 Motivation	97
II.F.2 Apparatus and Experimental Results	98
II.F.3 Low Pressure Measurements	100
II.F.3.1 Ne and Ne + SF ₆	100
II.F.3.2 N ₂ and N ₂ + SF ₆	102
II.F.4 Detection of Metastable Neon at Atmospheric Pressure.	102
III. OTHER ACTIVITIES	107
IV. CONCLUSION AND SUMMARY	108
V. REFERENCES	111
APPENDIX I	121
APPENDIX II	126
APPENDIX III.	130

LIST OF FIGURES

	Page
Figure 1. System for measuring electrical characteristics of corona pulses. Shown also are the measured impulse responses $h_1(t)$ and $h_2(t)$ at points A and B where the pulse repetition rates and pulse height distributions are measured respectively.	7
Figure 2. The measured response of the pulse counter (dashed line) and multichannel analyzer (solid lines) to application of two narrow pulses (~ 5 ns) separated by a time Δt . The left scale is the measured frequency and the right scale is the recorded amplitude	9
Figure 3. Typical positive corona burst pulses observed in SF ₆ at an absolute pressure of 300 kPa and applied voltage of 32.3 kV. These were observed with a time resolution of 0.1 μ s. Indicated are the sampling window t_p of the peakholder circuit and the minimum sampling interval t_s of the multichannel analyzer system	10
Figure 4. Multichannel analyzer channel number versus amplitude (in volts) of charge calibration pulse (see fig. 10)	12
Figure 5. Measured electrical characteristics of positive corona pulses in SF ₆ at an absolute pressure of 50 kPa. Shown are the corona pulse shapes, average corona current I , and pulse height distributions at the indicated applied voltages. The point electrode diameter is 0.1 mm and the gap spacing is 1.24 cm	13
Figure 6. Measured electrical characteristics of positive corona in SF ₆ at an absolute pressure of 200 kPa. Shown are the corona pulse shapes, pulse repetition rates f , average corona current I , and pulse height distributions at the indicated dc voltages. The point electrode diameter is 0.1 mm and the gap spacing is 1.24 cm	14
Figure 7. Measured electrical characteristics of positive corona in SF ₆ at an absolute pressure of 400 kPa. Shown are the corona pulse shapes, pulse repetition rates f , average corona current I , and pulse height distributions at the indicated dc voltages. The point electrode diameter is 0.1 mm and the gap spacing is 1.24 cm	15

LIST OF FIGURES (cont.)

Page

Figure 8.	Measured electrical characteristics of positive corona in SF ₆ at an absolute pressure of 500 kPa. Shown are the corona pulse shapes, pulse repetition rates f , average corona current I , and pulse height distributions at the indicated dc voltages. The point electrode diameter is 0.1 mm and the gap spacing is 1.24 cm.	16
Figure 9.	Measured electrical characteristics of negative corona pulses in SF ₆ at an absolute pressure of 100 kPa and applied voltage of 14.3 kV for freshly polished stainless steel electrodes. Shown are the average corona current I , the pulse repetition rate f , and typical pulse shapes recorded with a transient digitizer. The gap was not irradiated.	17
Figure 10.	Comparison of measured electrical characteristics of negative corona pulses in SF ₆ at 200 kPa for freshly polished electrodes (upper portion). Shown are the pulse height distributions, pulse repetition rates f , average corona current I , and applied voltage V . The gap was not irradiated	18
Figure 11.	Electron attachment cross sections for SF ₆ (from Asundi and Craggs)	23
Figure 12.	Calculated electron avalanching in 200 kPa SF ₆ controlled ionization zone.	26
Figure 13.	Avalanche radius with 100 kPa SF ₆ , 17 kV	28
Figure 14.	Avalanche radius with 200 kPa SF ₆ , 27 kV	28
Figure 15.	Calculated positive ion density left by an electron avalanche in the CIZ test cell at 100 kPa SF ₆	30
Figure 16.	Calculated positive ion density left by an electron avalanche in the CIZ test cell at 200 kPa SF ₆	30
Figure 17.	Calculated negative ion density left by an electron avalanche in the CIZ test cell at 100 kPa SF ₆	31

LIST OF FIGURES (cont.)

	Page
Figure 18. Calculated negative ion density left by an electron avalanche in the CIZ test cell at 200 kPa SF ₆	31
Figure 19. Calculated net ion density left by an electron avalanche in the CIZ test cell at 100 kPa SF ₆	32
Figure 20. Calculated net ion density left by an electron avalanche in the CIZ test cell at 200 kPa SF ₆	32
Figure 21. Model of avalanche used to evaluate space charge effects	33
Figure 22. Electron E-field/Laplacian E-field for SF ₆ at 100 kPa.	34
Figure 23. Electron E-field/Laplacian E-field for SF ₆ at 200 kPa.	34
Figure 24. Controlled Ionization Zone Technique	39
Figure 25a. Measured electron avalanche distribution for 100 kPa SF ₆ , at 17.6 kV.	41
Figure 25b. Measured electron avalanche distribution for 100 kPa SF ₆ , 17.6 kV, pulse rate = 89.	41
Figure 26a. Measured electron avalanche distribution for 100 kPa SF ₆ , 18.6 kV, pulse rate = 41.	42
Figure 26b. Measured electron avalanche distribution for 100 kPa SF ₆ , 18.8 kV, pulse rate = 50.	42
Figure 27a. Measured electron avalanche distribution for 200 kPa SF ₆ , 29.6 kV	43
Figure 27b. Measured electron avalanche distribution for 200 kPa SF ₆ , 29.6 kV, pulse rate = 11.	43

LIST OF FIGURES (cont.)

Page

- Figure 28. Observed pulse count rate versus applied voltage for positive and negative point-plane dc corona in SF₆ at a pressure of 200 kPa. The gap spacing was 1.24 cm and the radius of curvature of the point was 0.045 mm. The different symbols indicate data obtained from different runs. Included are all pulses with a charge in excess of 0.05 pC 47
- Figure 29. Observed pulse count rate versus applied voltage for positive and negative point-plane dc corona in SF₆ at a pressure of 400 kPa. The gap spacing was 1.24 cm and the radius of curvature of the point was 0.045 mm. The different symbols indicate data obtained from different runs. Included are all pulses with charge in excess of 0.05 pC 48
- Figure 30. Observed pulse count rate versus applied voltage for positive and negative point-plane dc corona in SF₆ at a pressure of 200 kPa. Also shown by the solid line is the average dc current observed prior to the inception of pulses. The gap spacing was 1.1 cm and the point radius was 0.47 mm. The data were obtained using uv-radiation and the different symbols correspond to different data runs 49
- Figure 31. Observed pulse count rate versus applied voltage for positive and negative point-plane dc corona in SF₆ at a pressure of 400 kPa. Also shown by the solid line is the average dc current. The gap spacing was 1.1 cm and the point radius was 0.47 mm. The data were obtained using uv-radiation and the different symbols correspond to different data runs 50
- Figure 32. Calculated average-maximum electron avalanche size versus applied voltage for the different indicated gas pressures and parameter $\epsilon = f - d$. The gap geometry corresponds to the conditions of figs. 28 and 29 53
- Figure 33. Collected ionization and attachment coefficients for SF₆. 56
- Figure 34. Measured and calculated ac and dc, positive and negative point-plane corona inceptions in SF₆ as a function of gas pressure. The gap spacing was 1.24 cm and the radius of curvature of the point electrode was 0.045 mm. 57

LIST OF FIGURES (cont.)

	Page
Figure 35. Measured and calculated ac and dc, positive and negative point-plane corona inceptions in SF ₆ as a function of gas pressure. The gap spacing was 2.28 cm and the radius of curvature of the point electrode was 0.045 mm58
Figure 36. Calculated boundaries of the initiation volumes for SF ₆ positive corona inception at the indicated applied voltages and for a gas pressure of 100 kPa64
Figure 37. Calculated growth in the electron initiation volume for two point electrodes characterized by the angles $\eta_0 = 11.575^\circ$ and $\eta_0 = 2.315^\circ$ plotted as a function of the ratio of applied voltage V to theoretical corona inception voltage V_i65
Figure 38. Electron drift velocity, W, for electrons in SF ₆ as a function of E/N80
Figure 39. Ratio of diffusion to mobility, D_T/μ , for electrons in SF ₆ as a function of E/N.81
Figure 40. Diffusion coefficients for electrons in SF ₆ as a function of E/N83
Figure 41. Attachment coefficient for electrons in SF ₆ as a function of E/N84
Figure 42. Ionization coefficient for electrons in SF ₆ as a function of E/N85
Figure 43. Electron growth constant (net ionization coefficient) for electrons in SF ₆ as a function of E/N.86
Figure 44. Relative concentration of H ₂ O in SF ₆ as a function of energy dissipated by a positive dc corona discharge for the indicated discharge power levels	94

LIST OF FIGURES (cont.)

	Page
Figure 45. Measured concentrations of SOF ₂ and SO ₂ F ₂ as a function of net energy dissipated in corona discharges operated at the indicated power levels	96
Figure 46. Schematic view of apparatus for performing optogalvanic measurements in a hollow cathode lamp.	99
Figure 47. Optogalvanic spectra of neon and a mixture of neon with 5% SF ₆ for comparable discharge current and gas pressure	101
Figure 48. Optogalvanic spectrum for N ₂ showing lines from the Ledbetter system and the (8,4) bandhead for the first positive system. . .	103
Figure 49. Measurement of neon optogalvanic spectrum at atmospheric pressure (100 kPa) and 3.6 mA discharge current. Optogalvanic transitions could be observed only in the negative glow region of the discharge	104
Figure 50. Simplified energy level diagram for neon. Optogalvanic signals are obtained when laser-induced transitions occur from the 2p ⁵ 3s states to the 2p ⁵ 3p manifold of excited states	106
Figure A.I.1 Coordinates for Swarm Equilibrium Calculations in the CIZ test cell arrangement	123
Figure A.I.2 Normalized average electron energy for swarms in the CIZ test cell arrangement	124
Figure A.I.3 Average electron energies in the CIZ test cell arrangement	124

LIST OF TABLES

	Page
Table I. Swarm parameters. Symbolic notation, scale factors, and units	73
Table II. Common units conversions for swarm data	74
Table III. Dipole moments, calculated dielectric constants at 20°C and 100 kPa, and calculated detection sensitivities for SF ₆ and contaminants commonly observed in SF ₆ after electric discharges	92

Abstract

A system for measuring the electrical properties of corona pulses has been characterized and is discussed. Additional data on the pulse height distributions of positive and negative corona pulses in pure SF₆ for point-plane electrode geometries are presented. Basic mechanisms for initiation of electric discharges in SF₆ for highly nonuniform fields have been investigated in a collaborative effort between NBS and the High Voltage Research Laboratory of the Massachusetts Institute of Technology. Effects of radiation, electrode geometry, and polarity on corona inception in SF₆ have been measured. Corona inception voltages and discharge initiation volumes have been calculated using the streamer criterion. Limitations of the streamer criterion as applied to SF₆ in highly nonuniform fields are discussed.

The statistics of electron avalanche growth in SF₆ have been measured and compared with results of theory. While the avalanche pulses, on average, followed expected theoretical behavior, the distribution was not found to be regular or to follow a simple stochastic theory. A thorough compilation and survey of electron swarm data for electronegative gases used, and proposed for use, as components of gaseous dielectrics was completed. The parameters considered include: electron drift velocity, attachment coefficient, ionization coefficient, electron growth constant, diffusion coefficient, detachment coefficient, and characteristic energy. These are quantities needed for prediction of breakdown and modeling of gas discharges. Some of the important gases included in this study are: O₂, CO₂, SF₆, H₂O, air, nitrogen oxides, halogens, and various halogenated hydrocarbons, e.g., CF₄, C₂F₆, C₃F₈, C₄F₁₀, CCl₂F₂, CClF₃, c-C₄F₈, c-C₅F₈, CH₃Br, CH₂Cl₃, CHCl₃, etc. In this report we include only an example of the data collected, namely that for SF₆. Using a gas-chromatograph/mass spectrometer, absolute concentrations of SOF₂ and SO₂F₂ and relative concentrations of H₂O in SF₆ have been measured as a function of total energy dissipated in corona discharges operated at power levels between 50 and 700 mW. The observed production rates for SOF₂ and SO₂F₂ appear to be proportional to power level, and the ratio of SO₂F₂ to SOF₂ concentrations for corona is considerably higher than that typically observed for arc discharges in SF₆.

Estimates have been performed to determine the sensitivity of a technique to detect polar gas contaminants in gaseous SF₆ using an accurate ppm measurement of changes in the low frequency (dc) dielectric constant of the gas. Measurements have been performed of optogalvanic spectra from glow discharges in Ne, N₂ and mixtures of these with SF₆. The effect of SF₆ in quenching metastables in these gases is discussed.

Disclaimer:

This is a report of an ongoing research project. Therefore, some of the results presented here, although believed to be correct, must still be considered preliminary. The conclusions based on the data given in this report must also be viewed as tentative and subject to possible revisions as additional information is acquired.

I. INTRODUCTION

The objective for this project is to develop measurement and diagnostic techniques for monitoring, identifying, and predicting degradation in future compressed gas electrical insulating systems under normal operating conditions. The focus is on providing fundamental information and data needed to improve test design and performance evaluation criteria for gaseous dielectrics. A basic understanding of the processes that can lead to failure of insulation materials is required before meaningful tests can be designed to evaluate long-time reliability of these materials. There is also a need for reliable fundamental electron transport data that can be used to predict electrical breakdown of gases under a variety of conditions that can occur in practical situations. The limits of applicability and validity of transport data, as well as the criteria used for predicting breakdown, must also be considered and understood before being applied to the design of insulation systems.

The emphasis of the studies reported here has been on the electrical and chemical properties of SF₆ because of its recent widespread use as an insulant, in advanced high-voltage systems. It serves as a convenient reference when considering the performance of other gaseous dielectrics, some of which might be considered as possible replacements for SF₆. In the development of new measurement techniques to be applied to the evaluation of gaseous dielectrics, it is desirable to start with SF₆. It is therefore important to have reliable data on the properties of this gas which can be used as bench marks. Although SF₆ has been studied extensively, much remains to be learned about its behavior under conditions of high electrical stress, such as the mechanisms that are responsible for various types of electrical discharges.

Major aspects of this project have included: 1) an investigation of the mechanisms that lead to electron avalanche formation and corona discharge inception in SF₆ under highly nonuniform field conditions, 2) an examination of the characteristics of corona discharges in SF₆, 3) a compilation and evaluation of electron swarm data needed to model electric discharge behavior in SF₆ and other electronegative gases, 4) an evaluation of optical techniques that can be used as diagnostics of gas discharges, and 5) an application of sensitive chemical analysis techniques to study corona-induced degradation of gaseous dielectrics and to investigate the effects of low-level gaseous contamination and decomposition on the behavior of gas discharges.

Most of the NBS-laboratory effort has been directed toward a study of partial discharge (corona) phenomena in gaseous dielectrics, particularly SF₆. Corona is important in practical high-voltage insulation systems because it can be responsible for power loss and can lead to deterioration of the insulating qualities of the gas as well as to production of toxic or corrosive by-products [1-3].¹ Corona is loosely defined as a localized gas discharge in a nonuniform electric field. The degree of nonuniformity of the field is assumed to be sufficient to limit the ionization associated with the discharge to a region in the immediate vicinity of the most highly stressed electrode, or electrodes. In the following discussions, the term

¹Numbers in brackets refer to the literature references listed at the end of this report.

corona refers to any detectable discharge phenomena in a nonuniform field which gives rise to ionization in the gas resulting in a multiplication of the number of free electrons in the gap.

Insulation systems are typically designed to minimize corona. However, the extent to which one can limit corona depends on one's ability to define, measure and predict corona onset (inception) as well as to understand the basic mechanisms that can influence the initiation and development of corona discharges. Measurement of corona onset voltages can also provide an indication of the dielectric strength of the gas since the basic theory used to predict onset in nonuniform fields is the same as that which applies to uniform-field breakdown [4].

Although there have been extensive studies of the properties of corona in air and in atmospheric gases such as N_2 and O_2 [5], there have been relatively few fundamental studies of corona in SF_6 . There is a need for better understanding of the basic factors that determine discharge inception as well as the basic characteristics of corona in this gas. In attempting to define corona onset, it is necessary to know how the discharge develops with applied voltage and how this development is affected by various conditions such as, for example, the waveform of the voltage, electrode geometry, the presence of radiation, and gas pressure and purity. Earlier investigations [6,7] of corona activity in SF_6 under direct-voltage conditions have shown that it appears predominately in the form of pulses or pulse bursts corresponding to electron avalanches and/or streamers. This appears to be true at least for positive corona with gas pressures above 20 kPa and for voltages from onset to breakdown. The statistical properties of the corona pulses, however, have not been quantitatively characterized in previous work. There is thus the need to explore new techniques to measure the electrical properties of corona in gaseous dielectrics in a statistically meaningful way.

Instrumentation developed at NBS to study the statistical properties of corona pulses in electronegative gases is described in this report. This technique is also discussed in a recent paper by Van Brunt and Leep [8], together with the results of an extensive study of the pulse characteristics of dc-point plane corona in SF_6 . Here we shall present only the main conclusions of this work, together with significant results obtained this year and some additional details of the measurement system not given previously.

The emphasis of the research at the MIT High Voltage Laboratory was on the development and testing of a model of prebreakdown partial discharge phenomena which can be used, for example, to understand and predict electron avalanche statistics in highly electronegative gases. Specifically, the basic objective of their research was twofold: (1) to develop a model which will enable a more complete fundamental understanding of inception and partial discharge phenomena in gases, and (2) provide basic information needed to develop new standard procedures for measurement of the insulation strength of gases. This activity is viewed as a collaborative effort which has supplemented and strengthened the research underway at NBS on partial discharge characteristics. A model which can be used to understand and predict discharge initiation in nonuniform fields is needed to interpret results obtained from measurements performed at NBS. Also, fundamental information obtained at NBS, e.g., from swarm data compilation and studies of contamination effects, should provide useful input to the modeling effort at MIT.

A description of the theoretical approach taken in this investigation is given in this report, together with results of calculations and measurements of electron avalanche statistics. Details of this work have been presented elsewhere [9].

Closely connected with the work at MIT was the effort at NBS to investigate the fundamental mechanisms of corona inception in SF₆. In addition to the preliminary results previously reported [10] on the comparison between ac and dc inceptions, we undertook a more thorough examination of the effects of uv-radiation, electrode geometry, and electrode conditioning on the measurement of corona inception in SF₆. Corona inceptions were also calculated using the streamer criterion and these were compared with our measured results. The connection between the streamer criterion and the nature of the corona phenomena observed near onset will be discussed, together with limitations of the streamer criterion for predicting inceptions.

A set of preferred discharge initiation mechanisms is proposed and shown to be consistent with the observed changes in discharge behavior with changing gap conditions. The results of this work will be published soon [11]. The major ideas which appear in this paper, and which were developed during the past year, will be reiterated in this report.

At the Atomic Collisions Data Center of The Joint Institute for Laboratory Astrophysics, a monumental survey of electron swarm data for electronegative gases was completed in the past year.

The types of data included in this survey are: ionization, attachment, detachment and diffusion coefficients, electron growth constants, drift velocities, and characteristic energies, all of which are relevant to modeling of electron transport properties and electric discharges in gases. Only electronegative gases of possible technical importance were considered, and these included, for example, O₂, CO₂, SF₆, H₂O, nitrogen oxides, air, the halogens, and halogenated hydrocarbons such as CF₄, C₂F₆, C₃F₈, C₄F₁₀, CCl₂F₂, CHCl₃, CH₃Br, C₂H₅Br, n-C₃H₇Br, n-C₄H₉Br, n-C₅H₁₁Br, n-C₆H₁₃Br, c-C₄F₆, 2-C₄F₆, 1,3-C₄F₆, c-C₄F₈, 2-C₄F₈, c-C₅F₈, c-C₆F₁₀, c-C₆F₁₂, C₇F₈, C₈F₁₆, 1-C₇F₁₄, c-C₇F₁₄, CCl₃F, and CClF₃. This survey has been submitted for publication in the Journal of Physical and Chemical Reference Data. The format of the paper is similar to that of an earlier survey of swarm data for atmospheric and rare gases by J. Dutton [12]. It was not possible to reproduce the entire manuscript in this report; however, we have included excerpts describing the approach taken, types of data considered, and examples of data included for SF₆, these being most relevant to other topics discussed in this report.

Estimates have been performed to determine the sensitivity of a technique to detect polar gas contaminants in SF₆ using an accurate ppm measurement of changes in the low frequency (dc) dielectric constant of the gas. Results of calculations presented here indicate that the technique can detect the presence of polar gases like H₂O only down to the 100 ppm level.

Work has continued on the use of the gas chromatograph-mass spectrometer (GC/MS) system to assist in determination of the effects of trace levels of H₂O on positive-corona discharges in SF₆. Preliminary results of this work

have been reported in a paper given at the Thirty-Third Gaseous Electronics Conference entitled "Pulse Characteristics of Positive DC Corona in SF₆: Effects of Trace Decomposition Products" by D. A. Leep and R. J. Van Brunt [13]. The GC/MS was also used to measure the rate of H₂O, SOF₂ (thionyl fluoride) and SO₂F₂ (sulfuryl fluoride) production from dc corona in SF₆ as a function of discharge power level. Preliminary results obtained from these measurements will be presented in this report. Additional information about this work has appeared in an Electric Power Research Institute Report [14] resulting from the 1980 Workshop on Arc By-Products in Gas Insulated Systems.

The use of laser-induced optogalvanic spectroscopy as a method for monitoring metastable species concentrations in corona and glow discharges continued during this year. Measurements were performed on discharges in Ne, N₂, and mixtures of these with SF₆ for gas pressure up to 100 kPa (~1 atm). The experimental results obtained and the observed limitations of the technique will be discussed in this report.

II. TECHNICAL PROGRESS

II.A. Characteristics of Corona Pulses in SF₆

II.A.1 Motivation

This work has been motivated by the need to develop new measurement techniques that allow characterization of corona-discharge pulses in a quantitative and statistically meaningful way. This is an extension of work reported last year [15]. Some of the results presented here have also been presented in a recent archival publication [8]. Included in this paper are a detailed description of the apparatus, and extensive data on the pulse characteristics of positive and negative point-plane dc corona in pure SF₆. Additional information can also be found in an earlier paper [16]. This report contains some new information about the characteristics of the instrumentation used which were not given in the above publications.

II.A.2 Instrument Development

A thorough analysis of the instrumentation developed at NBS to study statistical properties of corona pulses was completed in the past year. Possible sources of error and instrumental factors which can significantly affect the data have been carefully examined. A diagram of the instrument used for these measurements is given in figure 1. Basic features of this system have previously been discussed [8,15] and will not be repeated here. It is of interest to point out, however, the measured impulse response functions $h_1(t)$ and $h_2(t)$ at the critical points A and B. At point A, corona pulses are observed with either an oscilloscope or transient digitizer. At point B, the pulses are recorded with a multichannel analyzer (MCA), the input to which is a peak holding circuit. If $i(t)$ is the instantaneous current in a corona pulse, then the signal sensed by the peak holding circuit at point B is given by

$$q(t) = \int_{-\infty}^t i(t')h_2(t-t')dt'. \quad (1)$$

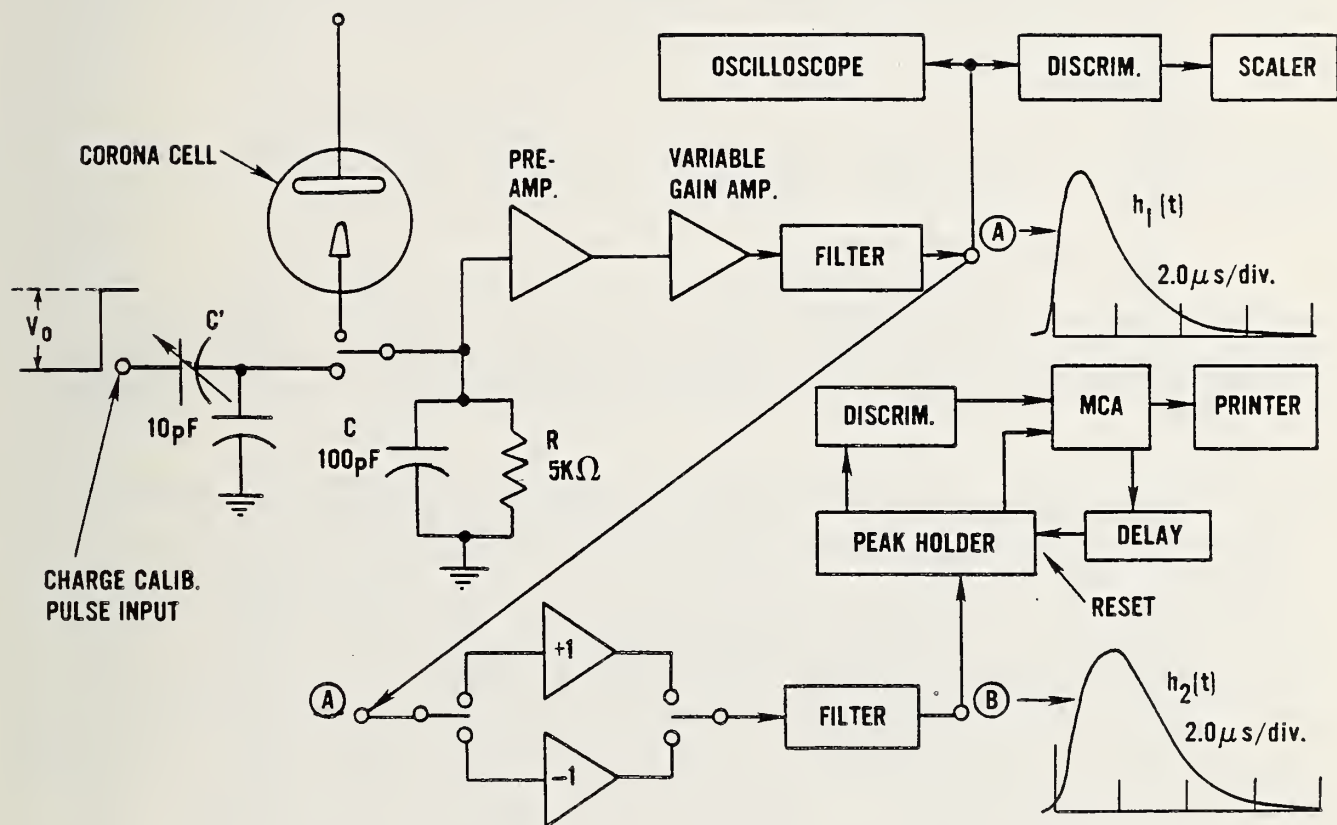


Figure 1. System for measuring electrical characteristics of corona pulses. Shown also are the measured impulse responses $h_1(t)$ and $h_2(t)$ at points A and B where the pulse repetition rates and pulse height distributions are measured respectively.

It is the maximum of this function which is actually recorded by the MCA. If the width of the corona pulse Δt is much smaller than the half width w of the function $h_2(t)$, and if the spacing between corona pulses is larger than w , then the measured pulse height distribution (PHD) of corona pulses is not affected by the details of $h_2(t)$. This becomes evident when the corona pulse is approximated by an impulse represented by a Dirac delta function, i.e.,

$$i(t) = Q\delta(t-t''), \quad (2)$$

where Q is the total charge contained in the pulse. Inserting this into eq (1) gives

$$q_m = Qh_2(t-t''), \quad (3)$$

which indicates that the maximum value of $q(t)$ will occur at the maximum of $h_2(t-t'')$, and will be proportional to the scale factor Q . This property of the measurement system has already been emphasized in a slightly different way [15].

The time resolving limitations of the instrument were examined in further detail during the past year. The results of such an investigation are illustrated in figure 2. Shown in this figure are the responses of the counter and the MCA system to two sharp (~ 10 ns) pulses separated by a variable time Δt . The dashed curve indicates that the counter cannot resolve pulses separated by less than $1.5 \mu s$, i.e., the maximum count rate at which it can record individual pulses is 6.7×10^5 Hz. The solid curve indicates that if the pulses are separated by less than about $0.4 \mu s$, then the MCA adds the amplitudes, i.e., it records a single pulse of amplitude $2 V$ for individual pulses with an amplitude of V . Only if the pulses are more than $1.8 \mu s$ apart does the instrument record an individual event of amplitude V , and only when the pulses are more than $8.0 \mu s$ apart does it record two events of amplitude V .

Figure 3 illustrates the way in which the instrument samples a pulse burst. The bursts shown are from positive corona in SF_6 , and were observed with a circuit of higher resolution ($\sim 0.1 \mu s$) than that used in figure 1. The first pulse in the burst triggers the peakholding circuit which remains on for a time $t_p = 2.0 \mu s$. In this case, smaller pulses immediately following the initial event are added to the amplitude of this event thus giving a recorded pulse amplitude which is somewhat greater than would be the case for a single isolated pulse.

While information is being transferred to the MCA there exists a dead time $t_s - t_p$ of $6.0 \mu s$ during which no new information can be accepted. The time $t_s - t_p$ is controlled by the delay indicated in figure 1, but is limited by the speed of analog-to-digital conversion in the MCA, which in the present system is approximately $4.0 \mu s$. After this time, if more pulses in the burst are present and exceed a predetermined threshold, then the cycle will be repeated. The burst will be sampled every $8.0 \mu s$ as long as it persists. The effect which this method of sampling can have in distorting the pulse height spectra of corona pulses has already been noted [8,15].

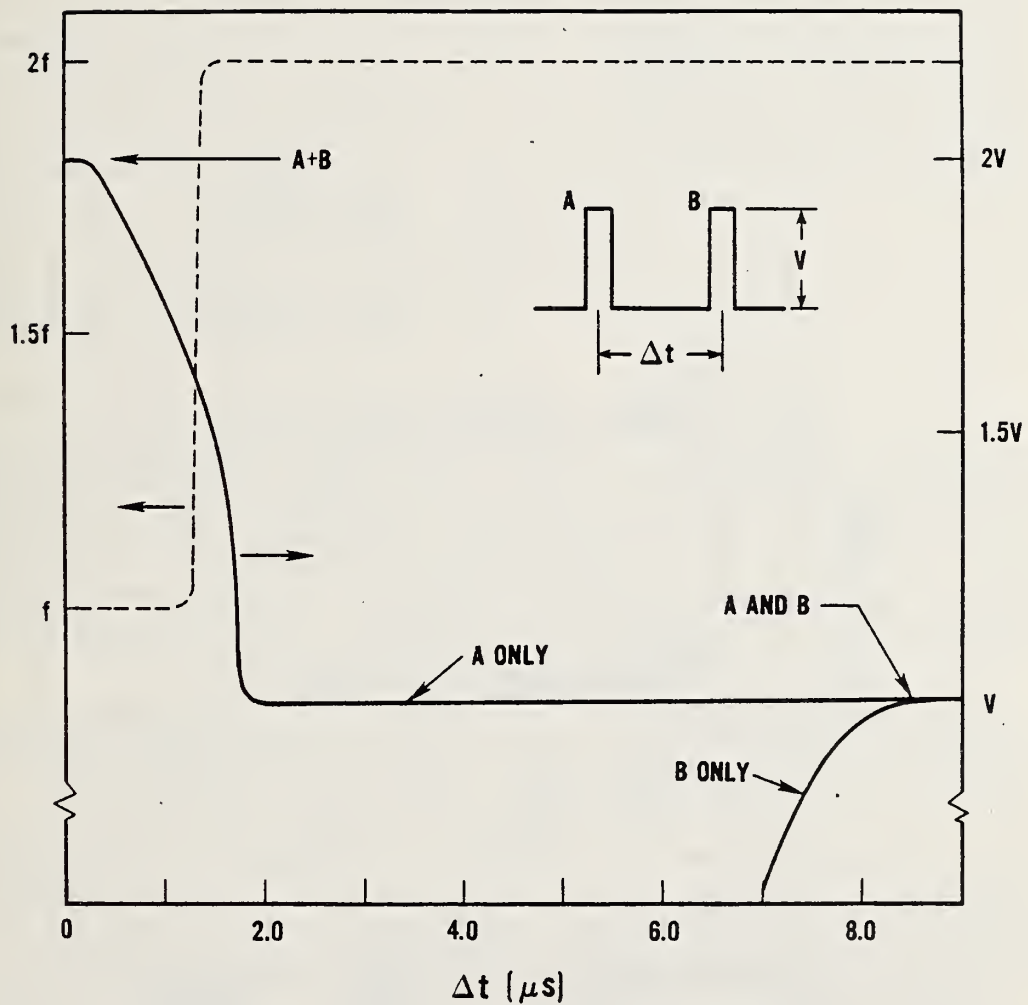


Figure 2. The measured response of the pulse counter (dashed line) and multichannel analyzer (solid lines) to application of two narrow pulses (~ 5 ns) separated by a time Δt . The left scale is the measured frequency and the right scale is the recorded amplitude.

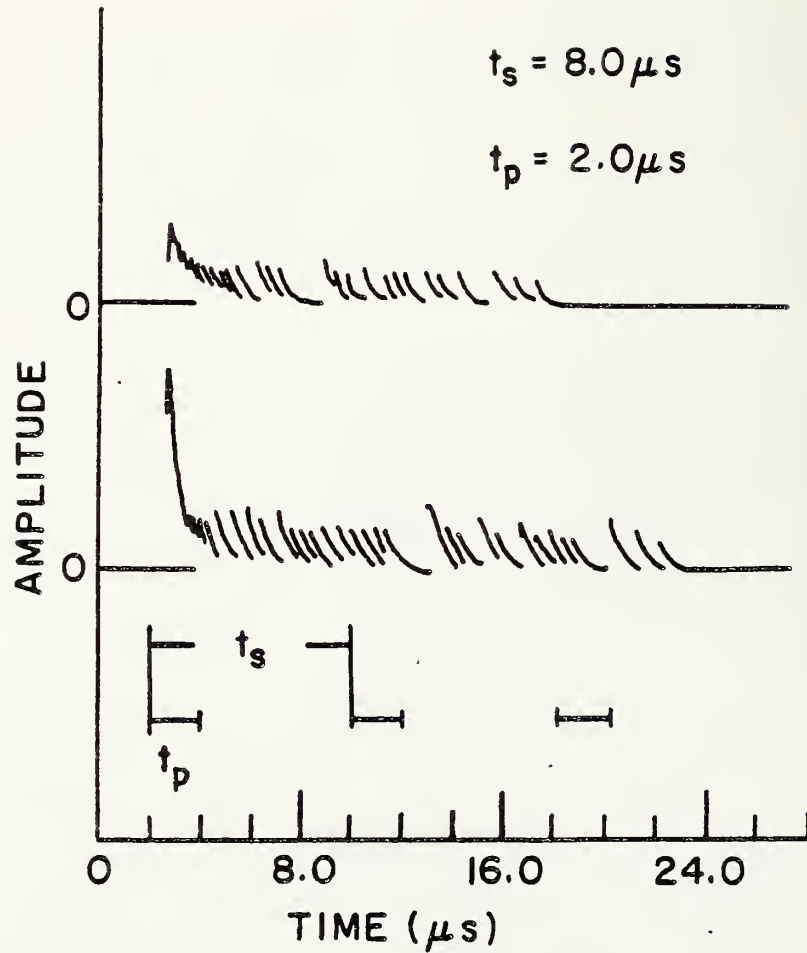


Figure 3. Typical positive corona burst pulses observed in SF₆ at an absolute pressure of 300 kPa and applied voltage of 32.3 kV. These were observed with a time resolution of 0.1 μs . Indicated are the sampling window t_p of the peakholder circuit and the minimum sampling interval t_s of the multichannel analyzer system.

Further tests were performed to evaluate the errors incurred in establishing a charge scale for PHD data. As indicated in figure 1, the system is calibrated by applying pulses of known amplitude V_0 to a standard capacitor C' to give a known injected charge $q = C'V_0$. The level corresponding to an injected charge q_i appears at a particular channel number n_i of the MCA, where it has been found that n_i is a linear function of q_i (see fig. 4). A least-squares straight-line fit to a set of observed calibration points ($q_i, n_i, i \geq 3$) was used to establish a charge scale from the MCA output. The uncertainties in the charge scale were found to be less than $\pm 10\%$ for the present method of calibration. The primary source of error appeared to be associated with uncertainty in matching the stray capacitance of the calibration circuit to that of the corona detection circuit. The uncertainties also appear to be greatest at the extreme low end of the charge scale where slight deviations from linearity in the relationship between q_i and n_i were noted (again see fig. 4).

II.A.3 Corona Pulse Characteristics for SF_6

As previously mentioned, a considerable amount of new data on the properties of dc positive and negative corona in SF_6 were acquired and presented in a recent publication [8]. Examples of some of these data are shown in figures 5-10. The results given in figures 5-8 on positive corona characteristics support our previously stated [15,16] conclusions concerning the voltage and pressure dependence of the pulse burst behavior. These results will not be repeated here.

Some new data were acquired in the past year concerning the properties of negative corona discharges, and examples of these are displayed in figures 9 and 10. The significant fact learned about negative corona is that in the absence of an external radiation source its characteristics near inception are quite dependent on conditions of the point cathode surface. It was discovered that characteristics of negative corona observed using freshly cleaned and polished stainless steel electrodes were drastically different from those observed after the electrodes had been "conditioned" by operating the discharge at a level of $1.0 \mu A$ or more for several minutes or by irradiating the point with uv light. Figure 9 shows the characteristics typically observed using "clean," unirradiated electrodes. The negative corona appears in the form of intermittent large pulses ($q > 10$ pC) of low repetition rate, even in some cases at voltages considerably in excess of onset. Depending on gas pressure, electrode diameter, and gap spacing the large pulses are usually followed by a long tail, or a burst of lower level pulses, such as for positive corona, or both. The inset in figure 9 shows two typical negative corona pulses recorded with a transient digitizer. The tails of the pulses are roughly of constant level and extend as much as $60 \mu s$ beyond the primary event. This characteristic of the pulses is reflected in the shape of the PHD, where the peak at $q \approx 64$ pC corresponds to the distribution of the relatively large primary events, and the sharp peak near 14 pC results from the first sampling of the tail. Actually, the tail, if it is longer than $16 \mu s$, is sampled more than once. Subsequent samplings which occur on the relatively level portion of the tail give rise to an even larger peak, not shown, at lower charge. This is more evident in the data displayed at the bottom of figure 10, which again corresponds to clean electrodes, but at a gas pressure of 200 kPa. The PHD peaks are broader in this case because here pulses with long tails

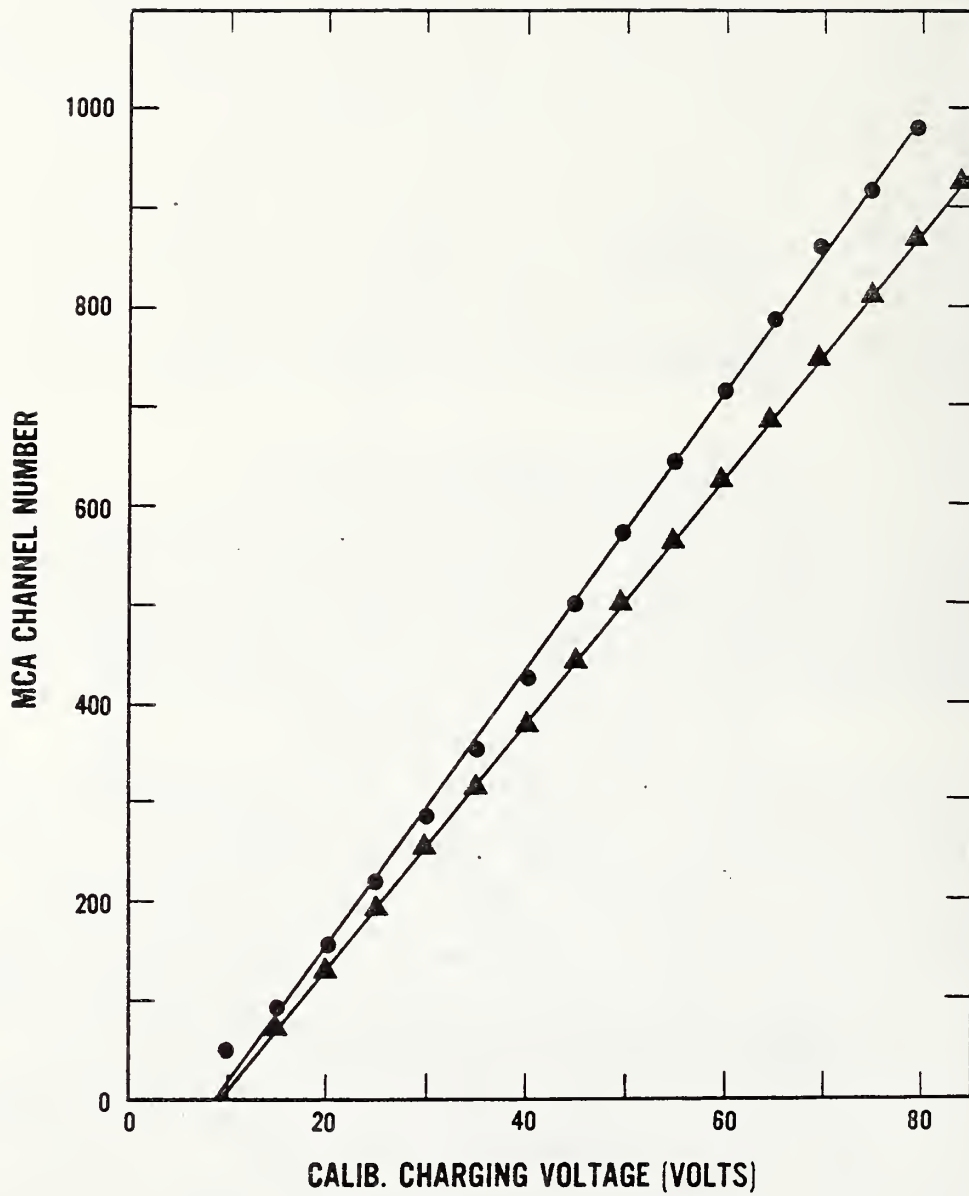


Figure 4. Multichannel analyzer channel number versus amplitude (in volts) of charge calibration pulse (see fig. 10).

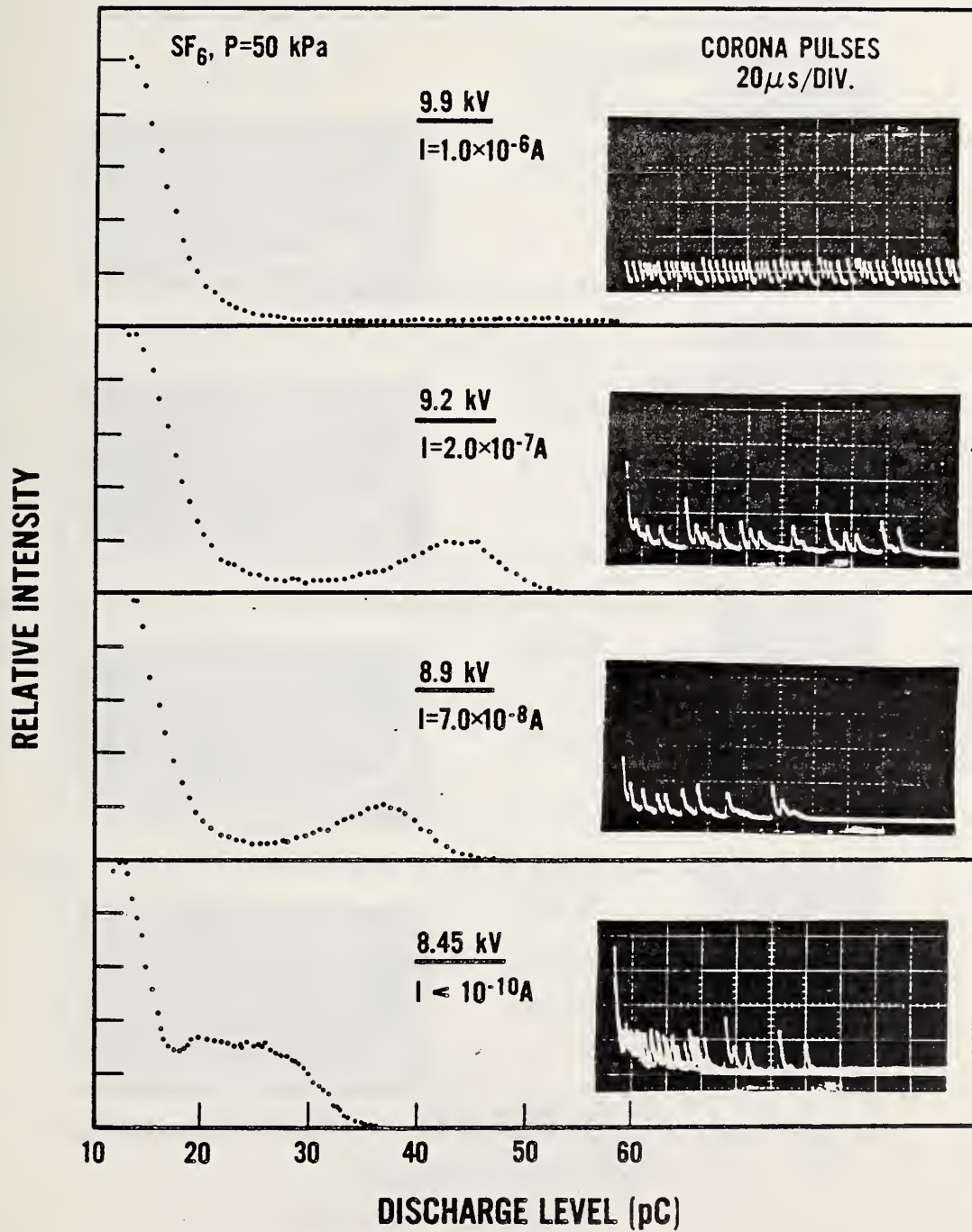


Figure 5. Measured electrical characteristics of positive corona pulses in SF₆ at an absolute pressure of 50 kPa. Shown are the corona pulse shapes, average corona current I, and pulse height distributions at the indicated applied voltages. The point electrode diameter is 0.1 mm and the gap spacing is 1.24 cm.

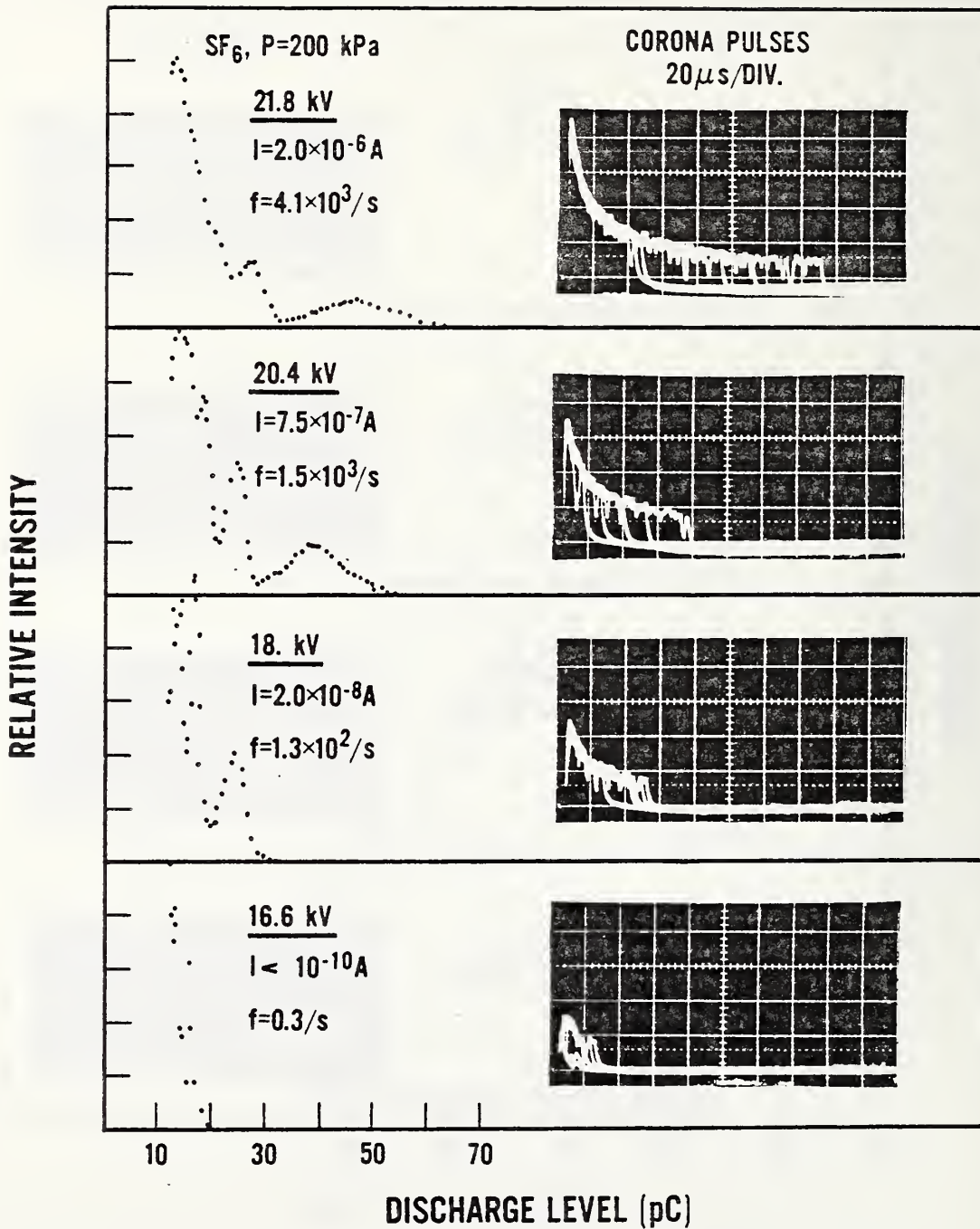


Figure 6. Measured electrical characteristics of positive corona in SF₆ at an absolute pressure of 200 kPa. Shown are the corona pulse shapes, pulse repetition rates f , average corona current I , and pulse height distributions at the indicated dc voltages. The point electrode diameter is 0.1 mm and the gap spacing is 1.24 cm.

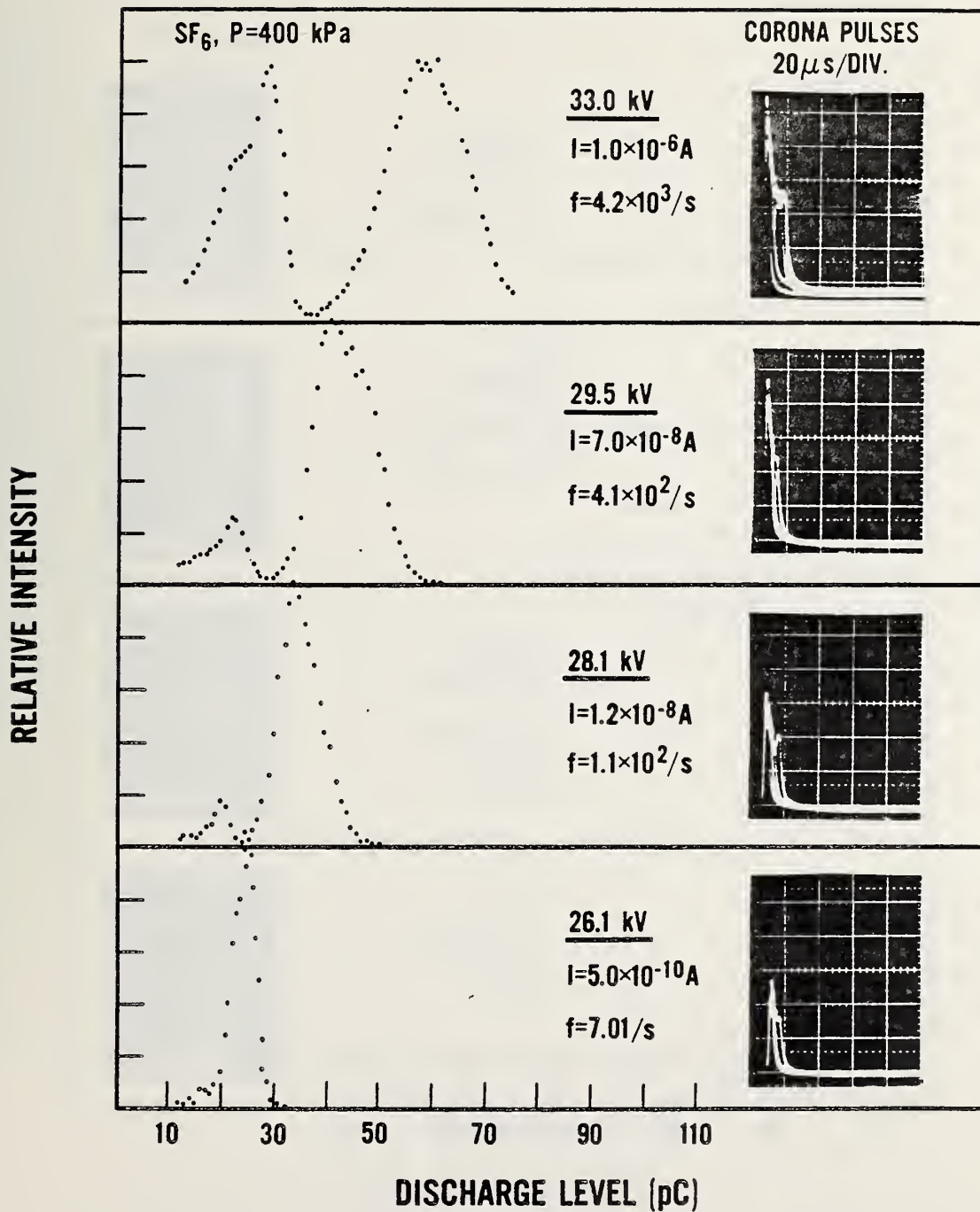


Figure 7. Measured electrical characteristics of positive corona in SF₆ at an absolute pressure of 400 kPa. Shown are the corona pulse shapes, pulse repetition rates f , average corona current I , and pulse height distributions at the indicated dc voltages. The point electrode diameter is 0.1 mm and the gap spacing is 1.24 cm.

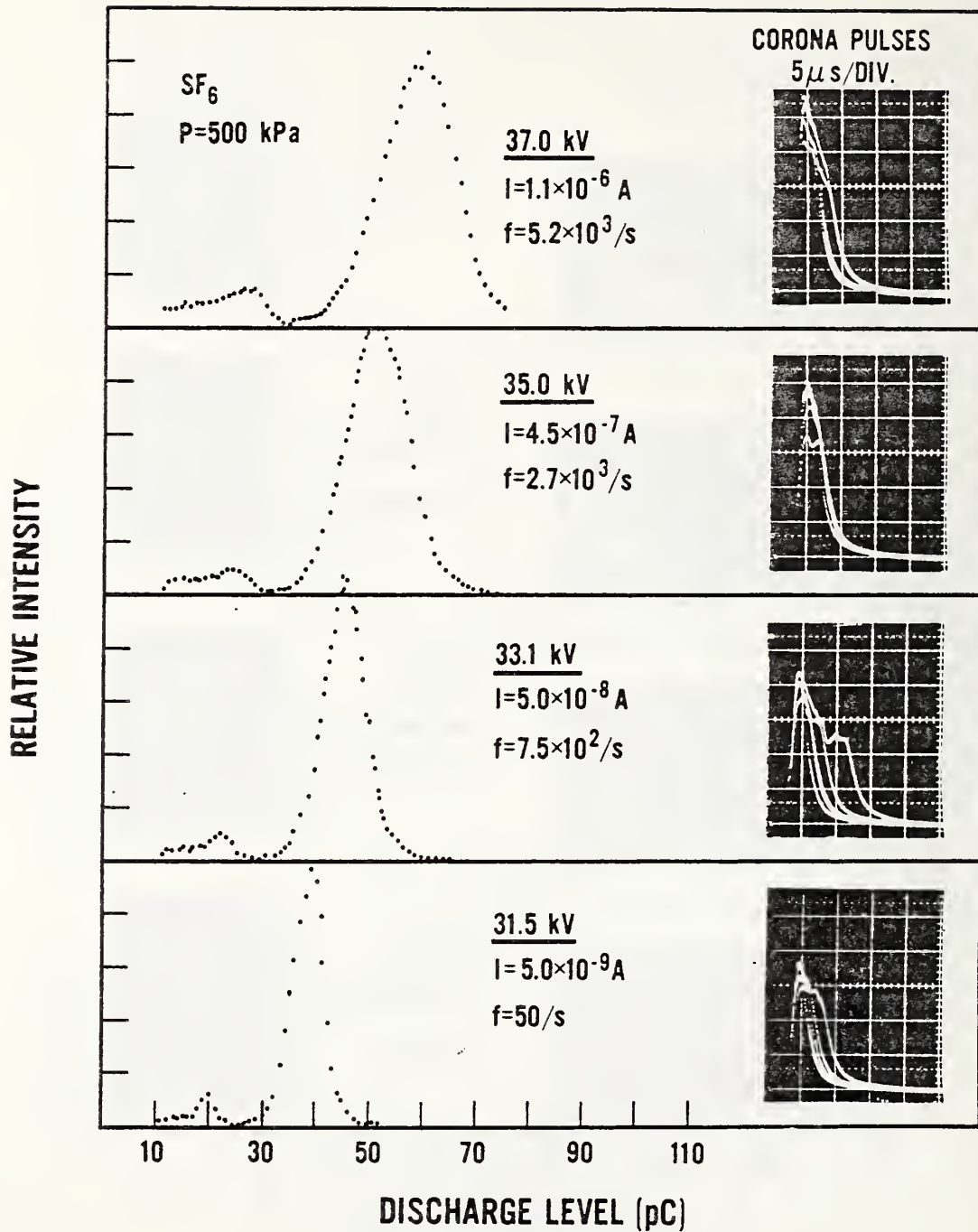


Figure 8. Measured electrical characteristics of positive corona in SF₆ at an absolute pressure of 500 kPa. Shown are the corona pulse shapes, pulse repetition rates f , average corona current I , and pulse height distributions at the indicated dc voltages. The point electrode diameter is 0.1 mm and the gap spacing is 1.24 cm.

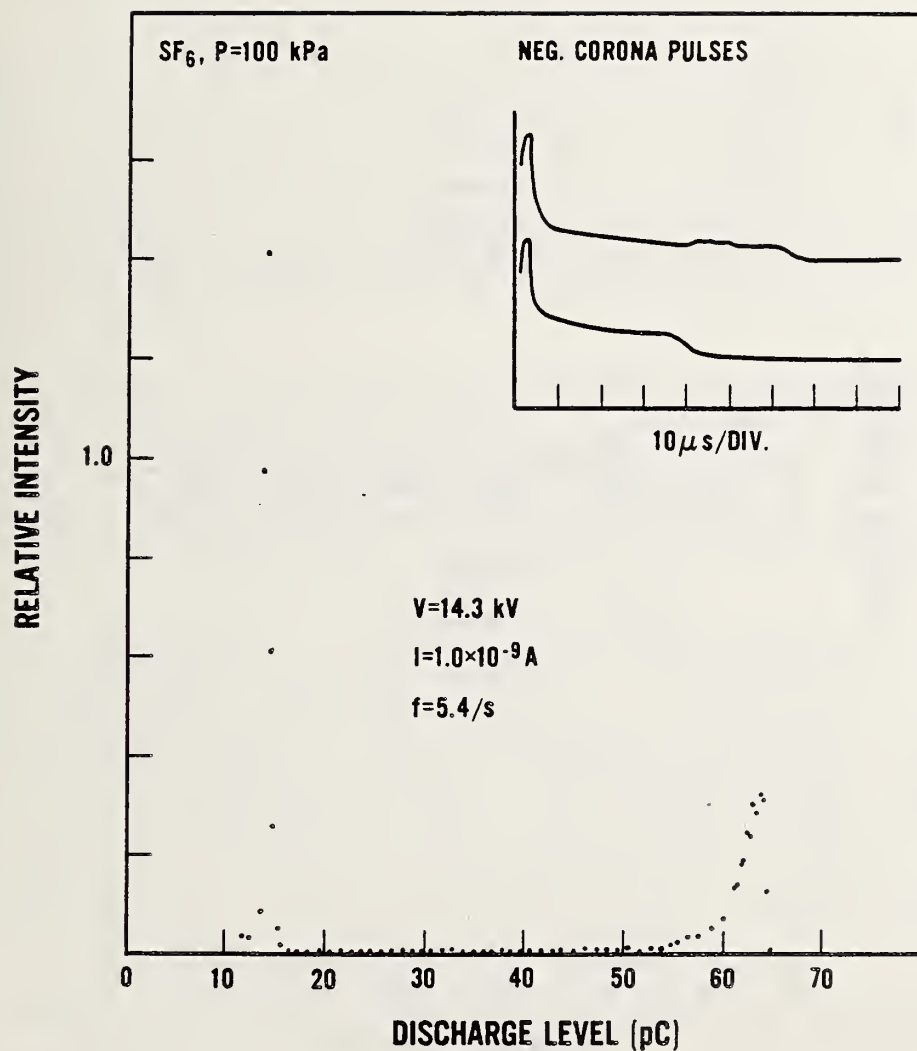


Figure 9. Measured electrical characteristics of negative corona pulses in SF₆ at an absolute pressure of 100 kPa and applied voltage of 14.3 kV for freshly polished stainless steel electrodes. Shown are the average corona current I , the pulse repetition rate f , and typical pulse shapes recorded with a transient digitizer. The gap was not irradiated.

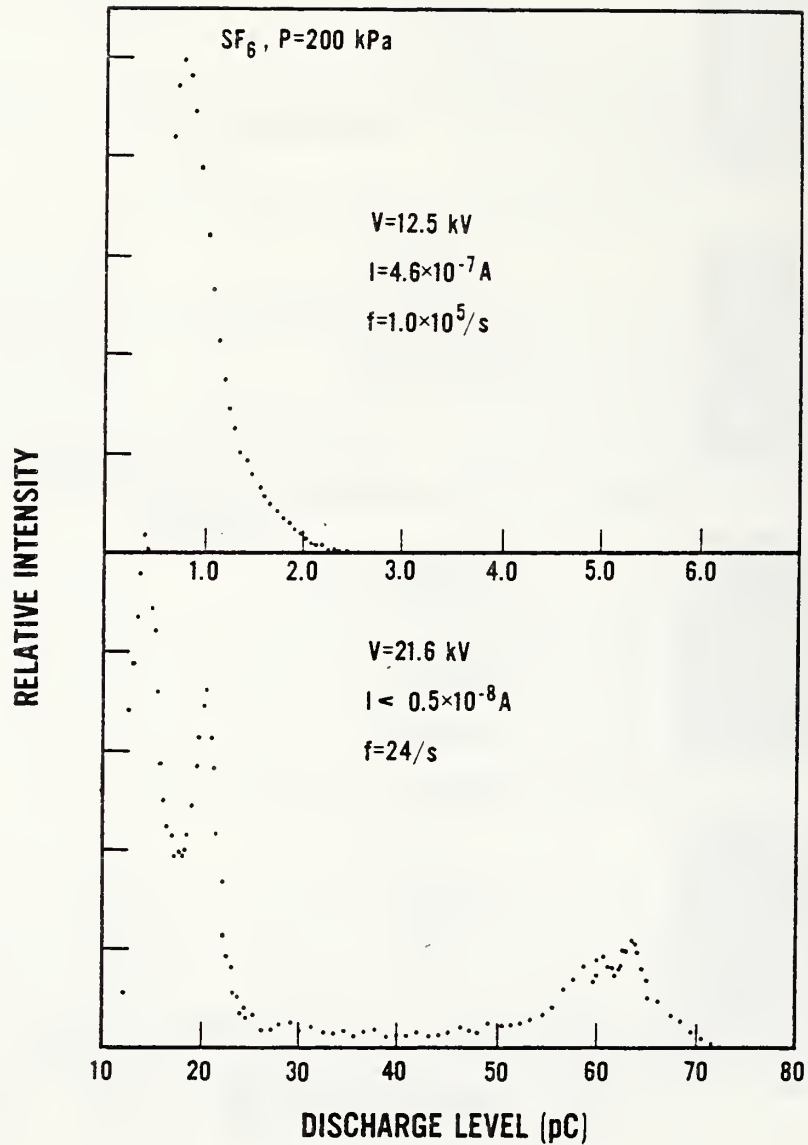


Figure 10. Comparison of measured electrical characteristics of negative corona pulses in SF_6 at 200 kPa for freshly polished electrodes (upper portion). Shown are the pulse height distributions, pulse repetition rates f , average corona current I , and applied voltage V . The gap was not irradiated.

were interspersed with large pulses followed by a burst of lower amplitude pulses. It is noteworthy that the larger pulses seen for negative corona from clean stainless steel tips have a fairly narrow distribution in amplitude, and in this sense they are similar to Trichel pulses [5] seen in negative corona discharges of other electronegative gases. However, unlike true Trichel pulses, their occurrence is random, i.e., they do not appear in regular intervals with a constant repetition rate.

The upper part of figure 10 shows the observed characteristics of negative corona for the same gas and electrodes, after the current had been operated at 5.0 μ A for a period of 70 s. The voltage for the upper graph in figure 10 is considerably below that for the lower graph corresponding to the clean electrodes, and yet the average corona current I is two orders of magnitude greater. It is also seen that the repetition rate for the pulses is considerably higher for the electrodes conditioned by prior discharges, although the mean amplitude of the pulses is now much lower (peaked below 1.0 pC).

Once conditioning of the electrodes had occurred, it was found that the general features of the negative corona in SF₆ remained fairly unchanged, i.e., the corona was found to "turn on" abruptly, as noted in earlier measurements [10], and it was predominantly in the form of high-frequency, low-amplitude pulses. Examination of the point electrode under a microscope after conditioning showed that it was slightly discolored and microscopic irregularities in the form of pitting had developed.

The effect of conditioning is to increase the electron emission of the point electrode, perhaps by a combination of lowering the work function of the surface and locally enhancing the field. It should be noted that this effect could be achieved with "clean" electrodes by irradiating the point with a sufficiently intense uv-source. The radiation insures electron production via the photoelectric effect, i.e., photon-enhanced field emission. However, once the electrodes have been conditioned by running a discharge, the uv-radiation has only a small influence on the way in which the corona develops with voltage. This is consistent with our previously reported observations [10,11,15].

II.B. Modeling of Discharge Inception and Electron Avalanche Growth in SF₆

II.B.1 Motivation

During the past year a grant was awarded by NBS to the High Voltage Research Laboratory at the Massachusetts Institute of Technology to support their participation in the NBS-DOE research program on gaseous dielectrics. The emphasis of their work has been on development and testing of a model of prebreakdown partial discharge phenomena which can be used, for example, to understand and predict the statistics of electron avalanche growth and the transition from avalanche to breakdown for electronegative gases in a highly localized nonuniform field region associated with a protrusion on a plane electrode. The specific motivation behind this work has been twofold: (1) to develop a model which will provide a more complete fundamental description of inception and partial discharge phenomena in gases, and (2) provide basic information needed to develop new standard procedures for measurement and evaluation of the insulation strength of gases. It

should be noted that this activity ties in closely with the NBS work on investigations of corona-inception mechanisms to be discussed in Sec. II.C, and with the effort to compile and evaluate fundamental electron swarm data to be discussed in Sec. II.D. Some results of this work have already been reported in a thesis by Gels [9].

In this report we give a brief description of the theoretical approach taken in this investigation and highlight some of the more significant results. Mention will be made of the problems that have been encountered and a proposed method for dealing with them. It is hoped that once a successful model is formulated which can predict electron avalanche size distributions and the transition to streamers in SF₆ for negative points (or protrusions), it can then be applied to the interpretation of results for positive-point discharges as given, for example, in the previous section of this report as well as in [8] and [16]. As will become evident from the discussions in Sec. II.C, the problem is more difficult for positive discharges because, in addition to considering the stochastic nature of the avalanche growth process, it is also necessary to consider the probability of initiatory electron release as a function of location in the gas containing gap. For negative discharges one can insure, by irradiating the point electrode, that electrons will be released at discharge inception predominantly from the tip of this electrode where the electric field is highest (see Sec. II.C). Thus, for the negative point case, the statistics of the electron release or injection process are of no concern, and the task of calculating the statistical distribution of avalanches is simpler.

The theoretical approach taken here resembles that used by Blair, et al. [17] in their investigation of avalanche statistics for uniform fields in SF₆. In that work it was shown that the probability that an electron avalanche will grow to the point where it leads to streamer breakdown is vanishingly small for E/p (field strength/pressure) below the limiting value corresponding to the condition $\alpha_i = \eta_a$, where α_i and η_a are respectively the ionization and attachment coefficients of the gas. The present work includes an attempt to extend these considerations to nonuniform field situations where a study of avalanche inception and growth are likely to be more successful because of the highly restricted nature of the ionization region. Moreover, this is more likely to represent the conditions under which breakdown occurs in practical situations. Rarely can one apply purely uniform fields considerations to compressed gas insulated equipment in which conducting particles may be present as well as surface irregularities. In practice, highly nonuniform electric fields can also appear at interfaces with solid insulators.

II.B.2 Theory

II.B.2.1 Introduction

The basic approach, as described here, is to use information on electron-molecule interactions in the gas phase to predict the development of an electron avalanche in a nonuniform electric field region, i.e., the spatial and temporal dependence of its growth. It should be kept in mind that electron avalanching, and for that matter breakdown, is a statistical phenomenon; thus, it is necessary to consider it from a statistical point of view. The

question of practical significance is: given a set of conditions, e.g., field nonuniformity, gas pressure, etc., what is the probability that an electron avalanche will grow to a sufficient size to lead to breakdown?

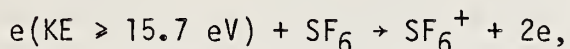
If electric fields are moderate, compressed gases exhibit remarkably little electrical conductivity. The conduction is very low because there are very few free charge carriers. The gas molecules, though mobile and constantly moving in thermal equilibrium, are normally neutral. An occasional charged molecule is created by background radiation effects so that a small but finite free carrier density exists. Because there are so few carriers, the electric current they provide is often not even measurable, typically being below 10^{-15} amperes.

The transition from the highly insulating to the conducting state of a gas, i.e., breakdown, can only occur when a great number of charge carriers are introduced into the gaseous gap. Hence, the basic phenomena associated with breakdown are the processes which influence the buildup and decay of free charge in the gas.

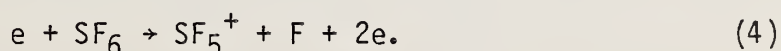
II.B.2.2 Basic Discharge Processes

Gas discharges occur when conditions allow ionization to take place. The energy needed for ionization of molecules or atoms in their ground state is typically 10 to 20 eV. Each ionizing event results in the liberation of at least one additional electron from a molecule, leaving behind a positive ion. The progressive release of liberated electrons causing further ionization, as in a chain reaction, is known as an electron avalanche.

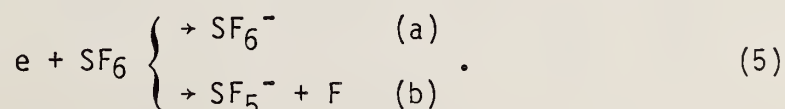
Although ionization can occur via other mechanisms such as through photon absorption or collisions with molecules in excited metastable states (see Sec. II.F), it will be assumed here that ionization by electron collision with ground state neutral molecules is by far the dominant mechanism responsible for electron multiplication, i.e., the process



where KE refers to the kinetic energy of the incident electron. Actually for electrons with energies above 15.7 eV, the formation of a stable SF_6^+ ion is highly improbable, and the most likely ionization process for SF_6 is one that involves dissociation [18-20], namely



Another process of fundamental importance in understanding electron avalanche growth is electron attachment, examples of which are



This is the process by which electrons are removed from the gas and rendered unavailable for ionization. The process (a) above, for the formation of a stable SF_6^- ion, requires a third body (molecule) to remove the excess energy [21]. The lifetime of SF_6^- exceeds 50 μs ; thus at high enough pressures, it will tend to collisionally stabilize before auto-detachment can occur. In the second process (b), referred to as dissociative attachment, the excess energy can be consumed as kinetic energy of the dissociation fragments, thereby insuring stability of the negative ion formed.

Given that an electron has sufficient energy to ionize (or attach), one must ask: what is the probability that such an event will occur in an electron-molecule encounter? The likelihood of an ionizing or attaching collision between an incident electron and a target molecule can be expressed by an "effective area," the cross section, which is the "size" of the region in space where the two particles must be at one time for the defined collision to occur. This formalism for describing what interactions take place at the atomic scale has proved remarkably successful over a very wide range of situations. In general form, the collision cross section, σ , is expressed as:

$$\sigma = \frac{\text{number of particles affected/unit time}}{\text{incident intensity}} .$$

The value of cross-section information is both in the visualization of what reactions take place and in its fundamental form which can be applied to most situations. Its generality also is a problem, though, since a thorough accounting of all significant reactions must be kept.

Each pair of colliding particles exhibits a specific cross-section pattern for a given event. This pattern is typically dependent upon the relative velocities or energies. As an illustration of the range and variation of cross-section values, data for electron attachment in SF_6 gas is presented in figure 11. These data were taken from [20].

Although one could use cross-section data directly to model electric discharge behavior such as with a Monte Carlo-type computer calculation in which an arbitrarily large number of individual collision events are considered, such an approach is time consuming and generally impractical. In applying cross-section data, it is convenient to first perform an average over the kinetic energy distribution of the electrons, and derive average quantities (swarm parameters) known as ionization and attachment coefficients (α_i and η_a) which give the number of ionizations (or attachments) per unit distance in the gas. This approach may not be valid under all conditions, but it is the approach that is commonly taken and will be useful in all cases where local equilibrium can be assumed (also see Sec. II.D).

If one knows the electron energy distribution function $f(u)$, then one can calculate the rates of ionization ν_i and attachment ν_a using

$$\nu_i = N\left(\frac{2}{m}\right)^{1/2} \int_0^{\infty} u^{1/2} \sigma_i(u) f(u) du \quad (6)$$

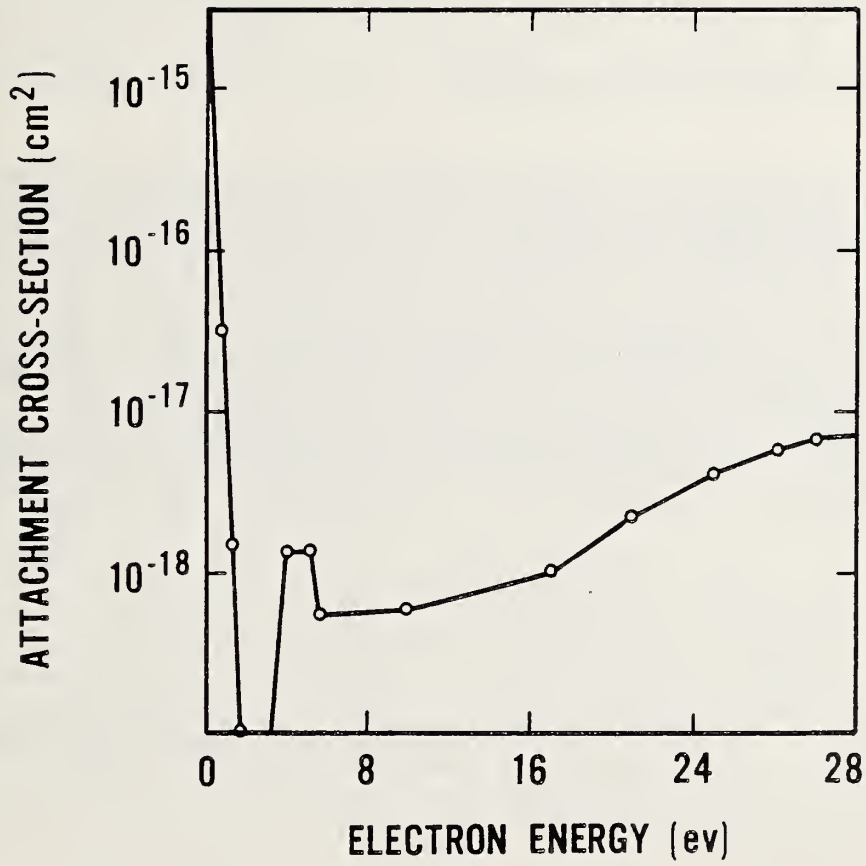


Figure 11. Electron attachment cross sections for SF₆ (from Asundi and Craggs).

and

$$v_a = N \left(\frac{2}{m}\right)^{1/2} \int_0^{\infty} u^{1/2} \sigma_a(u) f(u) du, \quad (7)$$

where m is electron mass, N is the gas number density and σ_i and σ_a are the ionization and attachment cross sections. The ionization and attachment coefficients are defined from the relationships

$$v_i = \alpha_i W \quad \text{and} \quad v_a = \eta_a W, \quad (8)$$

where W is the mean electron drift velocity. These coefficients are usually expressed as functions of E/N , the field-to-gas density ratio (see Sec. II.D). The electron energy distribution function can be obtained from solutions of the Boltzmann transport equation as discussed in Sec. II.D.

If the electric field resulting from ion-space-charge can be neglected so that the electric field is solely a function of position, and if the pressure in the gas is constant, then α_i and η_a will be solely functions of position. Thus, if ionization and attachment are the only important processes determining avalanche growth, then we can write the following approximate expression for the spatial dependence of the electron number density:

$$dn_e(x)/dx = n_e(x)[\alpha_i(x) - \eta_a(x)], \quad (9)$$

where $n_e(x)$ is the average number of electrons in the avalanche when it reaches position x . This equation allows for nonuniform electric fields to exist by allowing α_i and η_a to be functions of position in accordance with the electric field. More will be said about the validity of eq (9) in Sec. II.C.

There are, of course, other processes that can affect the growth or decay of an electron avalanche in a gas, and although these may not be important for most conditions considered here, they are nevertheless worth mentioning. For very high values of E/N , it may be necessary to include processes which lead to detachment of electrons from negative ions. The possible importance of this process in initiating electron avalanches will be considered in Sec. II.C. This process, like ionization and attachment, is usually described in terms of a detachment coefficient, i.e., the number of electron detachments per unit length. Collisions involving metastable species, i.e., atoms or molecules in long-lived excited states, may also be important in some cases as will collisions with ions. Absorption and emission of photons in the gas can also affect the production of free electrons.

II.B.2.3 Deterministic Model of Avalanche Growth

The number of electrons in a given avalanche, neglecting photoionization and ionization from ion or metastable collisions for the moment, depends on the accumulated likelihood for the various possible collision events during the travels of all the free electrons. For a given density of particles, the probability per unit distance of a collision event is simply proportional to the cross section. Individual events may include electron impact ionization, electron attachment, and detachment. As these events in the gas are not deterministic in nature, avalanche growth is statistical. Thus, for a given set of conditions, variations in avalanche size will occur and the result is best described by a distribution of sizes. The size is of special interest because it indicates when a self-sustained electrical discharge will occur.

As a first step in modeling avalanches, however, it is useful to consider a description in terms of average quantities as, for example, can be derived simply from a consideration of eq (9). Modeling discharges by considering phenomena only in terms of their average effects is sometimes referred to as deterministic, since the underlying stochastic nature of the phenomena is ignored. Later, when a stochastic model is formulated and the phenomena are described in terms probability distribution functions (PDF's), it is to be expected that averages generated from the PDF's should agree with the average solutions generated by the deterministic model. This, in fact, is found to be the case [9].

As a first approximation, we neglect space charges so that the electric field is Laplacian, solely a function of position. If the electric field is a function of position, then the ionization and attachment coefficients for the gas are functions of position. In this case, the growth-decay process is described by eq (9), from which the average number of free electrons in an avalanche, \bar{n}_e , when it reaches position x from the cathode is determined using swarm parameters by

$$\bar{n}_e = \exp\left[\int_0^x [\alpha_i(x') - \eta_a(x')]dx'\right]. \quad (10)$$

It was assumed here that the avalanche was initiated by a single electron. A numerical solution for eq (10) can be easily generated using a computer.

An example of calculated avalanching in SF₆ at a pressure of 200 kPa is shown in figure 12 for the case of a nonuniform applied field. The average number of free electrons contained by the avalanche as it moves from the cathode surface is depicted. The field nonuniformity in this example was provided by a cathode protrusion comprised of a hemispherically tipped metal rod, 0.2 mm radius, which protruded 2.0 mm into the gas gap from a planar cathode surface. The values of the ionization and attachment coefficients used are given in [9].

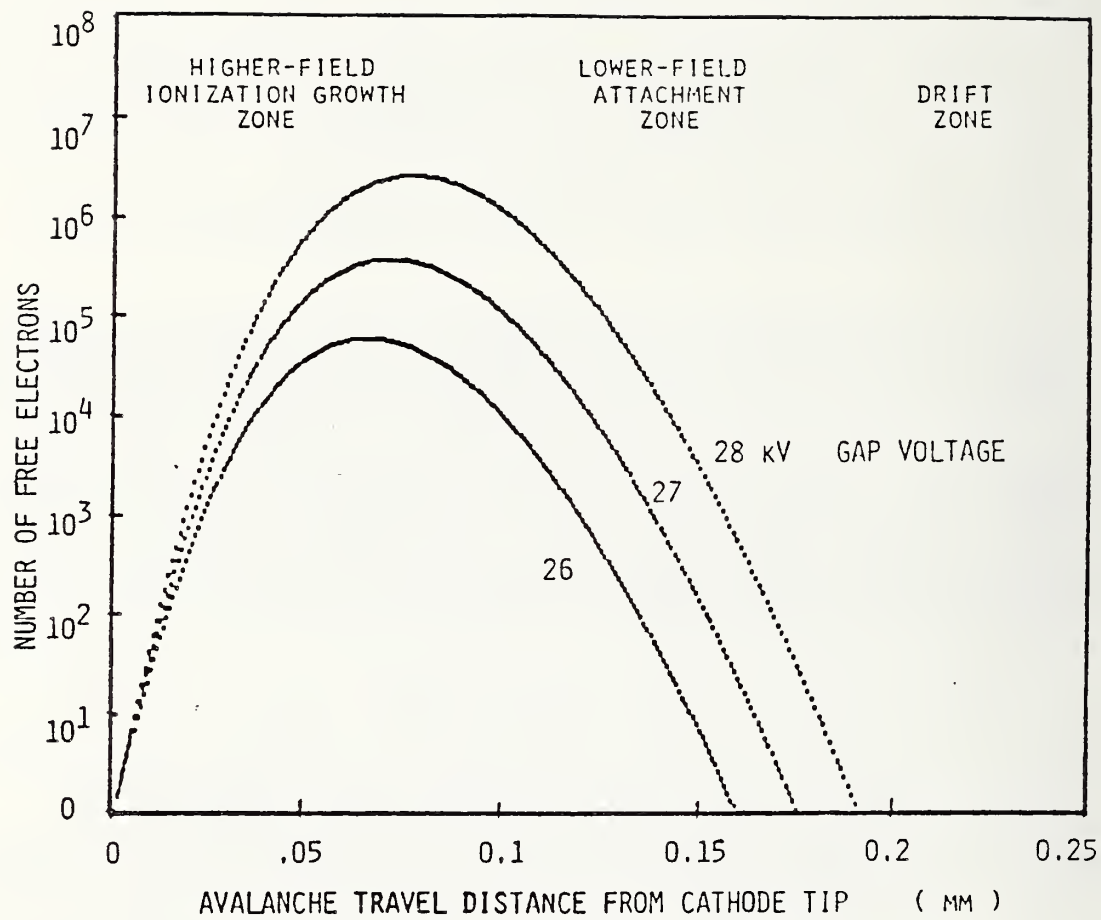


Figure 12. Calculated electron avalanching in 200 kPa SF₆ controlled ionization zone.

II.B.2.4 Effect of Space Charge on Avalanche Growth

To determine the effect of space charge on the electric field, which in turn affects the ionization and attachment coefficients, we must know not only the space charge magnitude, but also how it is spatially distributed. This can be determined by considering the distribution of electrons in the head of the avalanche.

Raether [22] has shown that, in the presence of diffusion, when at time 0 we start out with n_0 electrons at the origin, the density of electrons ρ_e at a distance r from the origin for time $t \geq 0$ is:

$$\rho_e(r,t) = [n_0/(4\pi Dt)^{3/2}] \exp[-r^2/4Dt], \quad (11)$$

with a mean-square radius of

$$\bar{r}^2 = (1/n_0) \int_0^\infty r^2 (4\pi r^2 \rho_e) dr = 6Dt, \quad (12)$$

where D is the diffusion constant for electrons. It can be shown [9] that even if the number of electrons is changing as a function of time in a manner dependent upon the number of electrons (this is the situation found in an avalanche), then the electrons still maintain the distribution above.

The avalanche can be viewed as a ball of electrons, with a density profile in the form of $\rho_e \sim \exp[-(r/R)^2]$, where r is the distance from the center of the ball. The center of the ball moves in the direction of the anode, the z -direction, with expanding root-mean-square radius given by

$$R = (6Dt)^{1/2} = [6(D/\mu) \int_0^z dz' / E(z')]^{1/2}, \quad (13)$$

where μ is the electron mobility. This radius is a function of z , the distance from the cathode. Figures 13 and 14 show calculated values of the avalanche radius as a function of the distance from a cathode protrusion.

A value of $D/\mu = 5$ eV has been taken from the data of Naidu and Prasad [23] (see Sec. II.D). For constant gas pressure, radii are not dramatically different for the different terminal voltages near the discharge inception levels.

As the avalanche head moves through the gas, it leaves a trail of positive and negative ions. Near the cathode, where the ionization coefficient exceeds the attachment coefficient, the ions are mostly positive. Further away from the cathode, the attachment coefficient exceeds the ionization coefficient, and the ions are mostly negative. Here, the electrons are taken to move many times faster than ions, due to relative mobilities.

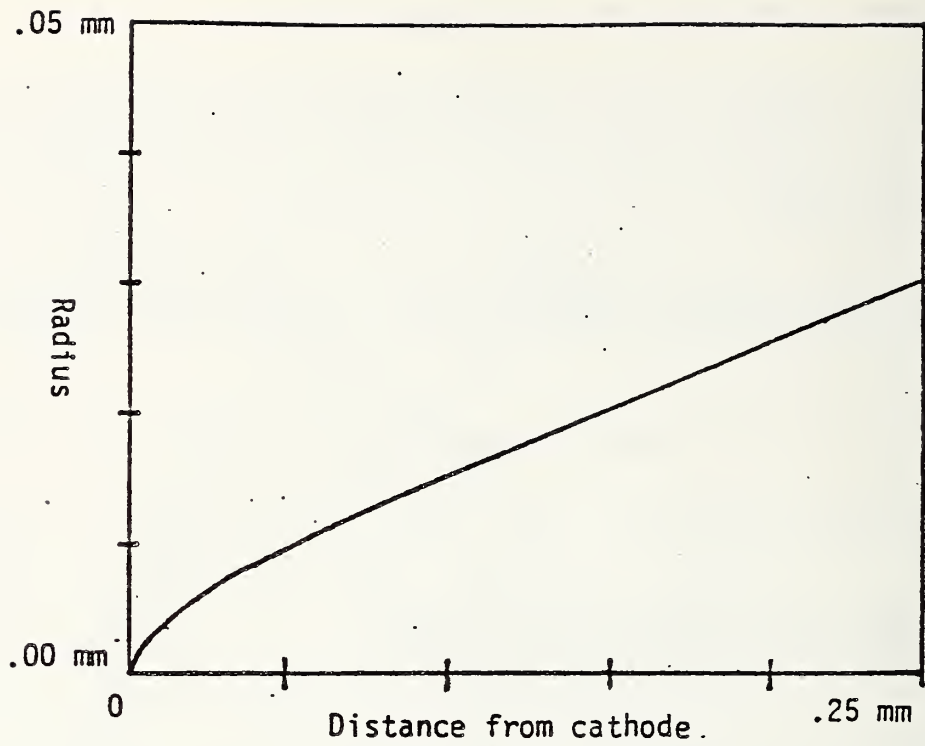


Figure 13. Avalanche radius with 100 kPa SF₆, 17 kV.

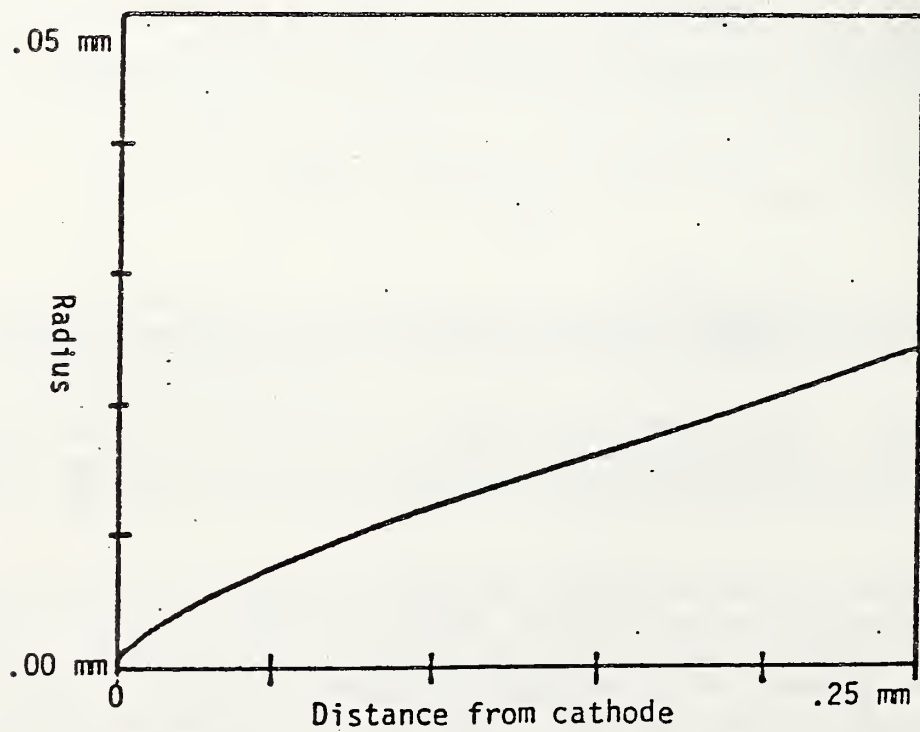


Figure 14. Avalanche radius with 200 kPa SF₆, 27 kV.

Thus, for any one avalanche, the ions are assumed to be stationary at their point of creation throughout the movement of the electron "wave" through the ionization zone. After all avalanche electrons have passed, the ions will slowly drift out of the gap.

For the electrode arrangement used in the experiment described in [9], ion densities (ions/mm path) were calculated at 100 and 200 kPa pressure SF_6 , figures 15-18. Net ion charge is shown in figures 19 and 20. Applied voltages which would create maximum free electron numbers just below and above 10^8 are used. Note the number of ions/mm exceeds the number of free electrons and that, as expected, the ions create a dipole, more positives in the growth region and more negatives in the decay region. Note also that as gas pressure is increased, these ions (and indeed) the whole avalanche moves closer to the cathode surface.

Taking into account electron diffusion, the avalanche leaves behind expanding cylinders of positive and negative ions, having approximate radii $\bar{r}(z)$ given by eq (13). To consider the effect of the ions on the field of the avalanche, we might break the charge trail up into disks of charge ΔQ having radii $\bar{r} = r$; the space charge field at the avalanche head is then obtained as the summed contributions of all the disks of charge. This is shown in figure 21. The electrons in the head of the avalanche will enhance the electric field, enhancing growth, in front of the avalanche head. On the other hand, the electrons will diminish the field in back of the avalanche head, diminishing growth there. Since the ionization and attachment coefficients are nonlinear functions of electric field, the net effects of enhanced and diminished growth do not cancel. Instead, the increased growth in front exceeds the reduction in growth in back. If the electrons in the avalanche head have radial distributions of the form $\rho_e \sim \exp[-(r/R)^2]$, where r is the distance from the center of the avalanche head, then the field distortion will be maximum at $r = R$.

Computer simulations were run using the assumptions and approximations explained above. The fields due to the avalanche head electrons were found to be several orders of magnitude greater than the fields due to the ions. The fields due to avalanche head electrons were divided by the Laplacian electric field, and plotted in figures 22 and 23.

Raether [24], investigating discharges in a cloud chamber, found that when the number of electrons in the avalanche reached a certain level, a channel formed, whose growth rate and speed suddenly increased by an order of magnitude. Raether [25] attributed this to the enhancement of the ionization process in front of the avalanche head, due to the space charge of the electrons in the avalanche head. He found that this critical number of electrons was approximately 10^8 . Raether was using a uniform field configuration to investigate a non-attaching gas.

Computer simulations of the nonuniform test system of [9], filled with sulfur hexafluoride, indicate the field due to electrons becomes roughly equal to the Laplacian field when the number of electrons approaches 2×10^6 . While this is lower than Raether's critical value, it is encouraging that the simple model employed shows that an avalanche growth instability can be expected. The lower critical number resulting from the computer simulation may be due to underestimation of the radius of the avalanche. The computer

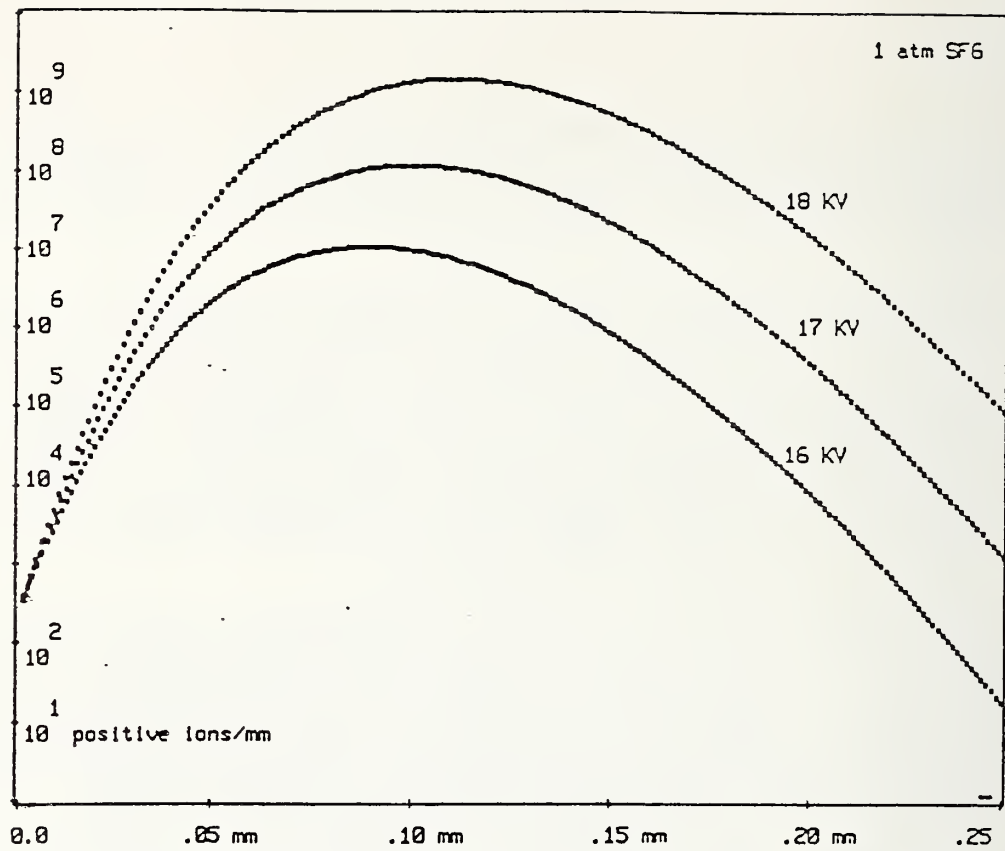


Figure 15. Calculated positive ion density left by an electron avalanche in the CIZ test cell at 100 kPa SF₆.

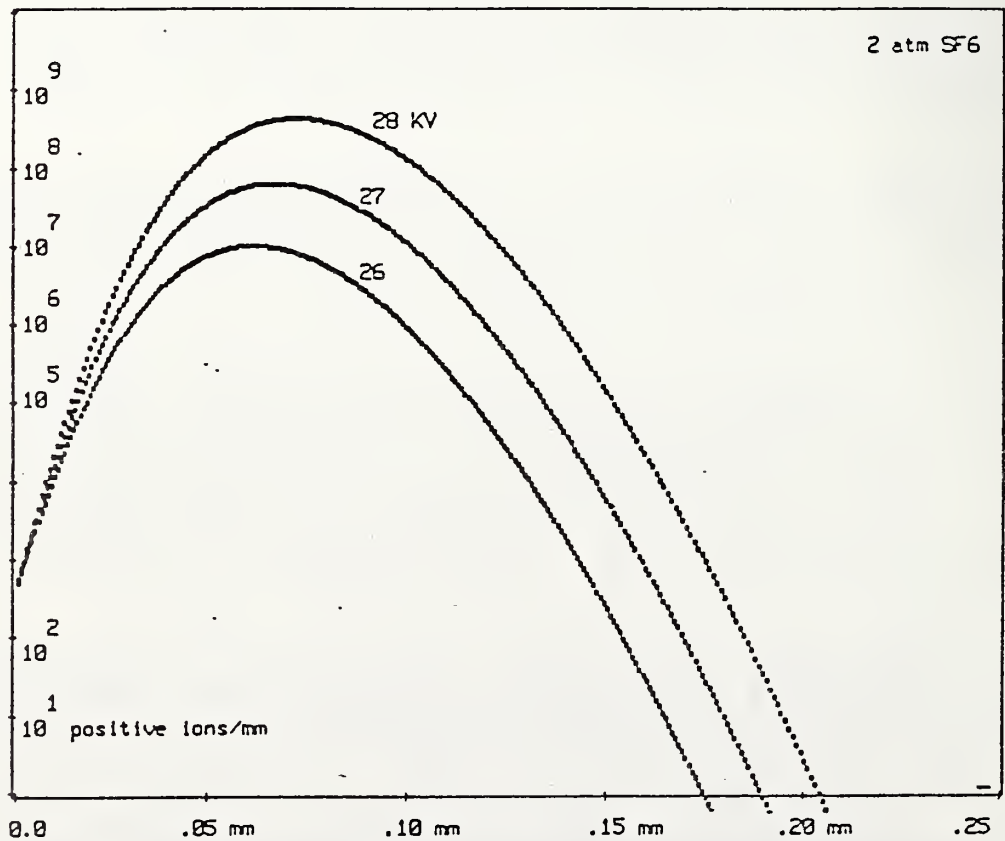


Figure 16. Calculated positive ion density left by an electron avalanche in the CIZ test cell at 200 kPa SF₆.

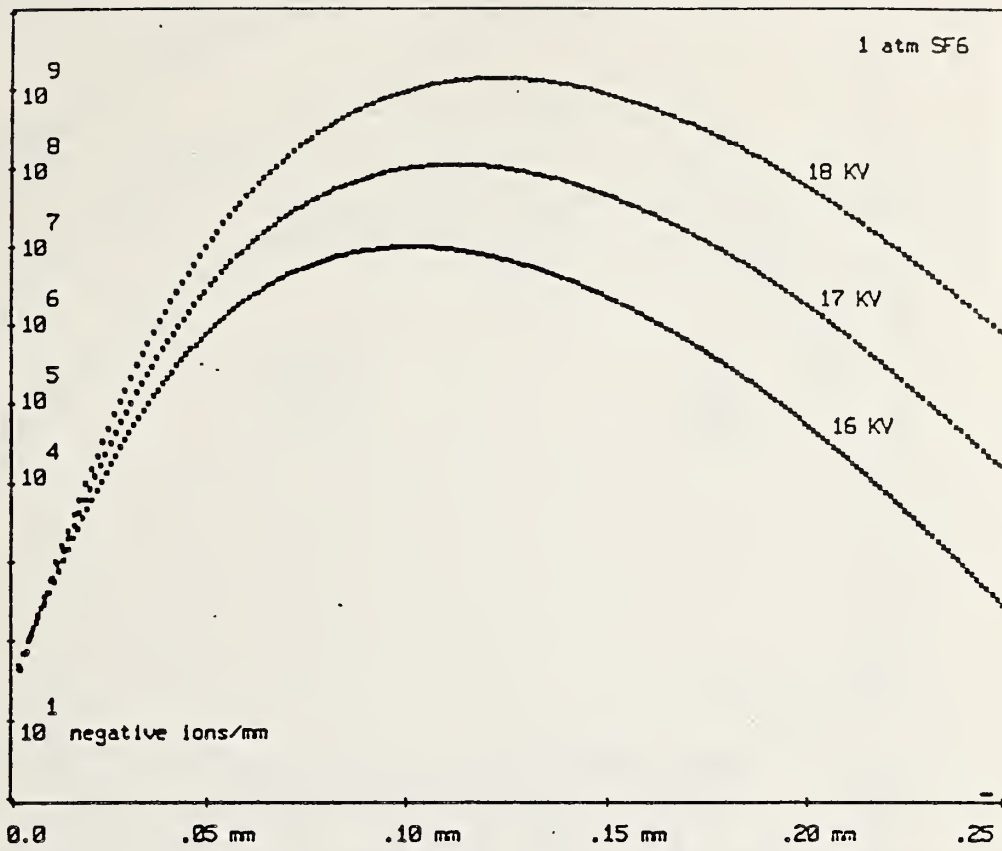


Figure 17. Calculated negative ion density left by an electron avalanche in the CIZ test cell at 100 kPa SF₆.

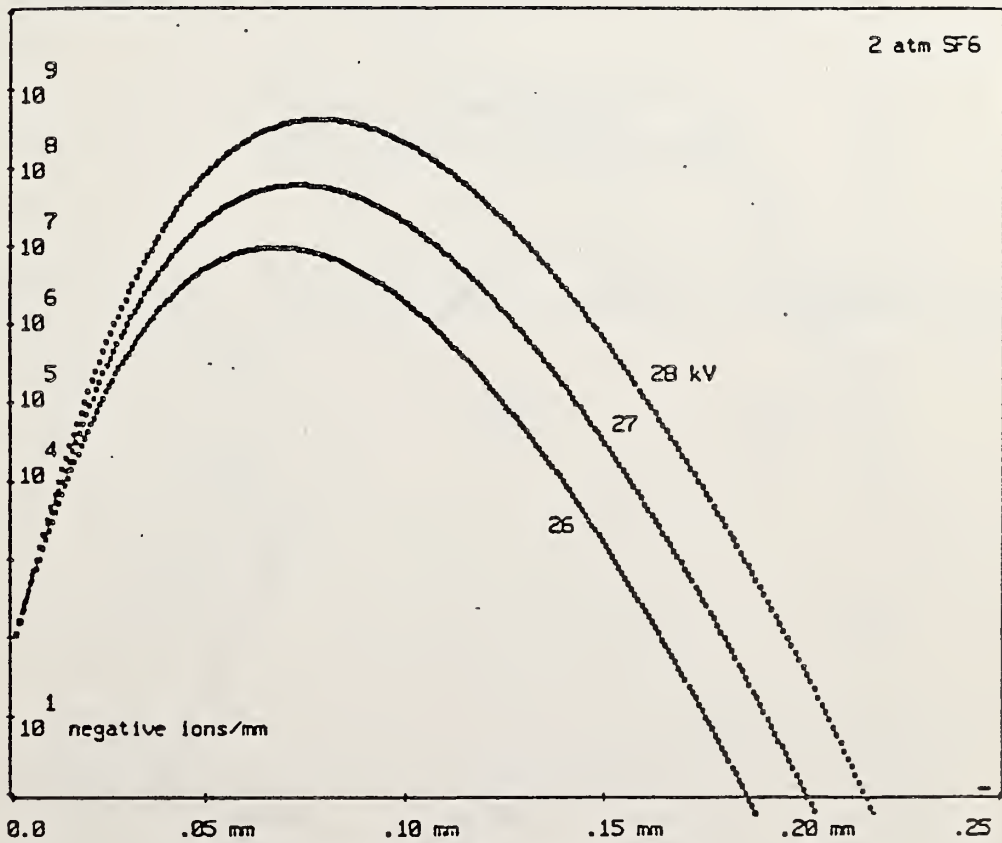


Figure 18. Calculated negative ion density left by an electron avalanche in the CIZ test cell at 200 kPa SF₆.

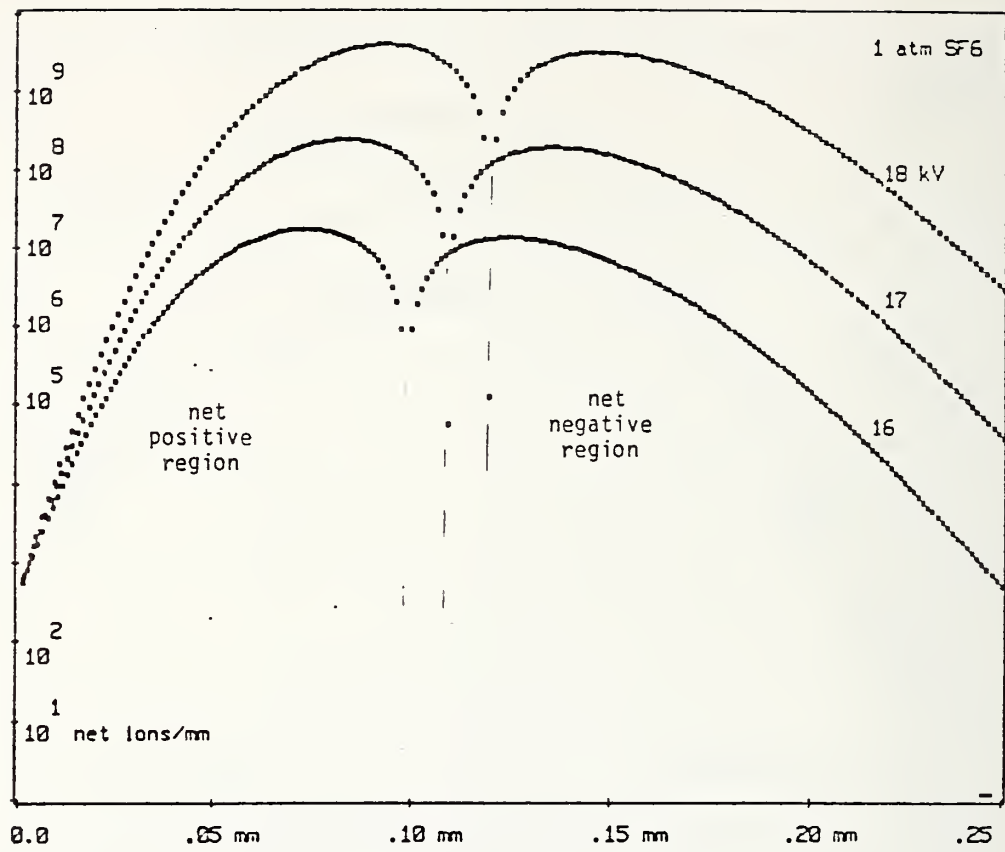


Figure 19. Calculated net ion density left by an electron avalanche in the CIZ test cell at 100 kPa SF₆.

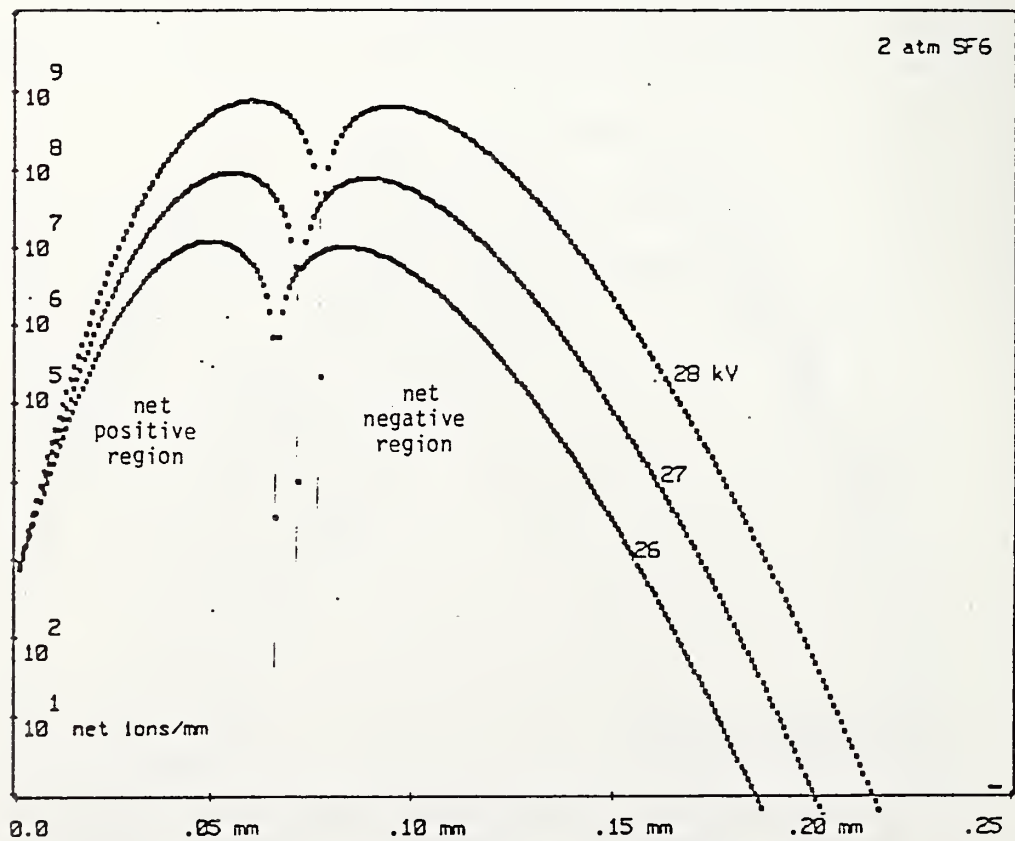


Figure 20. Calculated net ion density left by an electron avalanche in the CIZ test cell at 200 kPa SF₆.

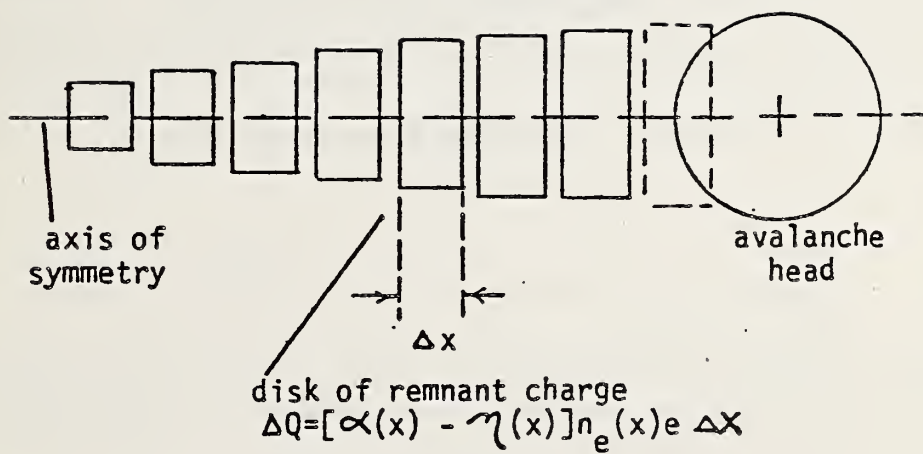


Figure 21. Model of avalanche used to evaluate space charge effects.

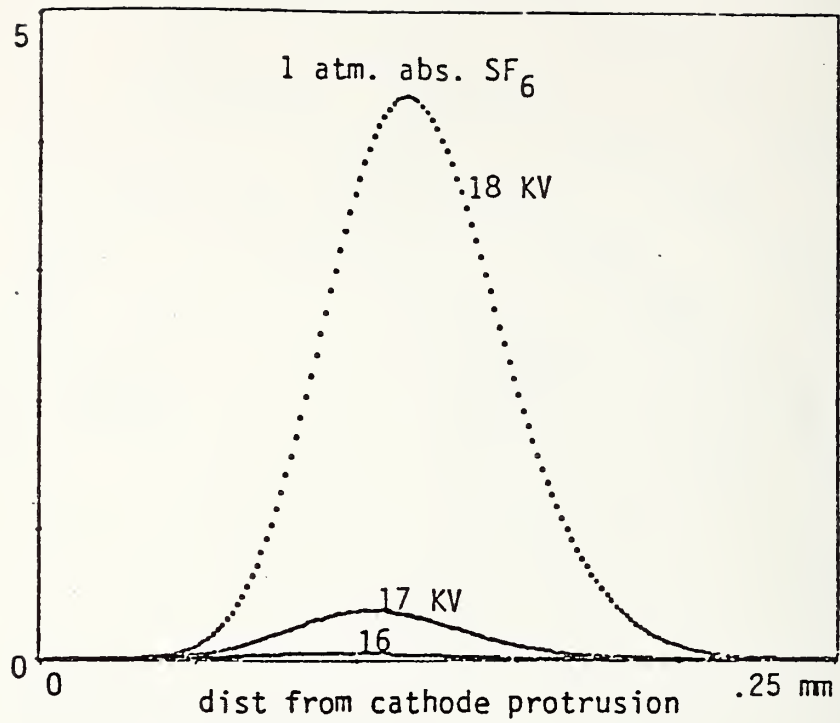


Figure 22. Electron E-field/Laplacian E-field for SF₆ at 100 kPa.

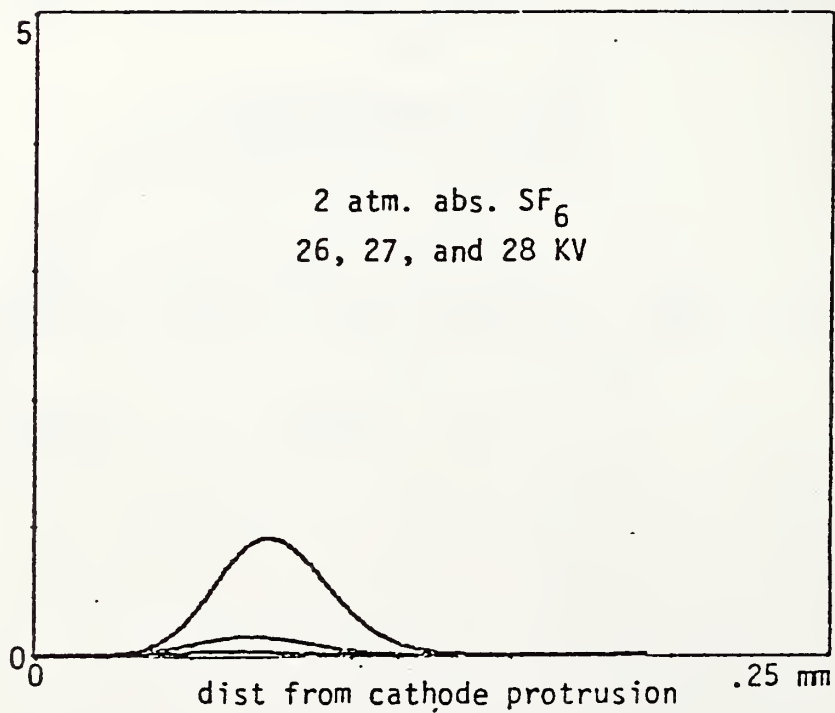


Figure 23. Electron E-field/Laplacian E-field for SF₆ at 200 kPa.

analysis considers radial motion from diffusive forces only and did not take into account the effect of the electron space charge field when calculating radial motion. This makes the computer analysis radii somewhat smaller than may actually occur. This may explain the discrepancies in critical sizes, since the computed critical size is highly dependent on the radius of the avalanche.

II.B.2.5 Stochastic Model of Avalanches

We now turn to the problem of determining the statistical variations in electron avalanches. In 1949, Wijsman [26] examined the avalanche process from a stochastic viewpoint for the case where there was no attachment and Townsend's first ionization coefficient, α_j , was constant. As in all stochastic modeling, space charge effects were considered to be negligible. Considering one dimensional growth, he assigned a coordinate x to every point along the discharge. He let $x = 0$ be the cathode, the origin for a single starting electron, and let $x = d$ be the anode. He considered $\alpha_j(x)dx$ to be the probability of an electron causing ionization when moving from point x to $x + dx$. He arrived at the probability distribution $p(n,x)$, the probability of the avalanche containing n electrons when it reaches point x . The result is the Furry [27] distribution,

$$p(n,x) = (1/\bar{n})[1-(1/\bar{n})]^{n-1}, \quad (14)$$

where

$$\bar{n} = \exp\left[\int_0^x \alpha_j(x')dx'\right]. \quad (15)$$

This expression can be approximated by $p(n,x) \cong (1/\bar{n})\exp(-n/\bar{n})$, for large n . It gives the same average value for the number of electrons at any point x in the avalanche's progression as the deterministic viewpoint. However, it shows that fluctuations from the mean are large.

If breakdown is considered from Raether's [24] streamer point of view, then these fluctuations can be very important. As an example, suppose the average avalanche size in a system is one half the critical avalanche size. The deterministic viewpoint suggests that streamers will not develop in this situation. The stochastic viewpoint, considering variations from the mean, suggests that $\exp(-2) = 0.14$ of all avalanches will exceed the critical size, and develop into streamers.

Measurements of electron avalanche distributions for non-attaching gases have yielded results which deviate from the Furry distribution in some situations. The results of these measurements are reviewed in [9]. Modifications and extensions of the statistical theory of avalanche formation have been made by Legler [28] and Byrne [29] to explain the discrepancies between predicted and measured distributions.

The statistical theory of avalanches for electron-attaching gases is somewhat more complicated, but as will be shown here, the resulting distribution is quite similar to the Furry distribution found for non-attaching gases. When electron attachment is included in the stochastic model, $n_a(x)\Delta x$ is considered to be the probability of an electron attaching when it moves from position x to $x + \Delta x$. If an electron avalanche starts out with exactly

one electron at the cathode, then the probability, $p(n,x)$, that the avalanche contains n electrons when it reaches point x will depend on three things: (1) the probability that there were n electrons at point $x-\Delta x$ times the probability that none of them attached or ionized in moving the distance Δx ; (2) the probability that $n-1$ electrons existed at point $x-\Delta x$ times the probability that one of them ionized in moving Δx ; and (3) the probability that one of them attached in moving the distance Δx . Stated mathematically, this means:

$$\begin{aligned}
 p(1,0) &= 1, \\
 p(n,x) &= p(n,x-\Delta x)[1 - n(\alpha_i(x) + \eta_a(x))\Delta x] \\
 &\quad + p(n-1,x-\Delta x)(n-1)\alpha_i(x)\Delta x \\
 &\quad + p(n+1,x-\Delta x)(n+1)\eta_a(x)\Delta x,
 \end{aligned}
 \tag{16}$$

where Δx is made asymptotically small, so that no more than one population-changing collision event can occur when the avalanche moves Δx . After some algebraic manipulation, and division by Δx , we get the differential-difference equations:

$$\begin{aligned}
 \frac{dp(0,x)}{dx} &= \eta_a(x)p(1,x), \\
 \frac{dp(n,x)}{dx} &= -p(n,x)n[\alpha_i(x) + \eta_a(x)] + p(n-1,x)(n-1)\alpha_i(x) \\
 &\quad + p(n+1,x)(n+1)\eta_a(x).
 \end{aligned}
 \tag{17}$$

The general case for this problem was solved by Kendall [30] for the case where "birth" (ionization) and "death" (attachment) were functions of time (position). Legler [28], apparently unaware of Kendall's work, solved this problem for the case when ionization and attachment are constants. Kendall's solution, of which Legler's solution is a special case, is given by:

$$\begin{aligned}
 p(0,x) &= 1 - \exp[-\rho(x)]/w, \\
 p(n,x) &= [\exp[-\rho(x)]/w^2](1 - 1/w)^{n-1}, \quad n \geq 1,
 \end{aligned}
 \tag{18}$$

where

$$\rho(x) = - \int_0^x [\alpha_i(x') - \eta_a(x')] dx',
 \tag{19}$$

and

$$w = 1 + \exp[-\rho(x)] \int_0^x \exp[\rho(x')] \alpha_j(x') dx' . \quad (20)$$

The distribution above has a mean of $\bar{n} = \exp[-\rho(x)]$, which is identical to the deterministic solution.

Because w is much greater than one for most cases of interest here, $p(n,x)$ has the asymptomatic solution

$$p(n,x) \approx \exp[-\rho(x)] \exp[-n/w(x)] / w^2 . \quad (21)$$

This follows from taking

$$\int_0^x \exp[\rho(x')] \alpha_j(x') dx' \sim 1, \quad (22)$$

and assuming $\bar{n}(x) \gg 1$, so that

$$w \approx \bar{n}(x) \int_0^x \exp[\rho(x')] \alpha_j(x') dx' , \quad (23)$$

which is obtained from eq (20) using eq (10).

Thus we have

$$p(n,x) \approx \exp[-\rho(x)] \exp[-\bar{n}/n(x) \int_0^x \exp[\rho(x')] \alpha_j(x') dx'] / w^2 . \quad (24)$$

For SF₆ under the conditions of interest here, the integral in eq (22) above ranged from 1.1 to 1.3. A plot of the PDF versus n on a log-scale gives a curve with a slope of

$$-1/(\bar{n}(x) \int_0^x \exp[\rho(x')] \alpha_j(x') dx') ,$$

as compared to the case for a non-attaching gas, where by eq (14), the slope should be $-1/\bar{n}$. As for non-attaching gases, deviations from this modified form for the Furry distribution are possible for very low n -values [28]. The effects of including detachment and secondary emission on the statistical distribution of avalanches is discussed in [9]. In general, the average quantities predicted from the PDF's are the same as those given by the deterministic model.

II.B.3 Measurement of Electron Avalanche Distributions

Experimental studies of electron avalanches in SF₆ were conducted using a test vessel described in [9]. Details of the measurement system will not be repeated here. The emphasis of the discussion in this report will be on the results, and a comparison of these with predictions based on the theory given above.

Briefly, in order to assess the avalanching model, a specific electrode configuration was selected. The configuration employed in the experiment is referred to here as a controlled ionization zone (CIZ). The configuration for the CIZ is depicted in figure 24. Electrons released from the cathode at a rate controlled by ultraviolet irradiation are exposed at first to a high-field ionization zone. Outside of this region the field quickly decays, so that ionization products drift without further ionization to be collected at the anode. The cathode tip employed had a 200 μm radius.

Tests of the CIZ system performance demonstrated that single avalanches could be initiated by uv stimulation of the cathode, and that avalanche growth in high-pressure gases could be detected. The degree of experimental stability necessary for accurate observations was also determined. The high-voltage supply stability was approximately ± 1.0 mV. A special effort was made to insure that the entire system was electrically quiet. Partial discharges in the all-connecting leads were eliminated in order to achieve the desired sensitivity for avalanche detection.

A corona detector-pulse height analyzer system was used for the measurements because it provided the greatest sensitivity. The noise level of the system allowed measurements of partial discharges as small as 0.05 pC. In general, almost no partial discharges above 3 pC were measured. The noise level of the system at each terminal voltage was determined by operating the system at that voltage with the ultraviolet lamp off. In this state, no avalanche initiating electrons were released from the cathode, so that any measured pulses that occurred under this condition could be attributed to system noise. To insure that what appeared to be discharges was not the result of electromagnetic coupling between the ultraviolet lamp and the system, the noise level was measured with zero terminal voltage and the ultraviolet lamp both on and off. It was determined that any noise that the ultraviolet lamp introduced into the system was well below the level of the other system noise.

At all pressures, the lower bound for the range of terminal voltages was determined by the threshold at which avalanches could be measured distinctly above the noise level. At a given pressure, as data was taken at incrementally higher voltages, there came a point at which the pulse rate began increasing suddenly. After this happened, the pulse rate was higher at lower voltages than it had been previously. This showed the discharges at the higher voltages had altered the rate of photoemission from the electrode surface. Since it was desired to run the experiments under conditions which were as constant as possible, no measurements were taken at or above the voltages which changed the pulse rate. This determined the upper limit of the terminal voltages for measurements made with SF₆ at 100 and 200 kPa. The upper voltage limit of the 300 kPa data was imposed by the limitations of the power supply.

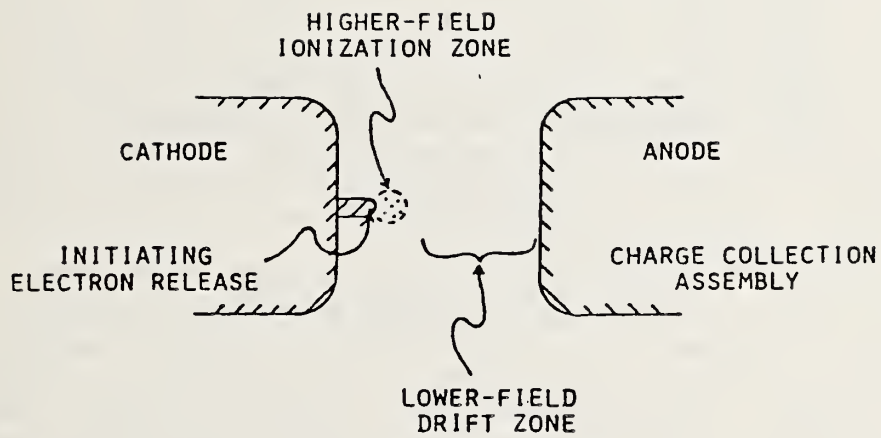


Figure 24. Controlled Ionization Zone Technique.

For a single test, the system was able to measure discharges over a range of 30 dB. Separate tests were necessary to acquire data over a wider dynamic range. The statistical distribution of avalanche sizes was measured for many different combinations of gas pressure and applied voltage. We present here only a few selected examples of the results obtained. Measured distributions obtained for the conditions indicated are shown in figures 25-27. In these figures the horizontal axis is charge, and the vertical axis gives, on a log scale, relative probability obtained from the number of pulses counted within an increment of charge.

It is clear that the measured distributions deviate, in some cases rather significantly, from the Furry distribution given by eq (24). Except for the data in figure 25, the distributions do not show a simple exponential decay with charge. At each gas pressure it was found that as voltage was increased, a distinct peak appeared in the distribution, and at even higher voltages a second well-defined peak appeared at higher charges (see figs. 26 and 27). At some pressure, as shown in figure 27, the second peak was associated with an isolated high charge feature well separated from the rest of the distribution. The charge level of both the first and second peaks increases as the terminal voltage increases, but does not increase as much as the average charge of the total distribution.

The average charge, determined by summing all the pulse charges and dividing by the number of pulses, was generally found to be much lower than the theoretically predicted value. However, the dependence on terminal voltage agreed fairly well with the theoretically predicted change. The discrepancy between predicted and measured average charge is probably accounted for by an 11% uncertainty in determination of the peak magnitude of the applied electric field [9].

The appearance of the lowest charge peak in the measured distributions represents a deviation from the Furry distribution similar to that seen for non-attaching gases as discussed in [9] and [28]. Namely, it seems to be accounted for by the fact that the likelihood of an electron causing ionization will in general depend on its history, i.e., it will have to move a minimum distance in the gas before it has enough energy to exceed the molecular ionization threshold. This history dependence makes it quite reasonable to expect considerable deviations from the Furry distribution. Nearly all the measured distributions appeared to follow a modified Furry distribution for at least part of their ranges.

The reason for the appearance of the second, higher charge peak in the distributions is more obscure. These peaks ranged between 1 and 3 pC. They may have been the result of space-charge effects. Calculations show that when the number of electrons in the avalanche approaches 3×10^5 , the space charge field due to the electrons in the avalanche head, which is assumed spherical and to expand only by diffusion, is equal to about 15 percent of the Laplacian field. An avalanche of 3×10^5 electrons would be expected to produce about 0.5 pC of ion charge. Measured discharges below this level tended to follow a modified Furry type of distribution [9]. Discharges above this level tended to be larger than would have been expected if space charges had been neglected. Furthermore, the second peak observed was

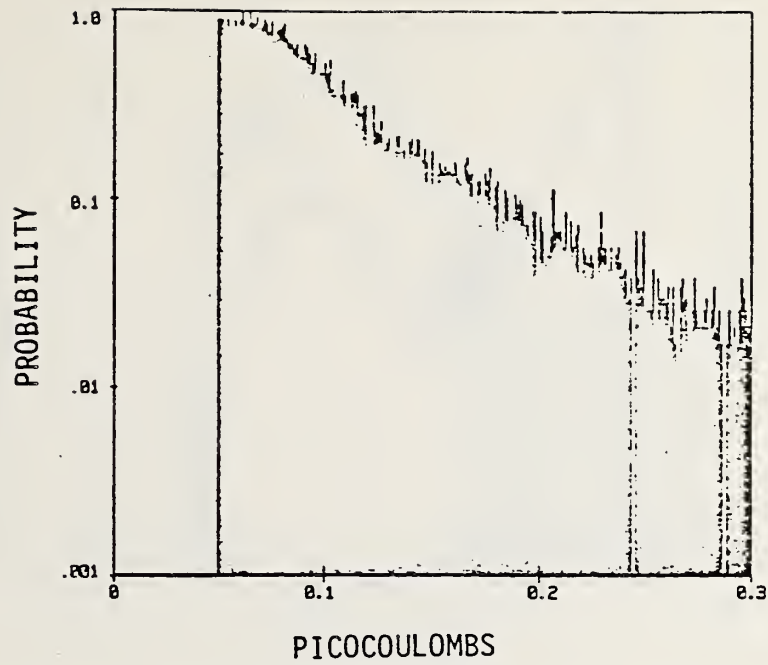


Figure 25a. Measured electron avalanche distribution for 100 kPa SF₆, at 17.6 kV.

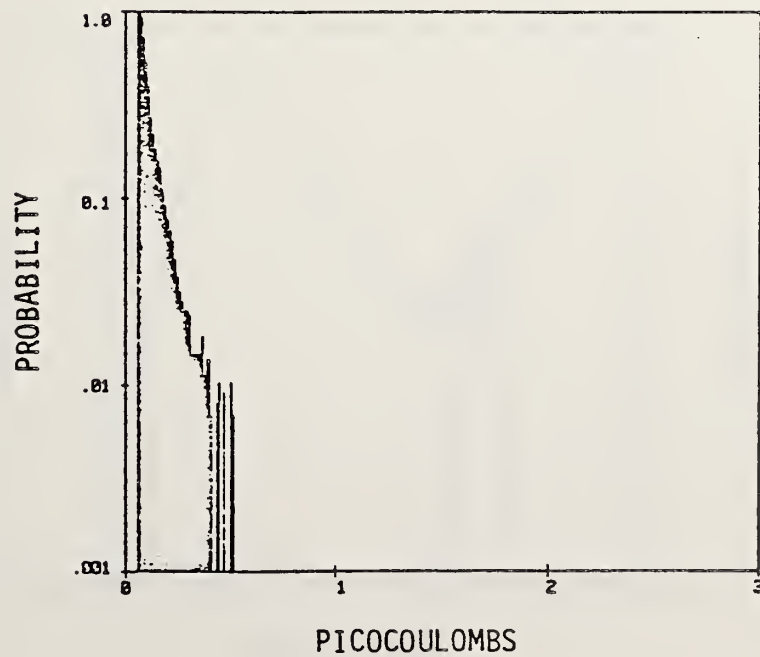


Figure 25b. Measured electron avalanche distribution for 100 kPa SF₆, 17.6 kV, pulse rate = 89.

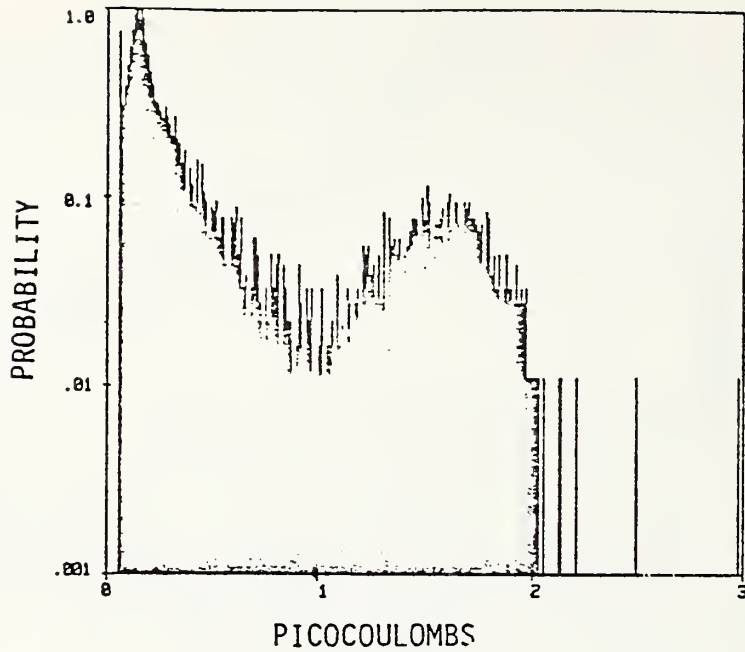


Figure 26a. Measured electron avalanche distribution for 100 kPa SF₆, 18.6 kV, pulse rate = 41.

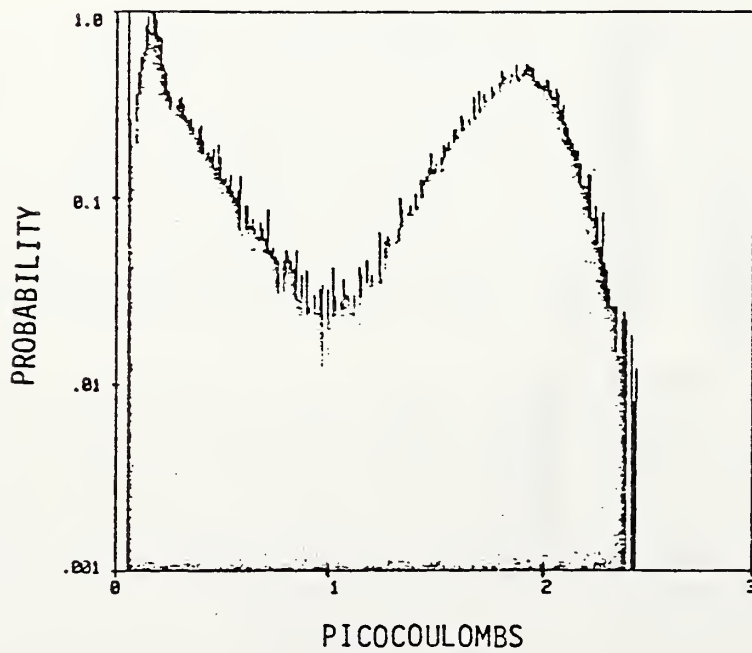


Figure 26b. Measured electron avalanche distribution for 100 kPa SF₆, 18.8 kV, pulse rate = 50.

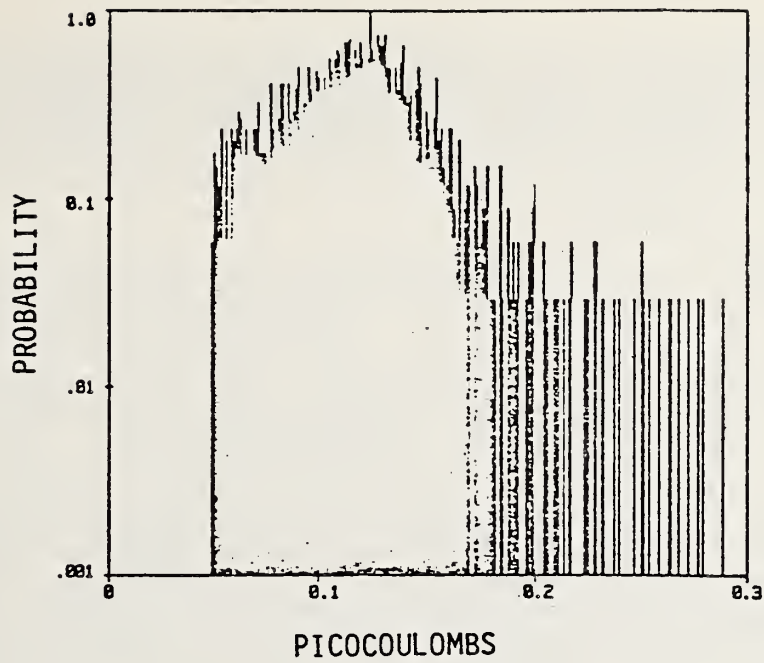


Figure 27a. Measured electron avalanche distribution for 200 kPa SF₆, 29.6 kV.

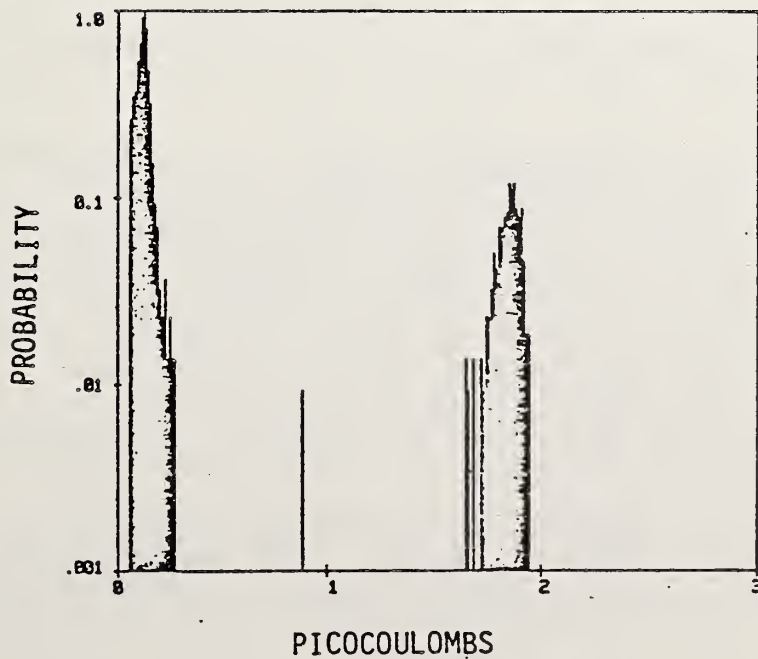


Figure 27b. Measured electron avalanche distribution for 200 kPa SF₆, 29.6 kV, pulse rate = 11.

always above the 0.5 pC level. Therefore, it is possible that the distribution of discharges above 0.5 pC was strongly influenced by space-charge buildup during the avalanche development. The transition to large pulses may also be the result of electrohydrodynamic instabilities in the gas (see appendix II).

II.B.4 Remaining Problems

It should be clear from the preceding discussions that there are a number of questions that remain to be answered. The relatively simple stochastic model of avalanche formation given here for highly electronegative gases appears to have only a limited range of applicability. Once the applied voltage exceeds a certain value, the model breaks down and can no longer explain features observed in the measured avalanche size distributions.

An understanding of the observed transition to "large" pulses not predicted by the Furry distribution may be the key to understanding the transition from electron avalanche to streamer and then to breakdown. It should be noted here that a similar abrupt transition from avalanches to large pulses was observed in the NBS laboratory measurements of both positive and negative corona pulses (see the previous section as well as [8] and [16]). The appearance of the large avalanches in the experimental results points to the need for better modeling, especially at very high values of E/N.

In attempting to improve the model of electrical discharge development in SF₆, two questions are currently being addressed. The first concerns the range of validity of swarm parameters such as the ionization coefficient for high E/N discharge environments where there may also be highly nonuniform fields. The second has to do with the effect of electrohydrodynamic (EHD) instabilities on the development of gas discharges.

Concerning the first question, an analytical theory, described in appendix I, can be used as a first approximation to determine when and when not to expect swarm parameters to be accurate representations for discharge studies. It should be noted that this question applies to a broad spectrum of expanding technologies where gas discharges are used. High and ultra-high power lasers; high energy density particle-beam and projectile accelerators; stable, high-speed mega-, giga-, and tera-watt switching and triggering systems; and super-high ($\approx 10^9$ V) voltage insulation systems are but a few areas in which one needs to know the range of swarm parameter validity in order to understand and predict device behavior. The approach given in appendix I provides a straightforward means of estimating the tendency of an average electron (i.e., one characterized as having the average of a distribution of energies) to attain and maintain equilibrium in an electric field. Special attention is given to the case of highly nonuniform fields.

Concerning the second question, an entirely new theoretical model is under consideration which is based on the use of perturbation analysis for the study of EHD instabilities. These are instabilities in the discharge parameters which may be superimposed on the developing electron avalanche. The formalism, as described in appendix II, requires the solution of coupled differential equations for conservation of mass, charged particles, and momentum, as well as Maxwell's equations for the electric field. The method appears to have broad generality in that it allows analysis of conditions which will inhibit, or if desired, promote breakdown, and hence

is applicable to insulation, switching, and lasers. The primary objective of the stability analysis in the present study is, of course, to attain an understanding of the sudden "avalanche-to-streamer" transition. Preliminary investigations of the feasibility of this method indicate that it should be quite promising.

II.C. Basic Mechanisms for Corona Inception in SF₆

II.C.1 Motivation and Introduction

The purpose of this work has been to examine the basic mechanisms for the initiation of corona discharges in highly electronegative gases such as SF₆. An understanding of these mechanisms will provide a basis for determining the effect of varying conditions on the measurement of corona inception voltage. These conditions, for example, include: gas pressure, electrode geometry, presence or absence of radiation, voltage waveform, electrode surface conditions, etc. The information acquired from this study will hopefully lead to more useful and physically meaningful definitions of corona inception which can be used in the testing of gaseous dielectrics as well as in the design of gas-insulated systems.

This work is closely related to the NBS-supported project at MIT described in the previous section. The emphasis in this section, however, is more on achieving an understanding of the discharge initiation processes, as opposed to the avalanche growth processes. Also both polarities are considered for the stressed electrode, whereas the MIT work was restricted to negative polarities in order that the source of initiating electrons could be precisely controlled. Information presented in Sec. II.A. on characteristics of corona pulses, together with the model of avalanche growth given in the previous section, is taken into consideration in the following discussion in evaluating applicability of the streamer criterion to prediction of corona onset.

The results reported here are an extension of preliminary results previously reported [10,16]. Most of the information presented in this section was given in a paper at the special symposium on corona and non-spark discharges which was part of the 1981 Conference on Electrical Insulation and Dielectric Phenomena. This paper will soon be published in archival form [11]. In addition to the comparison between ac and dc inceptions emphasized in the earlier work [10], we report here results of a more thorough examination of the effects of uv-radiation, electrode geometry, and electrode conditioning on the measurement of corona inception in SF₆. Corona inceptions have also been calculated using the streamer criterion and these are compared with our measured results. The connection between the streamer criterion and the nature of the corona phenomena observed near onset is discussed, and the limitations of the streamer criterion for predicting inceptions are considered. Discharge initiation mechanisms are proposed and shown to be consistent with the observed changes in discharge behavior with changing gap conditions.

Since details of the techniques used to measure corona inception voltages are covered elsewhere [10,11,16], we shall avoid discussion of the apparatus and measurement procedures and focus here instead on interpretation of the results.

II.C.2 Definition of Corona Inception

From the measurement point of view, there is a degree of arbitrariness associated with the definition of corona inception voltage. Corona can be measured by a variety of techniques of differing levels of sensitivity [31]. Thus, it is to be expected that one's preferred definition of a measured inception voltage will depend somewhat on the type of measurement method used. If, for example, one measures discharge current as a function of voltage, then inception is customarily defined as that voltage at which the current equals or exceeds a certain specified level. If one is detecting discharge pulses, then inception is usually defined as that voltage at which the charge in a pulse exceeds a certain level. Similar definitions would apply to optical or acoustical detection of corona. Unfortunately, the definition is more often determined by the sensitivity of the detection instrument used than by any knowledge about the properties of the discharge process itself.

If the corona discharge intensity as indicated by the current, for example, increases abruptly with increasing voltage, then it can be argued that the measured inception values will be relatively insensitive to the assumed definition. For the measurements reported here for SF₆, an abrupt onset is observed only for negative corona and then only when the point electrode is irradiated, or conditioned so as to insure electron emission. It would be desirable to have a phenomenological basis for defining inception, e.g., the voltage at which the discharge becomes completely self-sustaining. There are, however, difficulties with this approach because the conditions that determine the growth of the discharge, such as the microscopic nature of the cathode surface, or the presence of trace impurities in the gas, may be too numerous or uncontrollable. There are, nevertheless, theoretical criteria which have been successfully used in many cases to predict inception [32]. The relationship between these criteria and the measured inceptions reported here will be examined later.

For reasons previously mentioned [10,11], we have chosen here the count rate of corona pulses that exceed a certain level (0.05 pC) as a criterion for defining inception. In particular, inception was defined as the intercept of the voltage axis set at the 0.1 count/s level with a straight line fit on a semi-log scale to the data on count-rate versus applied voltage. Examples of such plots are shown in figures 28-31 for dc measurements corresponding to gas pressures and electrode gap conditions indicated.

There are difficulties that arise in assuming the same definition for both ac and dc conditions as are discussed in [10] and [11]. As a result, there are expected to be predictable differences between measured ac and dc inceptions based on the above definition. If the corona turns on abruptly with increasing voltage, then these differences should be small.

It has been known from earlier studies of corona phenomena [4,32], primarily for corona in air [33], that the initiation and development of corona discharges can depend significantly on the presence of radiation that is of sufficient energy to enhance the release of electrons either from the gas or from the cathode surface. The radiation reduces the formative time lag for discharge initiation associated with random fluctuations in the rate of initiating electron production [34], and can give rise to an increase

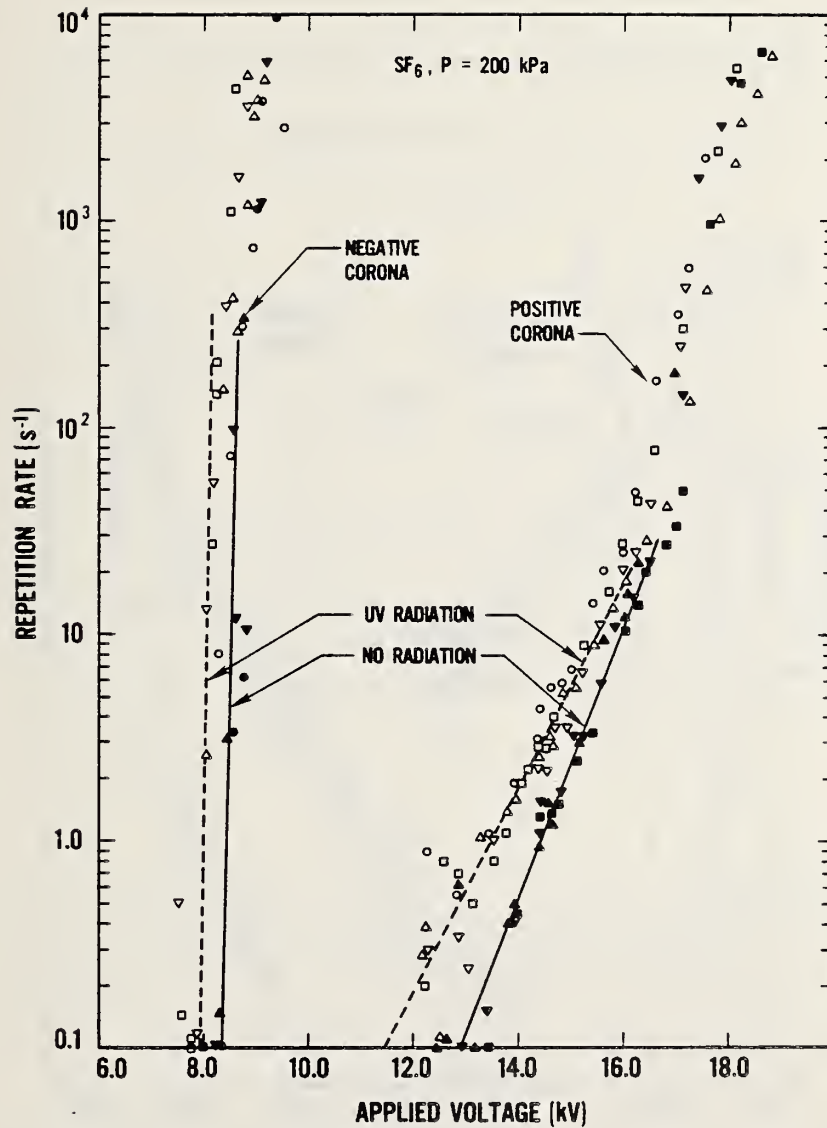


Figure 28. Observed pulse count rate versus applied voltage for positive and negative point-plane dc corona in SF₆ at a pressure of 200 kPa. The gap spacing was 1.24 cm and the radius of curvature of the point was 0.045 mm. The different symbols indicate data obtained from different runs. Included are all pulses with a charge in excess of 0.05 pC.

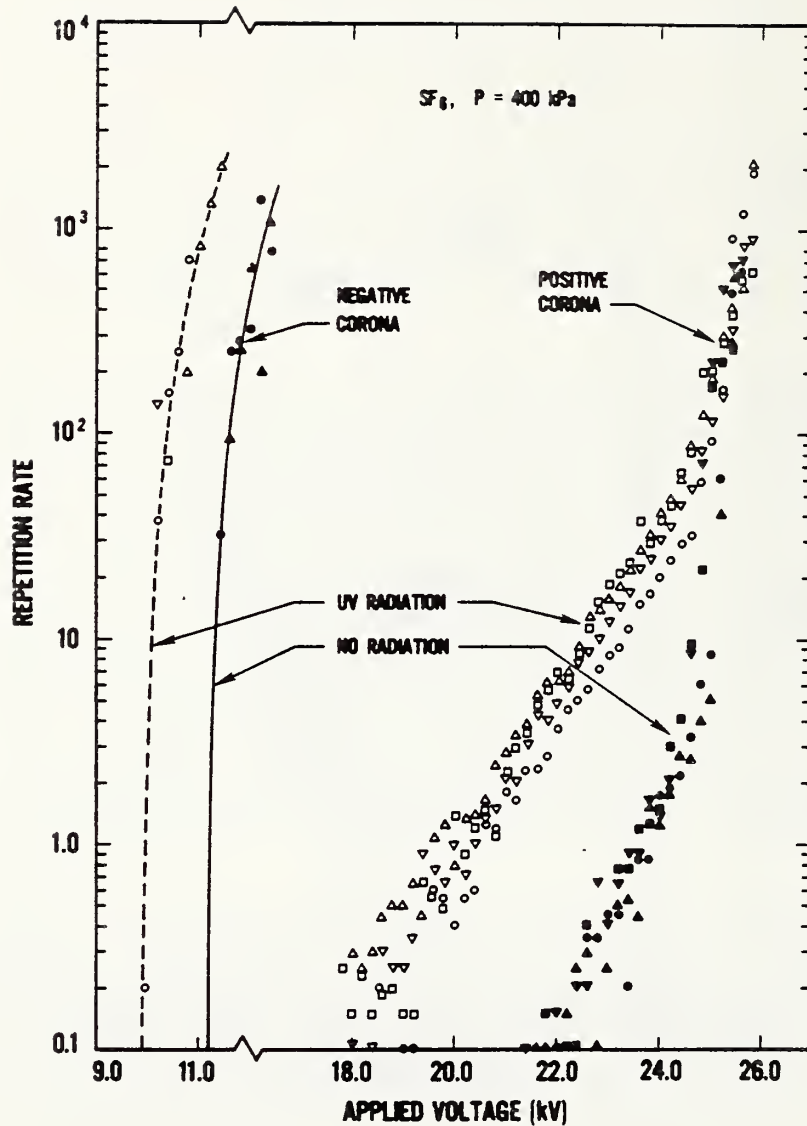


Figure 29. Observed pulse count rate versus applied voltage for positive and negative point-plane dc corona in SF₆ at a pressure of 400 kPa. The gap spacing was 1.24 cm and the radius of curvature of the point was 0.045 mm. The different symbols indicate data obtained from different runs. Included are all pulses with charge in excess of 0.05 pC.

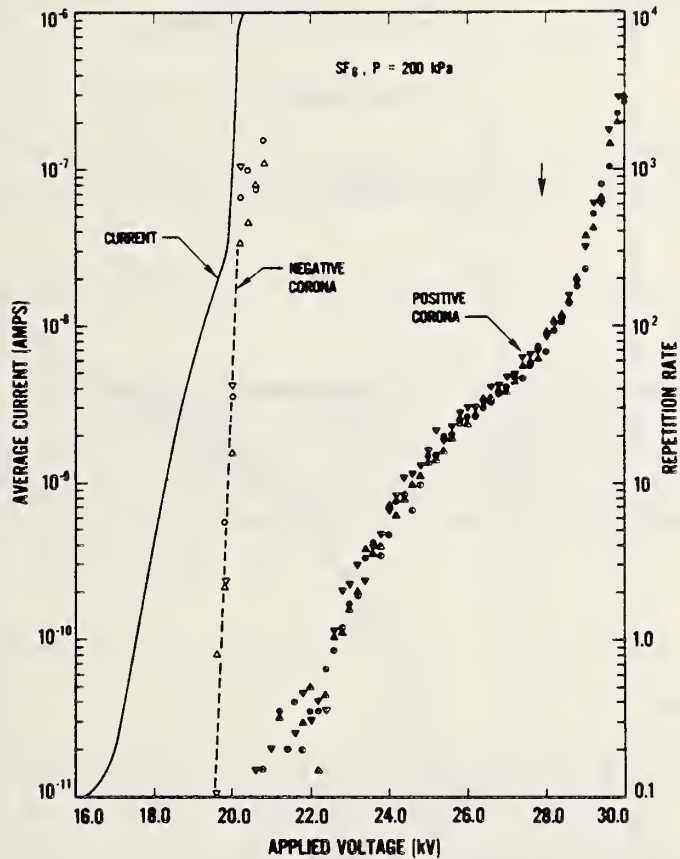


Figure 30. Observed pulse count rate versus applied voltage for positive and negative point-plane dc corona in SF₆ at a pressure of 200 kPa. Also shown by the solid line is the average dc current observed prior to the inception of pulses. The gap spacing was 1.1 cm and the point radius was 0.47 mm. The data were obtained using uv-radiation and the different symbols correspond to different data runs.

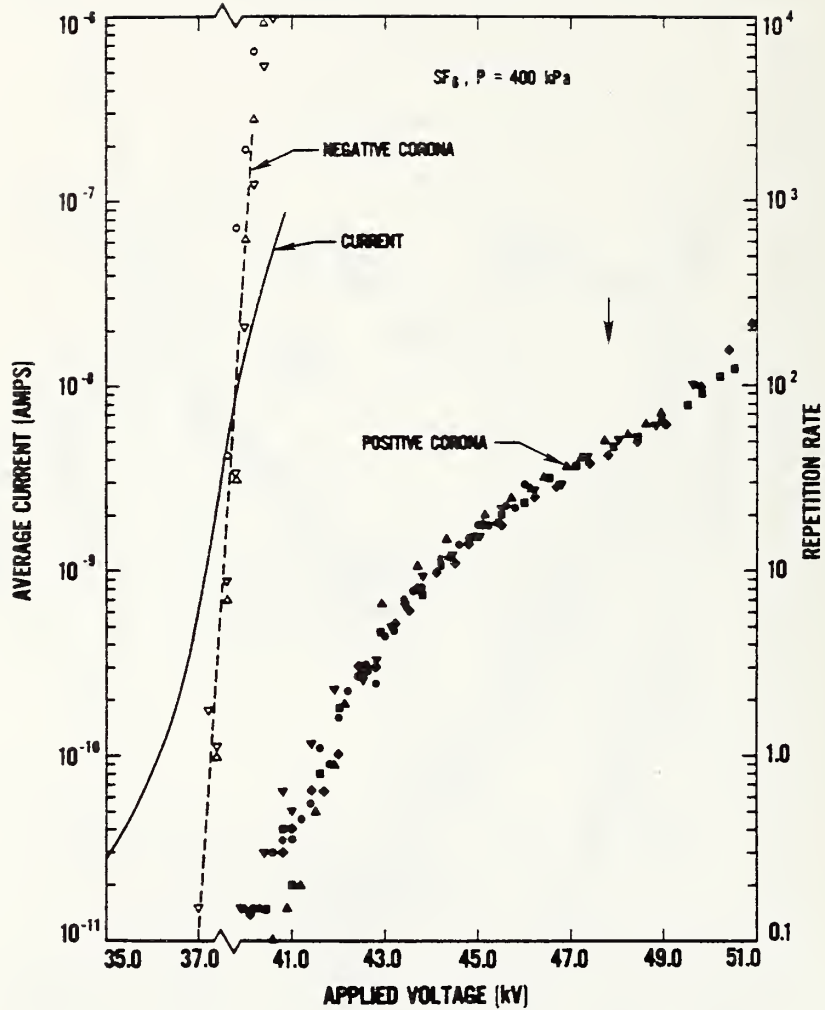


Figure 31. Observed pulse count rate versus applied voltage for positive and negative point-plane dc corona in SF_6 at a pressure of 400 kPa. Also shown by the solid line is the average dc current. The gap spacing was 1.1 cm and the point radius was 0.47 mm. The data were obtained using uv-radiation and the different symbols correspond to different data runs.

in the avalanche or streamer pulse rate which would therefore lead to a lowering of the apparent inception voltage. It is clear that the definition of corona inception may also depend on the intensity and energy of the radiation present in the gap. However, since the radiation serves only to insure that discharge initiating electrons will be present once the proper field conditions for inception are reached, it is expected that there will be an upper limit above which further increase in the radiation intensity will have no effect on the initiation of corona. For the measurements reported here, no attempt was made to guarantee that this limit was reached.

II.C.3 Calculation of Corona Inception

For the case of a nonuniform electric field, a net ionization which can lead to electron avalanche formation is possible only in the region where

$$\alpha_i(E/N) - \eta_a(E/N) > 0. \quad (25)$$

Here α_i and η_a are respectively the ionization and attachment coefficients defined in Sec. II.B. These coefficients are functions of E/N , the electric field-to-gas density ratio. Since E is a function of location in the gap, α_i and η_a will likewise be functions of location. As shown in Sec. II.B, the growth (or decay) of the number of electrons $n_e(x)$ between positions x and $x + dx$ in the gap is given by

$$\frac{dn_e(x)}{dx} = n_e(x)[\alpha_i(x) - \eta_a(x)]. \quad (26)$$

In this equation, we have assumed for simplicity that all of the electrons are located at a single point, i.e., we have neglected the effects of electron diffusion and delayed electron emission processes. This is a reasonable approximation only if the extent of the diffusion is small compared to the distance traveled by the avalanche where x can be associated with the centroid of the moving electron cloud.

Solving this equation one finds an approximate expression for the average avalanche size given by

$$n_e(\ell) = n_e(0) \exp\left[\int_0^{\ell} (\alpha_i(x) - \eta_a(x)) dx\right], \quad (27)$$

where it is assumed that the avalanche is initiated by $n_e(0)$ electrons which originate at the point $x = 0$. For the negative point discharges, the upper limit ℓ coincides with the critical electric field where $\alpha_i = \eta_a$. For positive point discharges, ℓ coincides with the location of the electrode tip and $x = 0$ is any point in the region where $\alpha_i > \eta_a$. The limits of integration have been conveniently chosen to exclude the region which does not satisfy eq (25), i.e., where growth in avalanche size ceases and decay begins. Equation (27) must be considered an approximate expression because

it is derived without consideration of the detailed stochastic nature of avalanche formation process [9,28]. Also it does not include possible contributions to the avalanche from secondary or delayed processes [35]. It is an average quantity in the sense that it is calculated from the swarm parameters α_i and η_a , which are themselves derived from averages over the electron energy distributions as given by eqs (6) and (7).

Using eq (27) for a single initiating electron, $n_e(0) = 1$, we have calculated the average-maximum electron avalanche sizes (of those that move along the electrode axis) as a function of applied voltage for the electrode gap conditions used in the measurements reported here. They are maximum in the sense that the limits of integration in eq (27) are between the point of maximum E/N and the point where $\alpha_i = \eta_a$. The results of such calculations are given in figure 32 for different indicated SF₆ gas pressures assuming gap conditions like those used to acquire the data given in figures 28 and 29.

In performing these calculations, the static electric field was expressed in terms of prolate spheroidal coordinates [36,37], so that the magnitude of the electric field is given by

$$E_n = V_0 [f \sin \eta (\cosh^2 \xi - \cos^2 \eta) \tanh^{-1}(\cos \eta_0)]^{-1}, \quad (28)$$

in which η and ξ are the meridian coordinates related to Cartesian coordinates by the transformations

$$x = f \cosh \xi \cos \eta \quad \text{and} \quad y = f \sinh \xi \sin \eta,$$

where x is taken to lie along the point-to-plane axis and azimuthal symmetry is assumed. The field is in a direction parallel to lines of constant ξ . In eq (28), V_0 is the potential applied to the point electrode which has been characterized by a surface of constant $\eta = \eta_0$, i.e., a hyperboloid of revolution for which f is the focal distance as measured from the plane electrode. For the gap conditions used here, the value of η_0 was determined at each gap spacing by a least squares fit of a hyperbola to a tracing of a photograph of the point electrode made using a microscope. Deviations of the electrode surface from these fits were generally quite small, even in regions far removed from the active discharge volume. The greatest uncertainty was in determining the exact shape and location of the tip, and this could lead to significant uncertainties in the calculations of n_e , as will be noted later.

The expressions used for α_i and η_a were obtained from polynomial fits to the data of Maller and Naidu [38] and are given by

$$\alpha_i(E/P) = [-1.743 + 0.0269(E/P) - 2.498 \times 10^{-5} (E/P)^2 + 9.131 \times 10^{-9} (E/P)^3]P, \quad (29)$$

for $E/P \geq 117$,

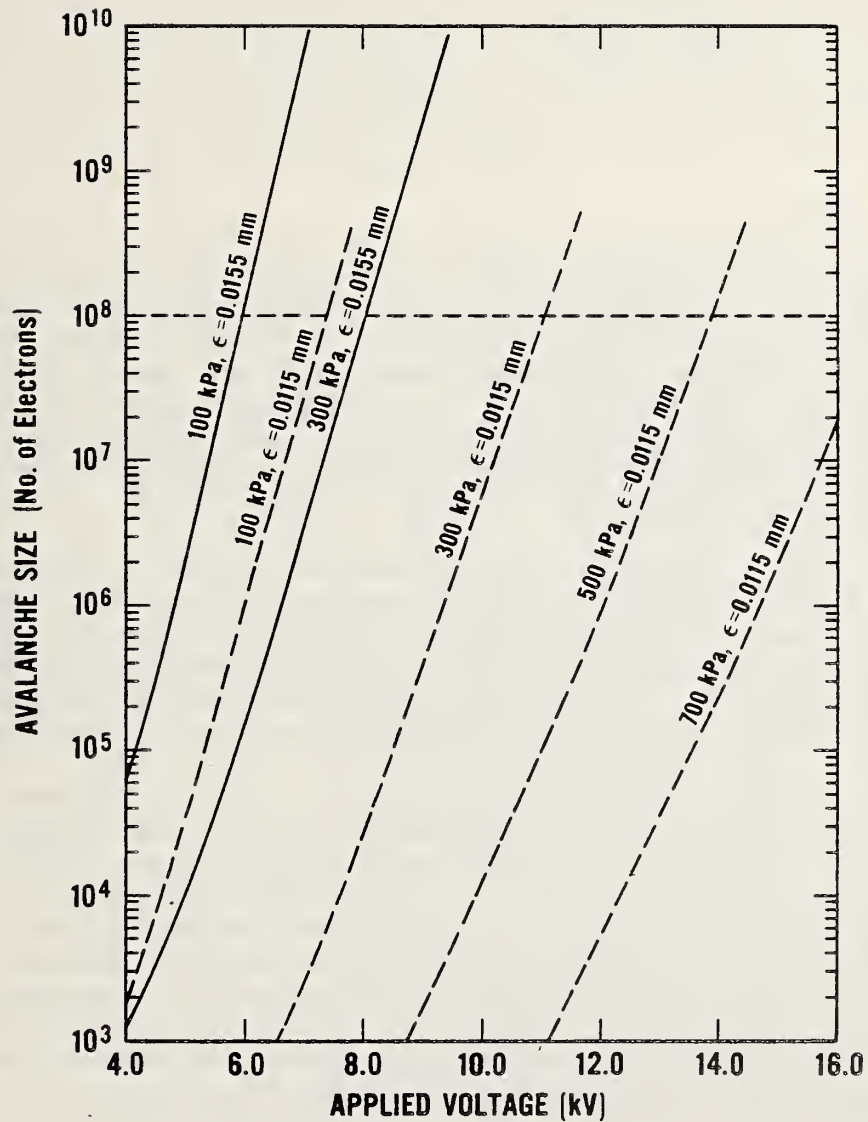


Figure 32. Calculated average-maximum electron avalanche size versus applied voltage for the different indicated gas pressures and parameter $\epsilon = f - d$. The gap geometry corresponds to the conditions of figs. 28 and 29.

$$\eta_a(E/P) = [3.408 - 0.0891(E/P) + 5.556 \times 10^{-4} (E/P)^2 - 1.017 \times 10^{-6} (E/P)^3]P \quad (30)$$

for $250 \geq E/P \geq 117$, and

$$\eta_a(E/P) = 0 \quad (31)$$

for $E/P \geq 250$,

where α_j and η_a are in units of cm^{-1} , P is the gas pressure in torr and (E/P) is expressed in units of $\text{V cm}^{-1} \text{ torr}^{-1}$, to be consistent with the published data. In order to obtain results consistent with the units used in reporting our data, the calculations were performed assuming the conversion $1 \text{ torr} = 0.132 \text{ kPa}$. The value $E/P = 117$ corresponds to the critical field where $\alpha_j = \eta_a$. In calculating n_e , eqs (29)-(31) were used in eq (27), and the integrations were performed numerically with a computer. The computer code used for these calculations is listed in appendix III.

The onset of corona is presumed to occur when the avalanche reaches some critical size such as would, for example, correspond to a detectable pulse, a streamer, or condition where the discharge is self-sustained. As we noted earlier, there have been attempts to find phenomenological bases for defining corona onset [32]. Perhaps the most successful and widely accepted theoretical criterion has come about from tying the onset of corona to the lowest voltage at which streamers are presumed to appear [39]. Although this "streamer criterion" may exclude some of the smaller electron avalanche pulses that were included in our measurements, it is, nevertheless, useful and constructive to compare onsets predicted on the basis of this criterion with our measured values. As noted in the previous section, an avalanche can presumably become a streamer when the number of electrons it contains is large enough that the space charge field it creates is comparable to the applied field [34], or according to Raether [39], when the avalanche contains on the order of 1×10^8 electrons. Using the streamer criterion, one obtains inception voltages which correspond to the points of intersection of the avalanche growth curves with a horizontal line at the 1×10^8 electron level as shown in figure 32.

The calculations giving the results shown in figure 32 were performed, as indicated, for different values of a parameter ϵ defined to be the difference between the focal length f and the gap spacing d , i.e., the distance from the plane electrode to the tip of the point electrode. This difference can be affected by the accuracy of the fit of a hyperboloid to the electrode surface near the tip. The degree to which we can determine the extent of the active region where $\alpha_j \geq \eta_a$ is determined by the uncertainty in ϵ . This uncertainty, it should be noted, is not an indication of how accurately we can measure the gap length but rather an indication of how accurately we can determine the size of the small active discharge region near the tip. From microscopic examinations of the point electrode surfaces and a consideration of the uncertainties in fitting hyperbolae to these electrodes, we must conclude that ϵ cannot be known to better than $\pm 0.002 \text{ mm}$. This can

lead to quite large uncertainties in the calculation of n_e , which are due to the fact that, especially for sharp points as considered here, a disproportionately large fraction of the ionization contributing to the avalanche size takes place in the immediate vicinity of the tip. This uncertainty will, of course, be reduced for point electrodes that are less sharp. This is evident in the work of Sangkasaad [40], in which the good agreement between experimental and theoretical corona inception values can be attributed, at least in part to the rather large point electrode radius of 5.0 mm as compared to a radius of 0.045 mm used for the calculations giving the curves in figure 32 and, also, for obtaining that data in figures 28-31.

For highly nonuniform fields such as used in the measurements reported here, there are likely to be additional large uncertainties in calculated avalanche size due to possible large uncertainties in the values of α_i at high E/N. This is demonstrated in figure 33 where the data of Maller and Naidu [38] (also see Sec. II.D) used in the present calculations are compared with data of Sangi [41] which have appeared in a thesis and conference proceedings which are not widely available. Also shown are data from Bhalla and Craggs [42] and Bortnik and Panov [43] for low E/N, and calculated ionization coefficients obtained from Cooke [44]. There is obviously considerable disagreement among the results for E/N > 500 V/cm torr, which is significant for highly nonuniform fields where E/N of this magnitude, or greater, can be expected. Moreover, for highly nonuniform fields at high E/N the electrons may fail to reach local thermodynamic equilibrium over a portion of the avalanche formation region. Therefore, use of ionization coefficients which are derived assuming equilibrium may not be justified in all cases. As already noted in Sec. II.B, this is a question that deserves careful consideration (also see appendix I).

In figure 34, we compare corona inceptions calculated assuming the streamer criterion (see fig. 32) with our experimental results. The calculated inceptions reflect the uncertainty associated with our inability to precisely determine the electric field near the tip of the point electrode, where rather than a single line we show a band of inception values. The measured values were obtained from data such as shown in figures 28 and 29 and have in fact been reported previously [10,11,15]. Results for both ac and dc measurements are shown, and for the dc case measurements were made both with and without uv-irradiation of the gap. For these measurements, the gap spacing was 1.24 cm and the radius of curvature of the point electrode was 0.045 mm corresponding to the conditions indicated for figures 28 and 29. The calculated corona inceptions appear to agree best with the results obtained for negative corona in an irradiated gap. As will be made evident later, this is consistent with the behavior expected on the basis of the proposed initiation mechanisms.

We now examine the relationship between the assumed streamer criterion and the properties of the discharge that have been observed near onset. There remains some question about the physical basis for this criterion as it relates to the nature of the measured phenomenon. In figure 35 are shown curves for corona inception corresponding to a critical avalanche size of 1×10^8 electrons for which the parameter ϵ was adjusted, within reason, to give a best fit to another set of data [10,11,15] for negative inceptions. Also shown are curves for a critical avalanche of 3.3×10^6 electrons from calculations performed for identical conditions. The former would correspond to pulses of roughly 10 pC whereas the latter correspond to

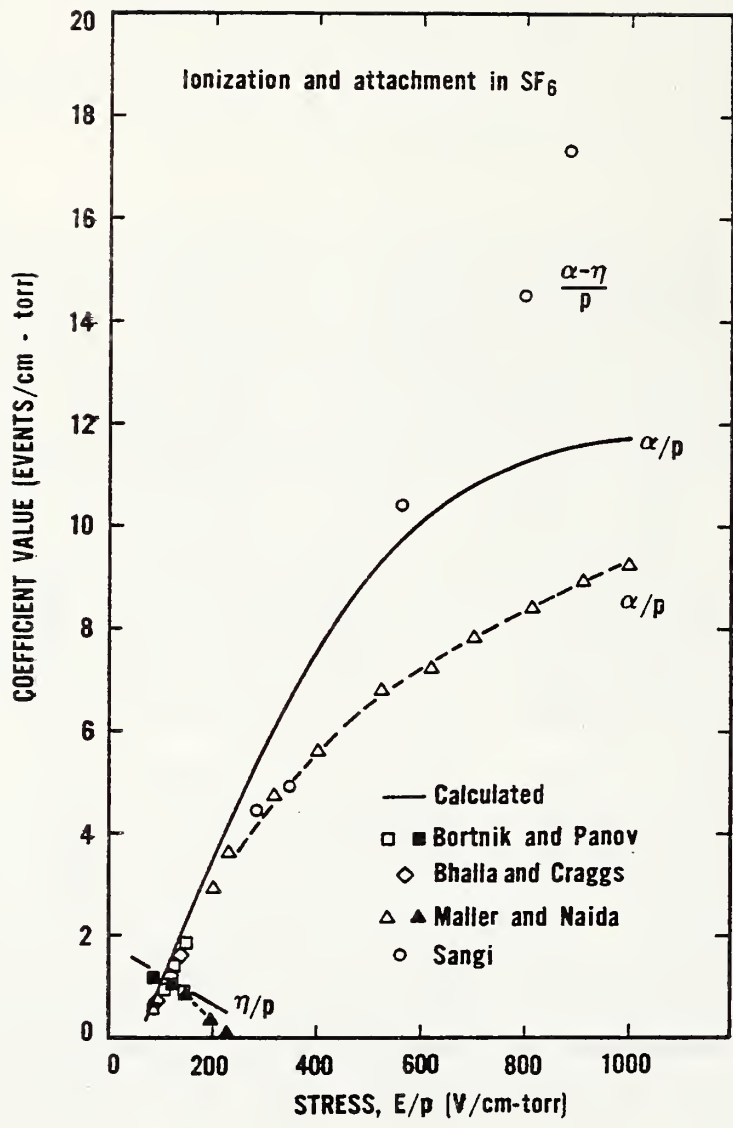


Figure 33. Collected ionization and attachment coefficients for SF₆.

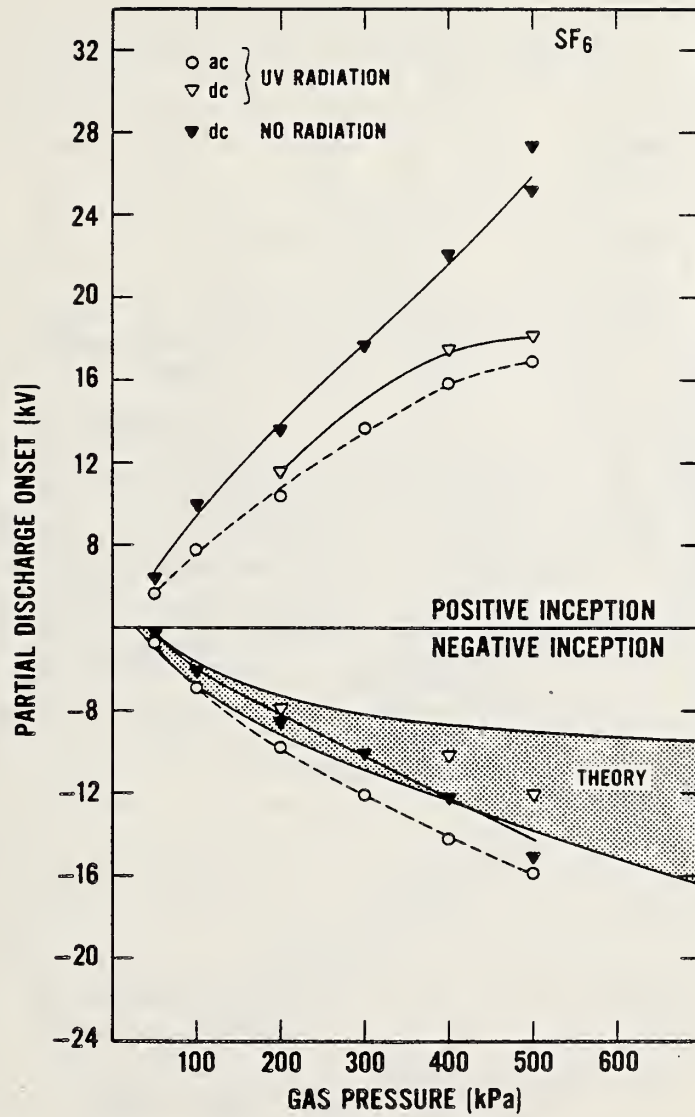


Figure 34. Measured and calculated ac and dc, positive and negative point-plane corona inceptions in SF₆ as a function of gas pressure. The gap spacing was 1.24 cm and the radius of curvature of the point electrode was 0.045 mm.

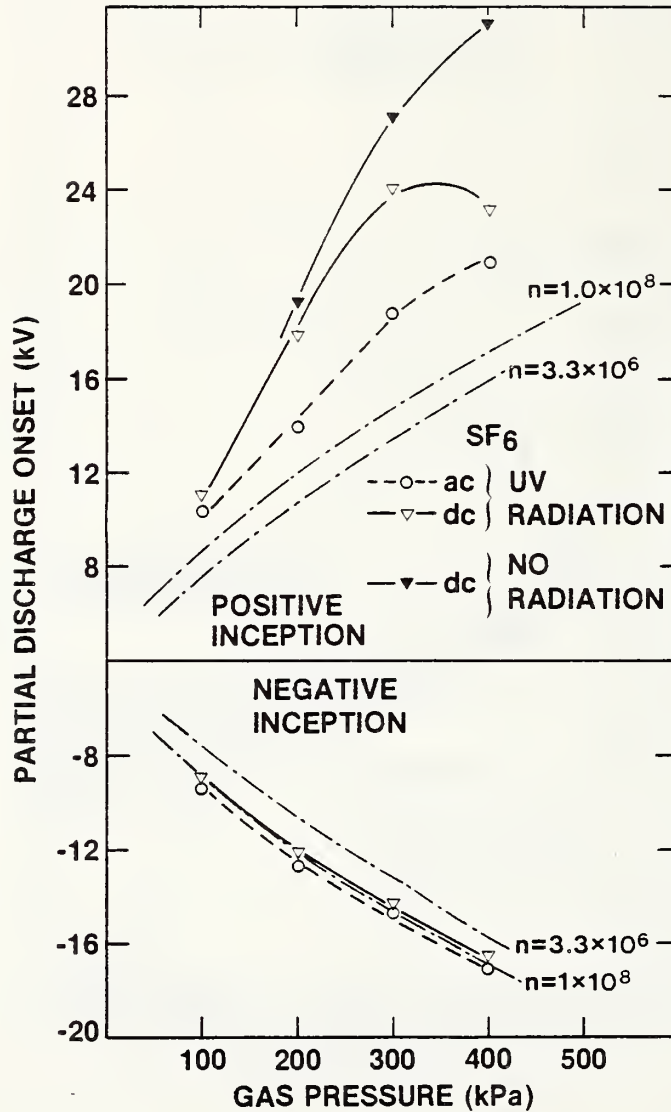


Figure 35. Measured and calculated ac and dc, positive and negative point-plane corona inceptions in SF₆ as a function of gas pressure. The gap spacing was 2.28 cm and the radius of curvature of the point electrode was 0.045 mm.

0.53 pC, which is somewhat closer to the mean value of corona pulse sizes that we have observed for both positive and negative coronas in SF₆ near onset [8]. It is evident that the curve for 3.3×10^6 electrons lies close enough to that for 1×10^8 electrons and that the differences between the two are within the expected uncertainties due to our lack of knowledge about the fields associated with a sharp point. This is expected on the basis of the curves shown in figure 32, which indicate that near onset the size of an avalanche can typically change by several orders of magnitude within a 2-kV variation of the applied voltage. Our onset results would, therefore, appear to be consistent with a fairly broad range of possible critical avalanche sizes. Our pulse height distribution results, however, suggest a value less than 1×10^8 . It should further be noted that the appropriate choice for the critical avalanche size under a given set of conditions has been brought into question in previous discussions [45,46], and it may very well be that this number depends significantly on the gas pressure, electrode surface conditions, and degree of field nonuniformity in the gap.

If one insists, in the theoretical definition of corona onset, that the discharge should be self-sustaining, then there are further complications that arise in addition to the question of critical avalanche size. First it should be realized that, in general, the occurrence of electron avalanches that satisfy the streamer criterion does not automatically guarantee that the discharge will be self-sustaining. By this it is meant that it persists in the absence of an external ionizing agent due to the fact that processes which occur in a given discharge pulse, e.g., ionization, excitation, or radiative emissions, supply mechanisms for the initiation of subsequent pulses. There may, of course, exist conditions under which the discharge, although present without irradiation, is significantly affected by the introduction of radiation. At low pulse repetition rates, i.e., where the time between pulses is long compared to the time required for ions and excited species to clear the gap, it is doubtful that processes occurring in one pulse could have significant influence on the initiation of subsequent pulses. Therefore, although pulses of low ($\leq 10/s$) repetition rate can occur without irradiation, as seen here under some conditions for positive corona in SF₆, it is unlikely that these could be considered completely self-sustaining. Thus, as observed (see figs. 28 and 29), one can expect radiation to have a big effect under conditions where low pulse count rates occur without radiation.

The extent to which a discharge is self-sustained will depend on electrode surface properties [32] and the degree of field nonuniformity. This is particularly true for negative corona in SF₆, evidence of which is supplied by the results presented here and in our earlier work [8]. For positive corona, the condition for a self-sustaining discharge will also be determined by the availability of negative ions in the gap as will be discussed in the next section. The experimental results given here (see figs. 28 and 29), together with data such as given in Sec. II.A, indicate that dc-positive corona in SF₆ is not completely self-sustaining, i.e., independent of external radiation, until large streamer burst-type pulses appear. The voltages at which this happens are usually considerably above the theoretical onsets based on the streamer criterion. As evident from the data in figures 34 and 35, even the first appearances of avalanches for positive dc corona with amplitudes considerably below that required by the streamer criterion occur at voltages above the theoretical onsets.

It thus appears from the discussion above that, at least for SF₆, the connection between measured corona inception voltages and conditions required for streamer formation, or for the discharge to become self-sustaining, is not always obvious. The behavior of the discharge near inception needs to be carefully considered and, as our results show, this behavior depends significantly on voltage and gap conditions. The reasons for these differences can be understood in part from a consideration of the predominant discharge initiation mechanisms for different gap conditions, as well as from a consideration of how electron avalanches grow and eventually develop into self-propagating streamers as discussed in Sec. II.B.

II.C.4 Discharge Initiation Mechanisms

The results presented here suggest that there are certain preferred mechanisms responsible for the initiation of corona discharges in SF₆. We propose that, in the absence of radiation, negative discharges are initiated mainly by field emission of electrons from the cathode tip, the efficiency of which is very much dependent on the condition of the surface, e.g., whether or not it has been "conditioned" by prior discharges (see Sec. II.A). If the cathode is exposed to radiation, the electron emission may be further increased by the photoelectric effect, or more properly, field-enhanced photoelectron emission. The presence of photons may be, in fact, essential to discharge initiation in cases, for example, where the tip is not sharp enough or the work function of the surface material is too high to permit spontaneous electron emission when the field is applied. The conditioning, as already noted, increases the spontaneous electron emission from the surface, e.g., by chemical changes that lower the work function or by introduction of microscopic surface irregularities that locally enhance the electric field [8,47].

For a positive polarity applied to the point electrode, we propose that, in the absence of radiation, collisional detachment of negative ions in the gas is the most likely corona initiation mechanism. However, as will be discussed, the probability for the occurrence of this process may be strongly dependent on the maximum electric field strength in the gap, and thus also on the degree of field nonuniformity. The probability will also depend on the density of negative ions in the gap, and in the dc case, the source of those ions for pre-corona conditions remains somewhat questionable. They could result, for example, from attachment of electrons released by ionization due to background cosmic radiation or by emission sites on the cathode surface due to microscopic irregularities, impact of metastable species, etc. No attempt was made in the present work to measure the negative ion density in the gap. When radiation is present, photodetachment of negative ions may become the dominant initiation mechanism for positive corona near onset. We will now argue that these proposed mechanisms are consistent with the effects observed.

II.C.5 DC Polarity Effect

As seen from the data presented in figures 34 and 35, the measured dc positive corona inceptions are always higher in absolute value than the negative inceptions. Moreover, this effect is greatest for unirradiated gaps at the highest gas pressure used. This polarity difference in inceptions is reduced under 60-Hz ac conditions. For dc it can also be reduced at a

given pressure by: (1) decreasing the gap spacing, (2) decreasing the degree of field nonuniformity in the gap, e.g., through the use of blunter point electrodes (compare data in figures 28 and 29 with data in figures 30 and 31), or (3) irradiating the gap with photons of sufficient energy to photodetach negative ions. The polarity effect observed here is consistent with that reported by Ibrahim and Farish [7,48], who suggested that it is most likely due to the long statistical time lags associated with the initiation of positive corona in SF₆.

In considering the reasons for this polarity difference, perhaps it should be noted first that if the electron avalanches always achieved the maximum-average size, then according to the streamer criteria the difference between positive and negative corona inception should be small in the first approximation. This is because the path length λ which an electron avalanche must travel in order to attain a critical size as calculated by eq (27) is the same for both positive and negative polarities, i.e., it is independent of the field direction. This, of course, assumes that space charge and diffusion effects on avalanche growth can be neglected (see Sec. II.B) and that initiatory electrons for positive corona originate at the point in the gas where $\alpha_i = \eta_a$. Although it can be assumed that the initial electron production for negative corona always occurs with greatest probability at the point of highest electric field, i.e., at the tip of the point electrode surface, it cannot be assumed for positive corona that the point at which $\alpha_i = \eta_a$ is necessarily the point of most probable electron release. Thus, from this consideration alone, there is reason to expect a polarity difference.

In order to attempt to understand this polarity effect, it is necessary to examine the factors that determine the probabilities of discharge initiation for each polarity. Since in the experiments reported here corona onset was defined in terms of discharge pulse repetition rate, it is appropriate to consider the probability per unit time, p_t for formation of a detectable electron avalanche. According to Goldman [32], we can write this as a product,

$$p_t = \frac{1}{\Phi_i} \int_{\Phi_i} p_1(\vec{r}) p_2(\vec{r}) p_3(\vec{r}) d^3r, \quad (32)$$

where p_1 is the probability per unit time at position \vec{r} that an electron source, e.g., a negative ion or a surface element with sufficiently low work function will find itself in a region Φ_i where the necessary conditions are satisfied for avalanche formation; p_2 is the probability of release of an avalanche-initiating electron from the source at \vec{r} ; and p_3 is the probability that if the electron is released, it will then yield an avalanche of the necessary critical size to be detected or satisfy the streamer criterion. The size of the region Φ_i where the field is high enough for initiation to occur can be expected to increase with increasing applied voltage. For negative corona, the active region is associated with a surface area around the tip of the point electrode, and for positive corona it corresponds to a volume in the gas referred to here as the initiation volume.

The probability factor p_1 is obviously proportional to the number of electron sources which appear per unit time at location \vec{r} . For positive discharges, it will be assumed that this is mainly given by the rate at

which negative ions become available for detachment at any location in ϕ_j , and for negative discharges it is the number of electron emission sites available per unit time within ϕ_j on the cathode surface. It will be assumed, as was the case for the experiments described here, that if external radiation is introduced, it has insufficient energy to ionize molecules in their ground state. Although ionization from metastable excited species may be possible, we exclude this mechanism on the basis of lack of information about the possible existence of long-lived excited electronic states of SF_6 which are less than 4.2 eV below the ionization limit [49]. For negative polarity, the number of emission sites will be quite large so that we can take $p_1 \sim 1$. However, for positive polarities, this may not be true because the number of negative ions in the gap at any time might be quite small unless their presence is enhanced by, for example, irradiation of the cathode which causes release of photoelectrons that can then attach to gas molecules.

The second factor p_2 , in eq (32), is determined by the basic mechanisms of electron release, such as, for example, the probability that a negative ion will detach its electron in an encounter with a neutral molecule at position \vec{r} . For negative discharges this can presumably be made arbitrarily large, i.e., $p_2 \sim 1$, by insuring field or photoelectric emission through proper surface preparation together with sufficient field strength, or via irradiation. It is not clear, however, that the assumption $p_2 \sim 1$ can be justified for positive discharges under conditions similar to those which apply for the present measurements. This will be discussed further in the next section.

The probability p_3 is determined by the statistical nature of the processes by which electron avalanches are formed in a gas. Given the release of an electron under a given set of initial conditions, one can calculate the probability that the avalanche will attain some critical size as was discussed in Sec. II.B. Our previous considerations have indicated that if we can neglect space charge effects and assume α_j and n_a are meaningfully defined everywhere in the gap, then the mean size of the avalanches should be nearly independent of the field direction. That is, if the field varies in the same way over a path length λ for avalanche formation, then n_e , as predicted by eq (27), will be the same for both polarities. Thus, if all initial electrons originated from comparable points for positive and negative discharges, then p_3 should be nearly the same for both polarities. This, however, is never the case. While avalanche initiating electrons for negative polarities are emitted predominantly from the tip of the point electrode, corresponding to the region of highest field, the electrons for positive polarity are liberated over a broader range of fields in the relatively lower field region of the gas. Also, the results presented in Sec. II.B. show that, in general, p_3 depends on the value of E/N at the point of initial electron release (also see [9]). Therefore, the positive avalanches can be expected to have a broader distribution in size than the negative avalanches. This implies that for the same maximum field in the gap the positive discharge initiating electrons will have a lower average probability for yielding avalanches of the necessary critical size as compared to the negative case, i.e., p_3 will generally be smaller for positive polarities.

Because p_1 and p_2 can be made to approach unity in the negative case, the rate of avalanche initiation should be quite high as soon as the proper

field conditions are met. One therefore expects a rapid development of this kind of discharge with applied voltage as observed. For the positive case on the other hand, p_1 and p_2 may be considerably smaller than unity, and one expects a slower development of the discharge with increasing voltage. Even if one could assure an abundant supply of negative ions that readily detach their electrons so that p_1 and p_2 approach unity, the initiation of positive discharges is still limited by the size of the initiation volume Φ_i .

To demonstrate this, we have computed the size of Φ_i as a function of applied voltage. These volumes were defined to be regions in which the condition

$$\int_{\ell} (\alpha_j(\ell') - \eta_a(\ell')) d\ell' \geq 18.5 \quad (33)$$

is satisfied, i.e., regions where the release of an electron could give rise to an avalanche containing at least 1×10^8 electrons. The computer program used for this calculation is listed in the appendix IV. In figure 36, we show the calculated boundaries of the initiation volumes for the different indicated voltages. These were calculated for gap conditions used to obtain the data in figure 34 and for a gas pressure $P = 100$ kPa. The outer part of these boundaries is determined by the requirement given in eq (25). The boundaries closest to the electrode are determined by the minimum length ℓ needed to give an avalanche of the critical size. Note that at the theoretical threshold corresponding to the lowest voltage at which the field conditions are first satisfied for the formation of an avalanche of the required size, the initiation volume is infinitesimally small, i.e., it corresponds to a single point. Therefore, $\Phi_i = 0$ at the lowest voltage for critical avalanche formation.

On the basis of these considerations, one is led to predict that conditions which increase either Φ_i , p_1 or p_2 for positive polarity will tend to reduce the polarity difference in corona inceptions. The factor p_1 can be increased by increasing the number of available negative ions. The reduction in the polarity difference in going from dc to 60-Hz ac conditions can be accounted for by the effect which corona on the negative half-cycle has in increasing the density of negative ions in the gap [10,11]. An increase in the rate of growth of Φ_i with voltage can be achieved by using more uniform fields, i.e., by increasing the size of the point electrode. For more uniform fields the initiation volume grows more rapidly with voltage. This is illustrated by the calculated results given in figure 37, where the curve for $\eta_0 = 11.57^\circ$ corresponds to the larger point. The size of the volume has been plotted versus the fractional increase in the applied voltage above inception, where V_i is the inception voltage. This trend was verified here experimentally as can be seen by comparing the data in figures 28 and 29 with the data in figures 30 and 31.

The factor p_2 can be increased by using radiation to photodetach negative ions in the initiation volume, and possibly by increasing the degree of field inhomogeneity as will be considered in the next section. The data in figures 34 and 35 clearly indicate a reduction in the polarity difference when uv-radiation is introduced.

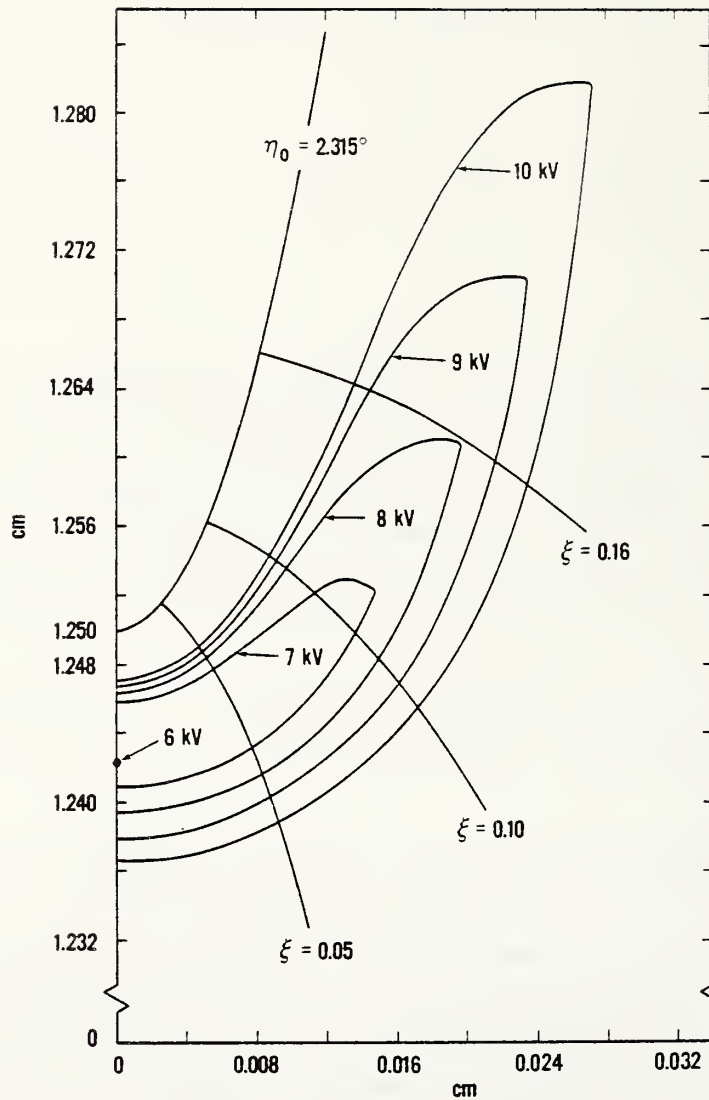


Figure 36. Calculated boundaries of the initiation volumes for SF₆ positive corona inception at the indicated applied voltages and for a gas pressure of 100 kPa.

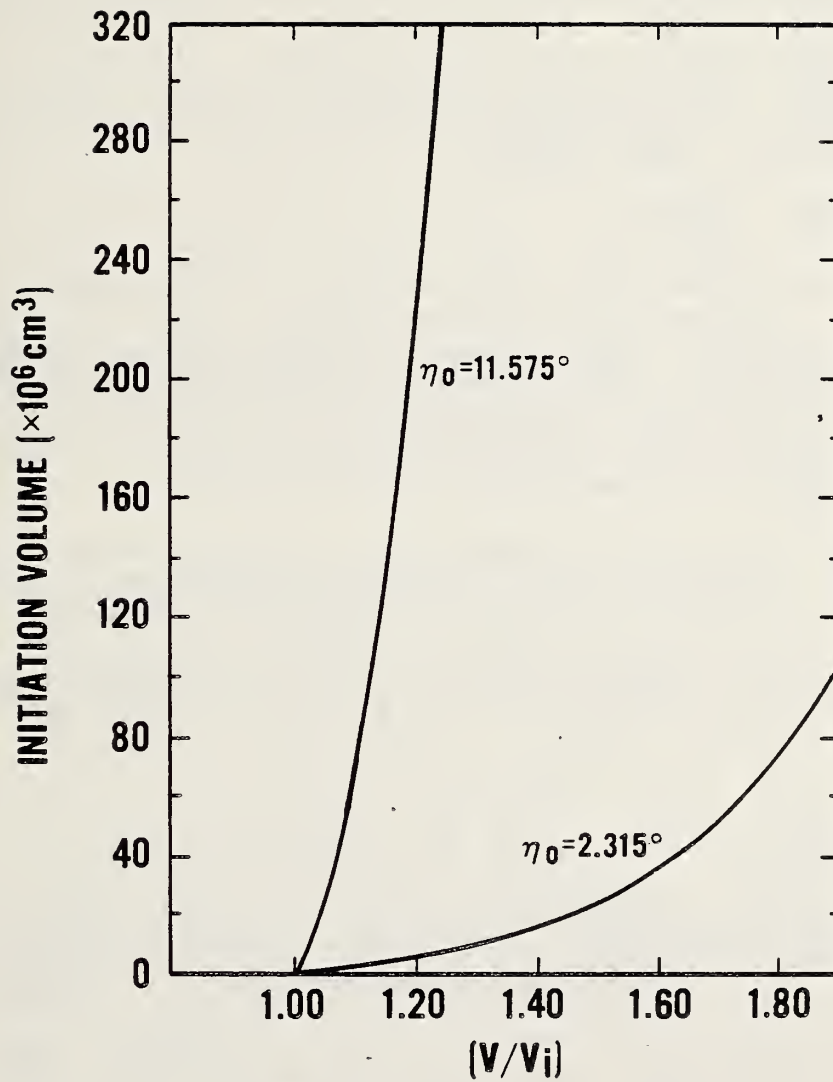


Figure 37. Calculated growth in the electron initiation volume for two point electrodes characterized by the angles $\eta_0 = 11.575^\circ$ and $\eta_0 = 2.315^\circ$ plotted as a function of the ratio of applied voltage V to theoretical corona inception voltage V_i .

The reason why the polarity difference is increased in going to longer gaps is not clear. If, for example, the ultimate source of negative ions in the positive point case is from release of electrons from the cathode region, then perhaps the effect is related to a reduction of ion densities due to longer drift lengths which allow ions to diffuse more so that fewer enter the initiation volume. The reason why the polarity difference is greatest at higher pressures also remains obscure. This effect may be related to changes in the predominant negative ions with increasing pressure, e.g., an increase in the relative abundances of ion clusters that move more slowly and detach less readily.

II.C.6 Geometrical Effects

In addition to the influence of electrode geometry on the magnitude of the polarity effect described in the previous section, there are other effects that need to be examined. The increase in corona inception voltages with increasing gap spacing and point electrode diameter can be understood simply from a consideration of the dependence of the electric field on gap geometry and applied voltage. These effects are readily predicted using the streamer criterion and need not be discussed further.

It is not immediately apparent, however, why it becomes necessary to use uv-radiation to initiate and sustain corona once the degree of field inhomogeneity becomes too low, i.e., for larger point diameters. We hypothesize that in the case of negative polarities the electric field at the surface of blunter points never attains sufficient strength near onset to permit field emission, i.e., $p_2 \sim 0$ in eq (32). Photons must then be used to insure electron production via the photoelectric effect. For positive polarities, one can argue that if the point is not sharp enough, then the field never reaches a value high enough to permit collisional detachment of negative ions to occur with sufficient probability.

For uniform field gaps, Frommhold [35] has pointed out the importance of collisional electron detachment in affecting the growth of electron avalanches once the field is high enough that the mean life-time of a negative ion is short compared to the time it spends traversing the gap. The probability that discharge initiation will occur in a given time has been formulated in terms of the life-times of negative ions by Berger and Hahn [50] and discussed by Goldman [32,45]. It is more appropriate in the present discussion to seek an expression for the rate of initiating electron production $(dn_e/dt)_0$ in the initiation volume.

Given that we know: (1) the flux of negative ions incident on the initiation volume ϕ_i , i.e., the current density $\vec{j}_0(a)$, (2) the detachment coefficient δ_d (number of detachments per unit length) as a function of E/N , and (3) the variation of electric field E in ϕ_i , we ask, what is the rate of initiating electron production, $(dn_e/dt)_0$ via collisional detachment?

The negative ion current density at any point is related to the negative ion density ρ_- and velocity \vec{v} by

$$\vec{j} = e \rho_- \vec{v}, \quad (34)$$

where e is the electron charge. Inside Φ_i the continuity equation holds, namely,

$$\partial \rho_- / \partial t + \nabla \cdot \rho_- \vec{v} = -Q, \quad (35)$$

where $-Q$ is a "sink" term giving the rate of destruction of negative ions inside the volume due to detachment. The above expression, of course, applies specifically to a pre-avalanche condition, i.e., an initiation volume in which electron multiplication has not yet begun. Once an initiation electron is released, it will either immediately attach again or lead to avalanche formation, thereby altering the condition implied by eq (35).

Assuming a steady-state condition in which the field E is constant in time, we have

$$(\partial \rho_- / \partial t) = 0. \quad (36)$$

It then follows from eqs (34)-(36) that

$$(1/e) \int_{S_0} [\vec{j}_0(a) - \vec{j}_\ell(a)] \cdot d\vec{a} = -(1/e) \int_{\Phi_i} Q d^3r = (dn_e/dt)_0, \quad (37)$$

where S_0 is the surface area enclosing Φ_i and $\vec{j}_\ell(a)$ is the exiting negative ion current density at surface area element da . The integral over volume on the right-hand side of eq (37) is the rate of loss of negative ions due to collisions and must therefore equal the rate of electron production, $(dn_e/dt)_0$. Consistent with eq (36), we can also write

$$\left(\frac{dn_e}{dt}\right)_0 = \left(\frac{dn_-}{dt}\right)_0 - \left(\frac{dn_-}{dt}\right)_\ell, \quad (38)$$

where the first term on the right gives the rate at which ions enter Φ_i and the second term the rate at which they leave.

It will now be assumed that if $dn_-(a)$ ions enter Φ_i at area element da , they will all travel a distance $\ell(a)$ before exiting if not destroyed. Allowing for destruction via collisional detachment, then the number of these ions that survive to leave the volume is given by

$$dn_\ell(a) = dn_-(a) \exp\left[-\int_0^{\ell(a)} \delta_d(\ell') d\ell'\right]. \quad (39)$$

It is preferable here to formulate the negative ion destruction in terms of $\delta_d(\lambda)$ rather than the collisional detachment cross section σ_d because the incident ions do not, in general, have a well-defined velocity and there may, in fact, be more than one type of ion involved. The relationship between δ_d and the cross sections $\sigma_{d,i}$ for detachment of the ions is given by

$$\delta_d = N \sum_i \frac{g_i}{\bar{v}_i} \int_0^{\infty} v \sigma_{d,i}(v) f_i(v) dv, \quad (40)$$

where g_i is the fraction of the total number of ions that correspond to the i th species. In this expression $f_i(v)$ and \bar{v}_i are respectively the velocity distribution and mean velocity of the i th ion species. The background neutral gas number density N has been assumed to be uniform throughout ϕ_j . Although the cross sections $\sigma_{d,i}$ appear to have fairly well-defined thresholds [51], the extent to which one can meaningfully define corresponding thresholds for δ_d depends on the width of the velocity distribution function. Only if one makes the simplifying assumption that all ions of a given species have the same velocity can one unambiguously refer to a threshold for δ_d . In that case, $f_i(v) = \delta(v_i - v)$, and eq (40) reduces to

$$\delta_d = N \sum_i g_i \sigma_{d,i}(\bar{v}_i). \quad (41)$$

Precluding this assumption, the terms "detachment threshold" as applied to δ_d will be taken here to mean the value of E/N at which $\bar{v}_i = v_{d,i}$, where $v_{d,i}$ is the threshold value for $\sigma_{d,i}$.

Now it should be noted that eq (40) applies only to a particular point inside σ_j , since $f_i(v)$ and \bar{v}_i will vary with location as determined by the field. Thus δ_d in eq (39) is expressed as a function of position λ' .

From eqs (38), (39), and $\vec{j}(a) \cdot d\vec{a} = dn_-(a)/dt$, we can write

$$\int_{S_0} \vec{j}_\lambda(a) \cdot d\vec{a} = \int_{S_0} d\vec{a} \cdot \vec{j}_0(a) \exp\left[-\int_0^{\lambda(a)} \delta_d(\lambda') d\lambda'\right]. \quad (42)$$

This, when combined with eq (37), leads to

$$\left(\frac{dn_e}{dt}\right)_0 = (1/e) \int_{S_0} d\vec{a} \cdot \vec{j}_0(a) \left(1 - \exp\left[-\int_0^{\lambda(a)} \delta_d(\lambda') d\lambda'\right]\right), \quad (43)$$

where S_0 represents the surface of the initiation volume and $\lambda(a)$ is the maximum path length along a field line that an ion could travel through the initiation volume if it enters at a particular surface area element da . The above equation is approximate in the sense that we have neglected ion diffusion. From eq (43) it is clear that the rate of initiating electron production increases as the integral over $\delta_d(\lambda')$ increases. The dependence of the detachment coefficient on position λ' is derived from its dependence on E/N .

In the category of collisional detachment, we include not only reactions of the form



but also detachment involving dissociation, such as



as well as associative detachment processes. Not included are reactions in which the electron is merely transferred to another species, or in which the character of the ion changes, e.g.,



It is quite possible that a negative ion will change its character in traversing the initiation volume, but that effect can, in principle, be included in δ_d . It is likely, especially at higher pressures, that more than one negative ion species is involved.

The dependence of the collisional detachment coefficient on E/N is important in determining the likelihood of this process occurring. Measurements have been made of δ_d for collisional detachment of negative ions such as SF_6^- , SF_5^- , and F^- in SF_6 [52,53]. These show that once E/N reaches a value, usually referred to as the detachment threshold $(E/N)_d$, δ_d increases abruptly with E/N . Actually, the term threshold is only properly ascribed to the dependence of the collisional detachment cross section on ion energy or velocity and, as previously noted, the extent to which one can meaningfully define a corresponding threshold for δ_d depends on the width of the ion velocity distribution function. For negative ions in SF_6 , $(E/N)_d$ appears to lie slightly below the critical value $(E/N)_c$ where $\alpha_i = n_a$. Below $(E/N)_d$ it is reported that δ_d is too small to be measured. The results of O'Neill and Craggs [53] further indicate that the assumption $\delta_d/N \ll n_a/N$ cannot be assured once $E/N > 1.4 (E/N)_c$, and, therefore, for high enough E/N , collisional detachment cannot be neglected in the calculation of electric discharge current growth.

Recent measurements [51] of the total collisional detachment cross sections of negative halogen ions by various molecular gases also show abrupt increases

in the detachment probability once the incident ion energy exceeds a threshold energy which is usually about twice the electron affinity. Several reported measurements [35, 54-66] of O^- and O_2^- detachment in O_2 show similar behavior, i.e., abrupt increases in the detachment rate, or cross section above a certain threshold.

Thus, the limited data on collisional detachment suggest that unless E/N is high enough, the negative ions never acquire enough kinetic energy between collisions to permit detachment to occur. If this is the case, then $p_2 \sim 0$ in eq (32), and the probability for avalanche initiation is negligibly small. As one goes to more divergent fields, i.e., sharper point electrodes, then the maximum value of E/N within the initiation volume ϕ_i will increase giving rise to a higher probability for collisional detachment. This can explain why spontaneous positive corona initiation was observed here in unirradiated gaps only for the sharper points.

It should finally be noted that for strong electric fields, the binding energy of the attached electron of a negative ion in the field may be reduced sufficiently to further enhance the collisional detachment process. In fact, Schweinler and Christophorou [57] have shown that if the field is strong enough (~ 1 MV/cm), field-induced detachment becomes possible. However, for negative ions with electron affinities greater than 1.0 eV, it is necessary to have fields in excess of 10 MV/cm in order for field induced detachment to occur with significant probability. For the measurements reported here, fields of this magnitude were not attained within the initiation volume ϕ_i . Thus, in agreement with the suggestion of Schweinler and Christophorou, we must argue that field induced detachment is unlikely to be an important discharge initiation mechanism.

II.D. Electron Swarm Data for Electronegative Gases

II.D.1 Motivation

The necessity of having reliable swarm data in the modeling of electric discharge phenomena was made clear from the discussions given in the previous three sections. The present survey is intended to provide information about the status of existing swarm data for gases which have application in electrical insulation technology. In this survey, data have been compiled from many different sources and presented with critical commentary. Major discrepancies and gaps in the data have been pointed out.

Most of the work was performed at the Atomic Collisions Data Center of the Joint Institute for Laboratory Astrophysics in a collaborative effort involving Prof. J. Dutton of the University College of Swansea and scientists at both NBS and the University of Colorado. The results of this survey have recently been submitted for publication [58]. In the present report we give only a description of the types of data included, and an example of the data compiled for SF_6 which tie in closely with the work described in the previous sections. Reference [58] will contain information on many other electronegative gases.

II.D.2 Definitions and Method of Data Handling

An electron swarm is a low density cloud of electrons of density n in a gas of much higher number density, N . The properties of the system are dependent

on the interactions of the electron swarm with the gas molecules (or atoms) and ions rather than with each other or with the container walls, typically in the presence of an electric field. The electric field increases the mean energy of the electron swarm so it can be substantially higher than that of the neutral gas, and electron collisions with the heavier gas molecules give them a large random component of motion. The electron motion is described by an energy distribution function which is dependent on the energy gain per mean free path from the electric field (see Sec. II.D.4). For an electric field of strength E , the latter quantity is proportional to E/N , the "reduced field strength." For the data considered here, the gas temperature T is relatively low and has little influence on the distribution function. The properties of swarms studied are those relating to spatial transport, the rates of creation and destruction of electrons, and the rates of energy transfer to the neutral gas. The parameters included in the data review are discussed briefly below.

In an electric field the velocity of the center of mass of the electron swarm drifts in the direction opposite to the field with a velocity known as the drift velocity, W . The electron mobility, μ , is defined as the ratio of the drift velocity to the electric field strength and, for present purposes, mobility is considered to be an alternate way of specifying the drift velocity.

Diffusion is the tendency of the swarm to spread as a result of its random motion in such a way as to make the density uniform and is characterized by a diffusion coefficient, D . When an electric field is present, the diffusion is not, in general, the same in all directions. Two parameters, the transverse diffusion coefficient, D_T , (perpendicular to the field) and the longitudinal diffusion coefficient, D_L , (parallel to the field) then characterize the diffuse motion. The ratio of diffusion coefficient to mobility, D/μ , has a rather special role, and data on this ratio are determined independently of the other quantities with D_T/μ treated separately. In the limit of small electric fields, this ratio tends toward the mean energy of the electrons and, as such, it is a measure of the electron temperature. At higher fields, the electron swarm is not in thermal equilibrium and no temperature is defined, but D/μ is a convenient measure of the energy content of the swarm. In this context D_T/μ is defined as the "characteristic energy." This terminology does not refer to D_L/μ .

The change in the number of the electrons in a swarm may come about as a result of electron attachment (coefficient η_a) to neutral particles, electron detachment (coefficient δ_d) from negative ions in collision with other gas molecules, and ionization (coefficient α_i) of neutrals. For some range of values of E/N the electron density will be simultaneously influenced by all three processes, but the spatial current growth in a Townsend discharge (see Sec. II.D.3.1) may be exponential over a large range of distance. It is convenient in these circumstances to define the parameter λ , the electron growth constant, as the multiplying constant in the exponential. In the case where only ionization and attachment occur, $\lambda = \alpha_i - \eta_a$, and is the average net gain of free electrons per unit distance of drift. Inelastic collisions other than those giving rise to ionization are quantified by excitation coefficients (ϵ). Another process which can cause a change in the number of electrons is recombination, but because of the low electron and positive ion densities in the swarms considered here, it is not included in the present review.

The swarm coefficients referred to in the previous paragraph are defined as the average number of events occurring when one electron drifts a unit distance in the direction of the electric field. In general, they are related to the corresponding two-body rate coefficients by $Nk_2 = SW$, where S is a coefficient (per unit drift distance) and k_2 the corresponding rate coefficient (also see Sec. II.B). In the case of three-body processes, the relationship is $N^2k_3 = SW$, where k_3 is the three-body rate coefficient.

As the values of the parameters characterizing the swarm behavior are determined by E/N and N , it is convenient to represent them as W , D/μ , DN , S/N as a function of E/N . Thus, most of the data of this survey are presented in graphs and tables of this form. The specific parameters and corresponding multiples of SI units in which they are expressed are summarized in table I.

When the original data were published in tabular form, the figures and tables were prepared directly from the original tables, and the number of significant figures of the tabular data retained. However, in most cases, the data were published in the form of graphs, and the graphs were enlarged and the coordinates of the data points obtained using standard digitization procedures. These procedures are estimated to introduce an error of no more than $\pm 3\%$. As a recording convenience, most of the data retrieved by this method were entered in the tables with three significant figures. In cases where experimental sources introduce higher errors, fewer significant figures were retained.

Data are frequently published in units other than the SI units given in table I. In these cases conversions to the SI units were made using the relationships listed in table II.

II.D.3 Experimental Techniques

Most of the experimental data reported were obtained using variations on a small number of general methods which are briefly described below. Although these methods are conceptually straightforward, the analysis of the measured data to obtain accurate transport and swarm coefficients is complex. Simplifying assumptions concerning the effects of boundaries, diffusion, secondary ionization and, especially in the case of electronegative gases, ion molecule reactions and detachment have frequently been made in the analysis of data obtained by these methods. Huxley and Crompton [59] give a comprehensive discussion of the impact of approximations based on these assumptions and the variations on experimental methods and related analyses which have been devised to avoid them.

II.D.3.1 Spatial Current Growth

In this technique [60], also referred to as a steady-state Townsend discharge, a swarm of electrons is photoelectrically released from the cathode of a drift tube, and the anode current, I , is measured as a function of gas pressure, electric field strength, and electrode separation, d . As discussed by Dutton [12], under especially simple conditions of ionization, i.e., absence of secondary ionization, attachment, and detachment and low E/N , the current can be expressed as

Table I. Swarm parameters. Symbolic notation, scale factors, and units.

Symbol	<u>Scale Factors</u>	
	Name	Units
N	Gas number density	10^{22} m^{-3}
P	Gas pressure	Pa
T	Gas temperature	K
W	Electron drift velocity	10^3 ms^{-1}
E/N	Reduced field strength	10^{-21} V m^2
$D_T N$	Transverse diffusion coefficient * N	$10^{24} \text{ m}^{-1} \text{ s}^{-1}$
$D_L N$	Longitudinal diffusion coefficient * N	$10^{24} \text{ m}^{-1} \text{ s}^{-1}$
D_T/μ	Ratio of transverse diffusion coefficient to mobility	V
D_L/μ	Ratio of longitudinal diffusion coefficient to mobility	V
η_a/N	Attachment coefficient/N	10^{-22} m^2
α_i/N	Ionization coefficient/N	10^{-22} m^2
δ_d/N	Detachment coefficient/N	10^{-22} m^2
λ/N	Electron growth constant/N	10^{-22} m^2
ϵ/N	Excitation coefficient/N	10^{-22} m^2
k_2	Two-body rate constant	$10^{-16} \text{ m}^3 \text{ s}^{-1}$
k_3	Three-body rate constant	$10^{-42} \text{ m}^6 \text{ s}^{-1}$

Table II. Common units conversions for swarm data^a.

Quantity	Symbols and SI units A	Conventional Units B	Conversion factor F to conventional SI units A = FB
Particle density	$N(m^{-3})$	$N(cm^{-3})$	10^6
Particle density	$N(m^{-3})$	P(torr)	$3.54 \times 10^{22} \frac{273 K}{T(K)}$
Temperature	T(K)	T(K)	1
Pressure	P(Pa)	P(torr)	133
Reduced Field	$E/N(V m^2)$	$E/P(V/cm torr)$	$2.83 \times 10^{-21} \frac{T(K)}{273 K}$
Reduced Field	$E/N(V m^2)$	$E/N(Td)$	10^{-21}
Drift velocity	$W(m s^{-1})$	$W(cm s^{-1})$	10^{-2}
Diffusion coefficient	$DN(10^{22} m^{-1} s^{-1})$	$DP(\frac{cm^2 torr}{s})$	$3.54 \times 10^{18} \frac{273 K}{T(K)}$
Diffusion/mobility	$D/\mu(V)$	$D/\mu(V)$	1
Swarm coefficients	$S/N(m^2)$	$S/P(cm torr)^{-1}$	$28.3 \times 10^{-21} \frac{T(K)}{273 K}$

^aPressure is incorporated into many of the units conventionally used. The related conversions to SI units used in this paper are not a simple numerical factor, but require incorporation of the ratio $T(K)/273 K$ in the conversion factor F, where $T(K)$ is the temperature at which the measurements were made.

$$I \propto \exp(\alpha_j d) \quad , \quad (47)$$

and the ionization coefficient can be determined from measurements of the current as a function of d . Similarly, for systems in which only attachment occurs, i.e., no detachment or ionization and low E/N ,

$$I \propto \exp(-\eta_a d) \quad , \quad (48)$$

and the attachment coefficient can be determined. Of course, these special conditions are rarely satisfied, especially for high E/N , and extensive analysis incorporating ionization, attachment, detachment and ion-molecule reactions is required to accurately determine swarm coefficients from these measurements (see [12] eq (16)). Although in some cases experimental conditions can be selected so that some parameters are negligible, measurements in electronegative gases for a reasonable range of E/N require fitting measured current growth curves with analytical expressions containing several swarm coefficients (e.g., α_j , η_a , δ_d). The values of these coefficients which fit the experimental data are often subject to large uncertainties. Recently, advances in computer techniques have enabled analyses with more sophisticated fitting procedures.

II.D.3.2 Transverse Diffusion Coefficient

In a modification of the steady-state Townsend discharge used to measure D_T/μ , the cathode emission is confined to a point source and the anode is divided into concentric rings. Townsend's original analysis was refined by Huxley and Bennett [61] and subsequent work, as described in [59] chapter 11. The ionization coefficient can also be obtained from analysis of these data.

II.D.3.3 Temporal Current Growth

A pulsed Townsend discharge [62,63], which has been used since high-speed electronics have become available, involves the production of a pulse of photoelectrons and the observation of the time dependence of the transient current. Because the electrons have much higher drift velocities than ions, the related components of the current are distinguishable. Concerns involving interpretation and analysis of results to give swarm coefficients are similar to those for steady-state Townsend measurements.

If the energy of the electron swarm exceeds the ionization energy of the gas molecules, an electron avalanche is initiated. Measurement of the electron density as a function of time, either electronically or by observation of the light emitted from the discharge, provides values of the ionization coefficient and electron drift velocity [39].

II.D.3.4 Sampling Techniques

These techniques, also referred to as time-of-flight and Bradbury-Nielson techniques, use a drift tube in which two or more electrical shutters are placed in the path of the drifting electrons, the first to function as a gate to admit electrons into the drift space at a known time and the second

to sample the density of electrons traveling the distance between the shutters as a function of time. From these measurements, electron drift velocities and, with more extensive analysis, longitudinal diffusion coefficients are obtained. Many variations on the construction and operation of the shutters and on the analysis of the resulting data are included in the comprehensive discussion of drift velocity measurements in chapter 11 of [59].

II.D.3.5 Errors

When available, the original authors' uncertainty specifications are quoted with the data. However, because different researchers use different standards for their uncertainty statements, the data with the smallest specified uncertainty is not necessarily the most reliable.

There are several specific sources of error common in swarm measurements. One is gas impurities which may have a significant influence on the quantities observed as evidenced by measurements in intentional mixtures. A second is the effect of surfaces in both distortion of the electric fields and the spatial distribution of electrons and as a source of secondary electrons. A third is the measurement of partial pressures in mixtures.

There are also error sources related to the interpretation of measured quantities to obtain swarm coefficients, especially in electronegative gases where the electron number density varies due to attachment and, at higher E/N, ionization. Various aspects of the complete reaction scheme such as detachment from negative ions and charge transfer, as well as more complex (and perhaps unidentified) reactions such as formation and attachment to clusters, may be unidentified by the investigator or ignored in the interest of reducing the analysis to manageable proportions. The use of mass spectrometric techniques is essential to identification of a complete reaction scheme, as well as to monitor impurity concentrations.

Additional sources of error in the analysis of experimental data include the assumption of idealized geometry, the neglect of diffusion effects (see e.g., chapter 5 of [59]) and inelastic collisions. As discussed in Sec. II.D.3.1, the reported transport and swarm coefficients are often derived from curve-fitting procedures in which the parameters describing the reaction scheme are incorporated into an analytic expression which describes the observations. Often a range of parameters gives a satisfactory fit, resulting in a large uncertainty.

II.D.3.6 Computations Using the Boltzmann Equation

The swarm parameters discussed so far are measures of the macroscopic properties of an electron cloud moving through a neutral gas under the influence of an electric field. Because there is no macroscopic theory of electron transport (drift velocity and diffusion coefficients) or electron excitation (here excitation is defined as reactive collisions), it is necessary to go back to the details of the microscopic electron-neutral scattering cross sections to calculate swarm parameters. The Boltzmann equation provides a connection between these microscopic cross sections and the measurable macroscopic parameters.

The Boltzmann equation is the equation of continuity for electrons in a six-dimensional phase space and describes the time evolution of the electron energy distribution function, $f(r,v,t)$. Electron transport and excitation coefficients are calculated as averages or integrals involving f (see eqs (6)-(8)). The electron energy distribution function contains all the information about the electron swarm, and the calculated swarm parameters are averages in the same sense that the experiments measure average quantities. The key to a model or theoretical calculation is then the electron energy distribution function.

The Boltzmann equation may be written as [59],

$$\frac{\partial f}{\partial t} + \vec{v} \cdot \nabla_r f + \vec{a} \cdot \nabla_v f = C(f) , \quad (49)$$

where \vec{a} is the acceleration due to the applied field and C is the collision operator. In order of the terms above, the time evolution of f is due to a spatial flux, a flux in velocity space, and a redistribution of electron energy due to collisions with neutral particles. Electrons may lose recoil energy in elastic collisions with neutrals, gain recoil energy if the electron energy is less than the neutral energy, and gain or lose discrete amounts of energy in exciting or de-exciting the neutrals to or from the various rotational, vibrational, or electronic levels. For cases of interest here, space-charge fields and Coulomb collisions are negligible.

Solutions of the Boltzmann equation are complicated because f depends on the six phase-space variables and time. An additional complication is that the collision operator C is a combination of multiplicative and integral operators. However, in the hydrodynamic regime, i.e., the regime of interest in typical swarm situations where the measured parameters are free of boundary effects and any change in current is exponential in both time and distance, several simplifying assumptions can be made which cast the Boltzmann equation into a form amenable to numerical solution. Even in the hydrodynamic limit, however, much effort has been devoted to techniques for solving the Boltzmann equation and studying the various approximations that make numerical solutions of the equation practical.

By far the most common solution is the "two-term" approximation. Here the spatial dependence of f is assumed small and is treated in second order. Thus, since the current growth is exponential, $\partial f / \partial t = (\text{constant}) \times f$ and $f(r,v,t) = f(v)$. The two-term approximation is then invoked, i.e., the angular dependence of f (the angle being that between the electron velocity vector and the field direction) can be approximated by the first two terms of a spherical harmonic (or because of the cylindrical symmetry, Legendre polynomial) expansion. This approximation leads to calculated values of electron transport and rate coefficients (see Sec. II.B) that agree reasonably well with the more rigorous calculations in most cases.

An alternate technique for the calculation of swarm parameters is a Monte Carlo calculation which avoids entirely the use of the Boltzmann equation. In these numerical simulations of the swarm motion, the trajectories of individual electrons are followed through a large number of collisions with the exact outcome of each collision being modeled on the basis of a random number. This

technique offers the advantage that boundary effects may be included, and no assumptions are made about either the r or v dependence of the distribution. This advantage is offset by the comparatively long computational times involved. Also, for calculations of equilibrium or steady-state swarm phenomena, the boundary effects may be safely neglected.

There are two general categories of applications for the solution of the Boltzmann equation:

- 1) Iterative extraction of low-energy electron-neutral scattering cross sections from measured swarm data, and
- 2) Calculations of swarm parameters from a given set of cross sections.

These two categories differ in purpose but are the same computationally. In the first category, the cross sections may be extracted from swarm data in a trial and error sense by comparing calculated values of swarm parameters with measurements using an estimate for the cross sections. Cross sections are then adjusted using the comparison as a guide until the calculated and measured values agree. The cross sections in He, for example, thus determined are considered to be some of the most accurate available.

The second of the applications listed above is of more interest here. The electron energy distribution function in a gas mixture can be very different from those of the individual mixture components under the same experimental conditions. In general, the distribution function for a gas mixture cannot simply be determined from considering the separate distributions for the gas components. It is necessary to go through the Boltzmann equation using as input the component gas cross sections. Thus swarm parameters in mixtures may be calculated from the constituent gas cross sections.

Calculations of swarm parameters may be made quite accurately depending on the method used to solve the Boltzmann equation. For many applications, the "two-term" approximation yields sufficient accuracy. With few exceptions, the theoretical values of swarm parameters reported here were calculated using that approximation.

II.D.4 Data for Sulphur Hexafluoride

A dominant fact of electron swarms in SF_6 is that low energy electrons are very rapidly attached to form negative ions, and the rapid disappearance of free electrons greatly complicates the measurement of other swarm parameters. At high E/N ionization helps balance the loss by attachment. Small shifts in the energy distribution function can substantially change the balance between electron gain and loss. In two papers published in 1979, Kline, Davies, Chen, and Chantry [64] and Yoshizawa, Sakai, Tagashira, and Sakamoto [65] reviewed the available cross section data for collisions of electrons in SF_6 . In each of these papers, the electron energy distribution function was calculated by solving the Boltzmann equation, and the swarm parameters were computed using the distribution function and the relevant cross sections. The paper by Kline and co-workers also reported some new, presumably more reliable, cross section data which are rather different from those assumed by Yoshizawa and co-workers. On the other hand, Yoshizawa and co-workers

used a more accurate method of solution of the Boltzmann equation. These papers support the conclusion that the dominant phenomena of electron swarms in SF_6 are well understood, but there are considerable uncertainties in the magnitudes of some of the transport coefficients.

II.D.4.1 Drift Velocity

Naidu and Prasad [23] used sampling techniques to measure the electron drift velocity for the E/N range $340-640 \times 10^{-21} \text{ Vm}^2$, and the results are displayed in figure 38. These data are the only measured values available from a direct and recognized method and are counted as the most reliable. The authors estimate the uncertainties to be 5 percent. Teich and Sangi [41] also reported data for the same E/N range in a conference proceedings which is not widely available. They provide no description of experimental method and give their results in the form of a simple equation. These data are also displayed in figure 38. Harris and Jones [66] reported data on the drift velocity of electrons in SF_6 for the range $E/N = 15 - 150 \times 10^{-21} \text{ Vm}^2$. (The same results with less explanation were also given by Dutton, Harris, and Jones [67].) Their method involved a detailed accounting for electrons removed by diffusion back to the cathode. While this method is indirect, in other gases it yielded data in error by only 15 percent. The results of these measurements are given as an equation which is represented in figure 38 by a line.

Kline et al. and Yoshizawa et al. both calculated drift velocities which are displayed in figure 38. The data from Yoshizawa et al. are W_M , the velocities of the center of mass of an isolated group of electrons, which is the definition most appropriate to the measurements of Naidu and Prasad. Yoshizawa et al. considered the consequences of spatial inhomogeneity in the distribution function and found surprisingly large effects. For instance, they report that W_y , the average velocity, is lower than W_M by about 25 percent at $E/N = 600 \times 10^{-21} \text{ Vm}^2$. Calculations were also performed using other definitions of the drift velocity. Kline and co-workers, who were primarily concerned with attachment and ionization phenomena, did not consider these higher order effects since they used the conventional two-term approximation and included new electrons produced by ionization.

II.D.4.2 Ratio of Diffusion-to-Mobility and the Diffusion Coefficients

Naidu and Prasad [23] also reported values for D_T/μ . These data were derived from measurements of the ratios of currents to concentric ring electrodes. Taken as a whole the data set displays inconsistencies which the authors discuss. The authors note that most of the discordant data involved use of the outermost rings, and these data are defined to be the result of "anomalous" diffusion. Anomalous diffusion is defended as a significant physical effect and not the result of measurement error; however, no explanation is given for the causes. The authors suggest that data derived from the inner rings are reliable, and these data are represented in figure 39 as a short straight line. Maller and Naidu [68] later reported similar measurements which are also shown in figure 39 and are quite close to the results of Naidu and Prasad. Kline and co-workers calculated values of D/μ along with other swarm parameters, and their results are included in figure 39. For applicable values of E/N the experimental values are the preferred data. The calculated data represent a reasonable basis for extrapolation to higher and lower values of E/N .

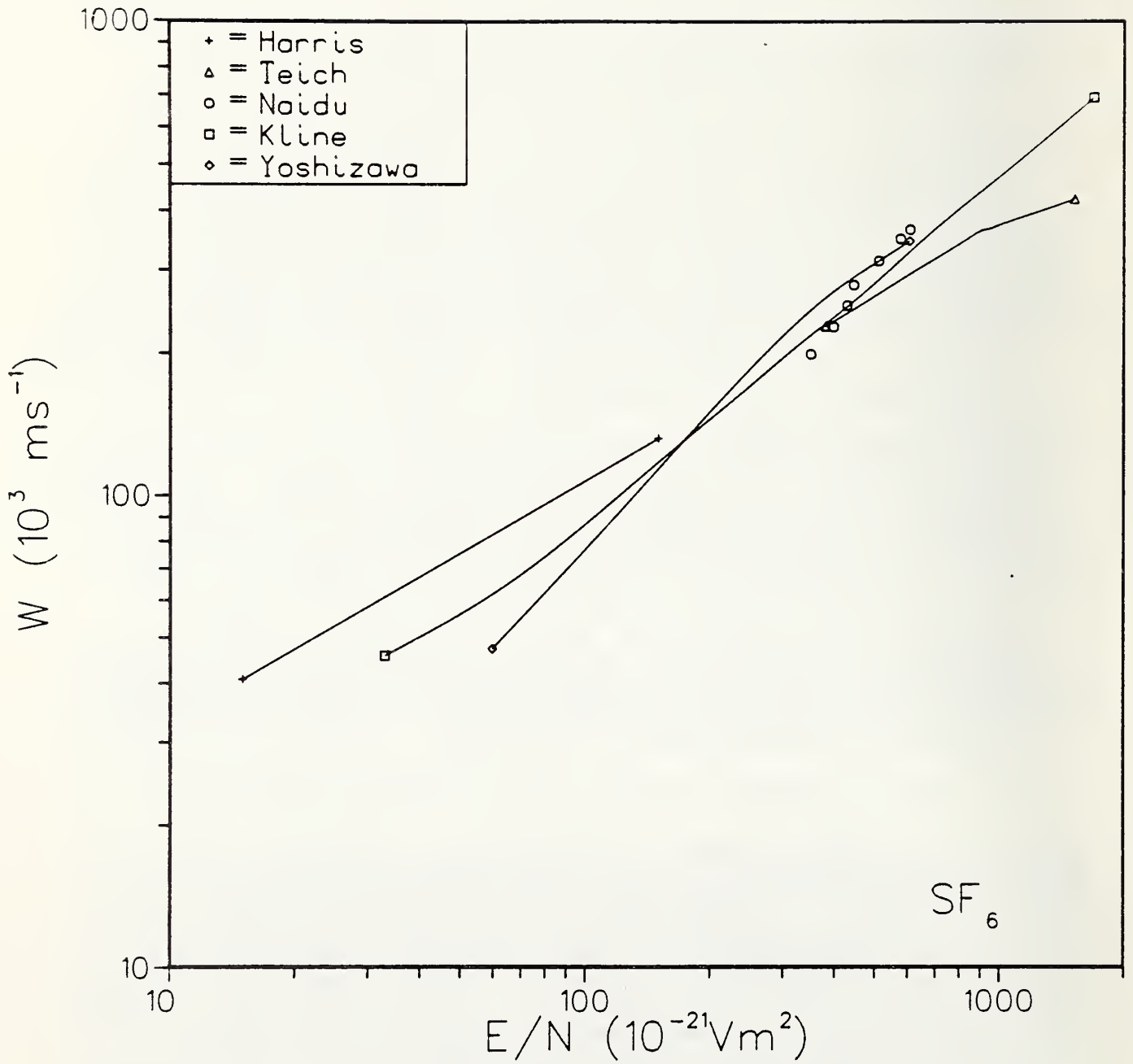


Figure 38. Electron drift velocity, W , for electrons in SF_6 as a function of E/N .

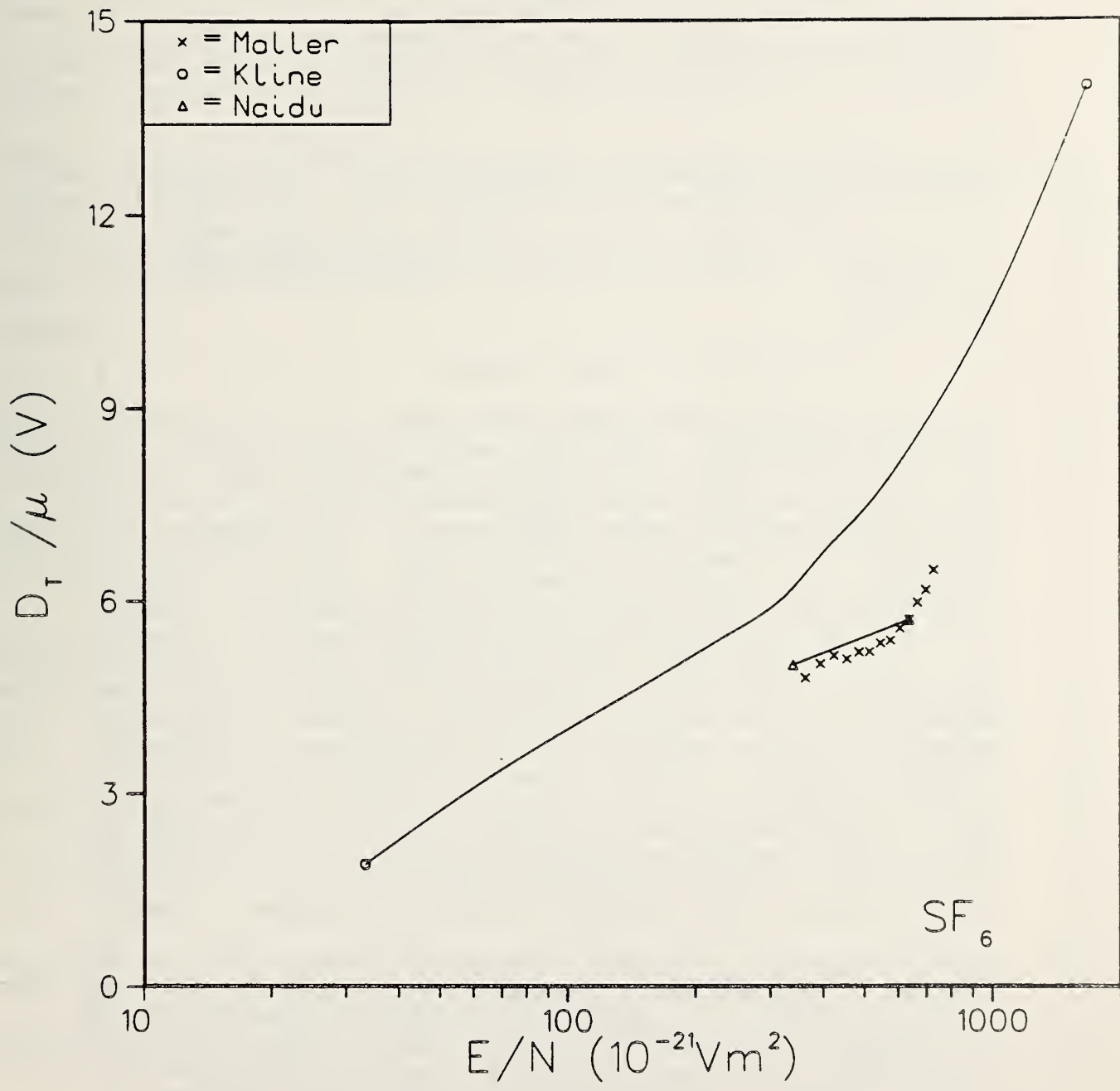


Figure 39. Ratio of diffusion to mobility, D_T/μ , for electrons in SF_6 as a function of E/N .

No direct experimental data are available on the diffusion coefficient for electrons in SF₆. Yoshizawa et al. included diffusion coefficient calculations as part of their Boltzmann equation analysis. As with drift velocity, data were calculated using several definitions, but in this case the different definitions yield data which vary only slightly (for the relatively low values of E/N investigated). Figure 40 includes the results which they label as D_L and D_T values appropriate to a steady-state Townsend discharge.

Also included in figure 40 are values of DN which were calculated from the W and D/μ values reported by Kline and co-workers. What appears to be "noise" in these data arose from reading a rather small logarithmic graph. At low E/N these results are not significantly in disagreement with those of Yoshizawa. At high E/N the Kline data must be considered uncertain because of the way in which the effect of new electrons produced by ionization was handled.

II.D.4.3 Electron Gain and Loss Processes

SF₆ is known to have a very large cross section at low energies for attaching electrons to make SF₆⁻. Kline and co-workers report that this cross section is $5.5 \times 10^{-10} \text{ m}^2$ at 0.01 eV. They conclude that at higher energies the cross section falls rapidly, decreasing to $3 \times 10^{-12} \text{ m}^2$ at 0.3 eV. Chutjian [69] reported further measurements at very low energy which offer the possibility of being more reliable. Above about 0.3 eV dissociative attachment is the dominant attachment process. Fehsenfeld has reported in a conference paper [70] that the zero field attachment rate constant is $2.2 \times 10^{-7} \text{ cm}^3/\text{s}$ at temperatures in the range 290-500 K. Crompton et al. [71] recently gave a preliminary report of a more precise experimental method which yields a similar conclusion. In view of the weak temperature dependence k_2 can be expected to be weakly dependent on E/N for small E/N. Fehsenfeld found the reaction rate to be proportional to gas density indicating a two-body reaction. Actually a two-step process is involved with the initial attachment collision producing an excited negative ion. For the gas densities normally used in electron swarm and gas discharge work, there is a high probability that the excited state will be collisionally quenched [21]. Foster and Beauchamp [72] reported that at low densities radiative decay is also important in stabilizing excited SF₆ negative ions.

Several dissociative attachment processes are known to occur in SF₆, producing a variety of negative ions. Kline et al. report that for the energy range 0.3-2.5 eV, the dominant negative ion is SF₅⁻ and above about 2.5 eV, it is F⁻. Other ions formed are SF₄⁻, F₂⁻, and SF₂⁻, none of which are dominant at any energy. The principal reason for concern with the identity of the ions is the impact on interpreting data relating to detachment.

Most of the available data on electron reactions in SF₆ have come from analysis of spatial current growth in Townsend discharges. The first electron swarm data on SF₆ were reported by Hochber and Sandberg [73], who gave values of the ionization coefficient inferred from observations of a Townsend discharge. However, their analysis did not recognize the possibility of electron attachment. Data on SF₆ including attachment were obtained by Geballe and Harrison (as reported by Loeb [74]) and by Bhalla and Craggs [42], and these results are given in figures 41-43. In the case of the attachment coefficient, displayed in figure 41, some of the data points of Bhalla and Craggs fall below the

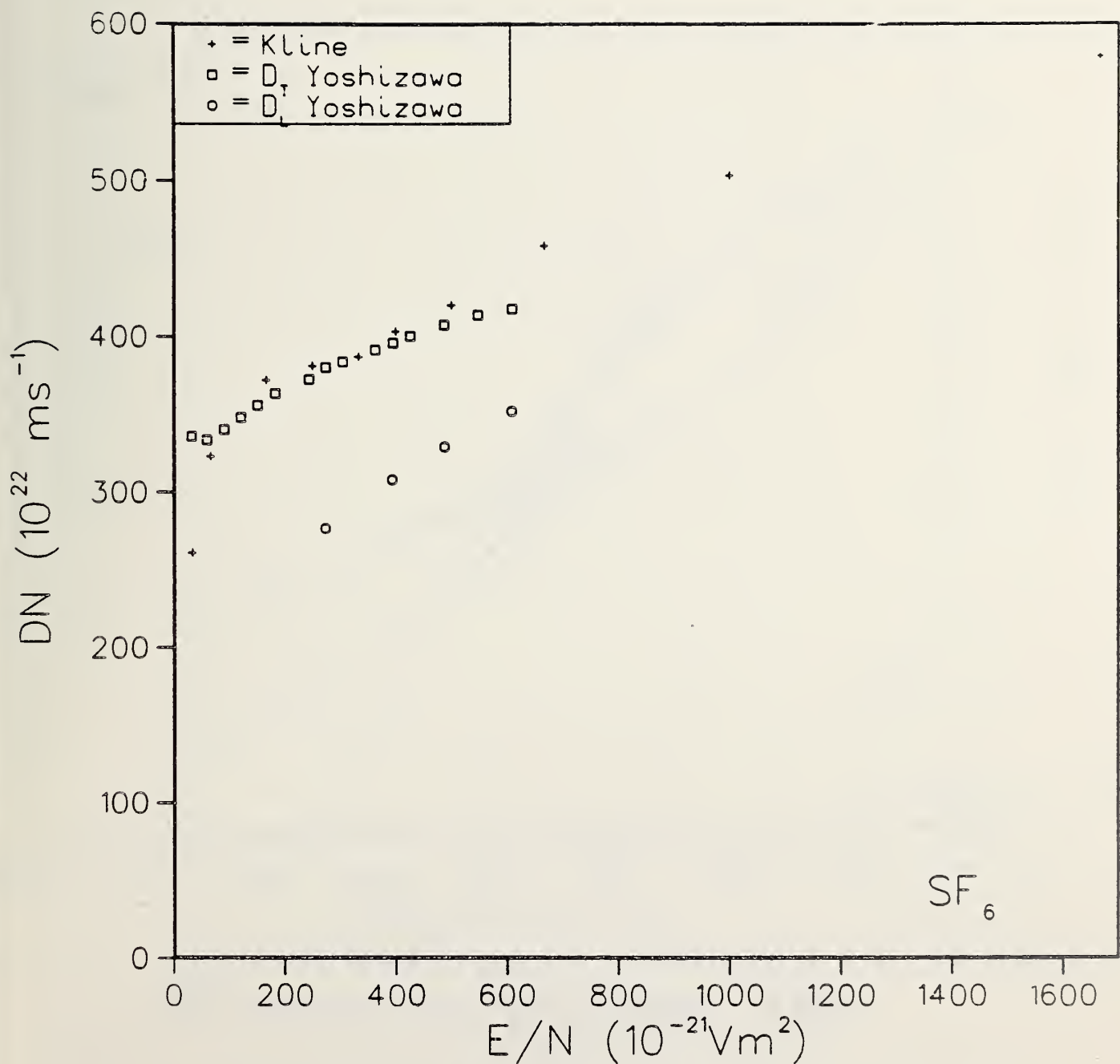


Figure 40. Diffusion coefficients for electrons in SF₆ as a function of E/N.

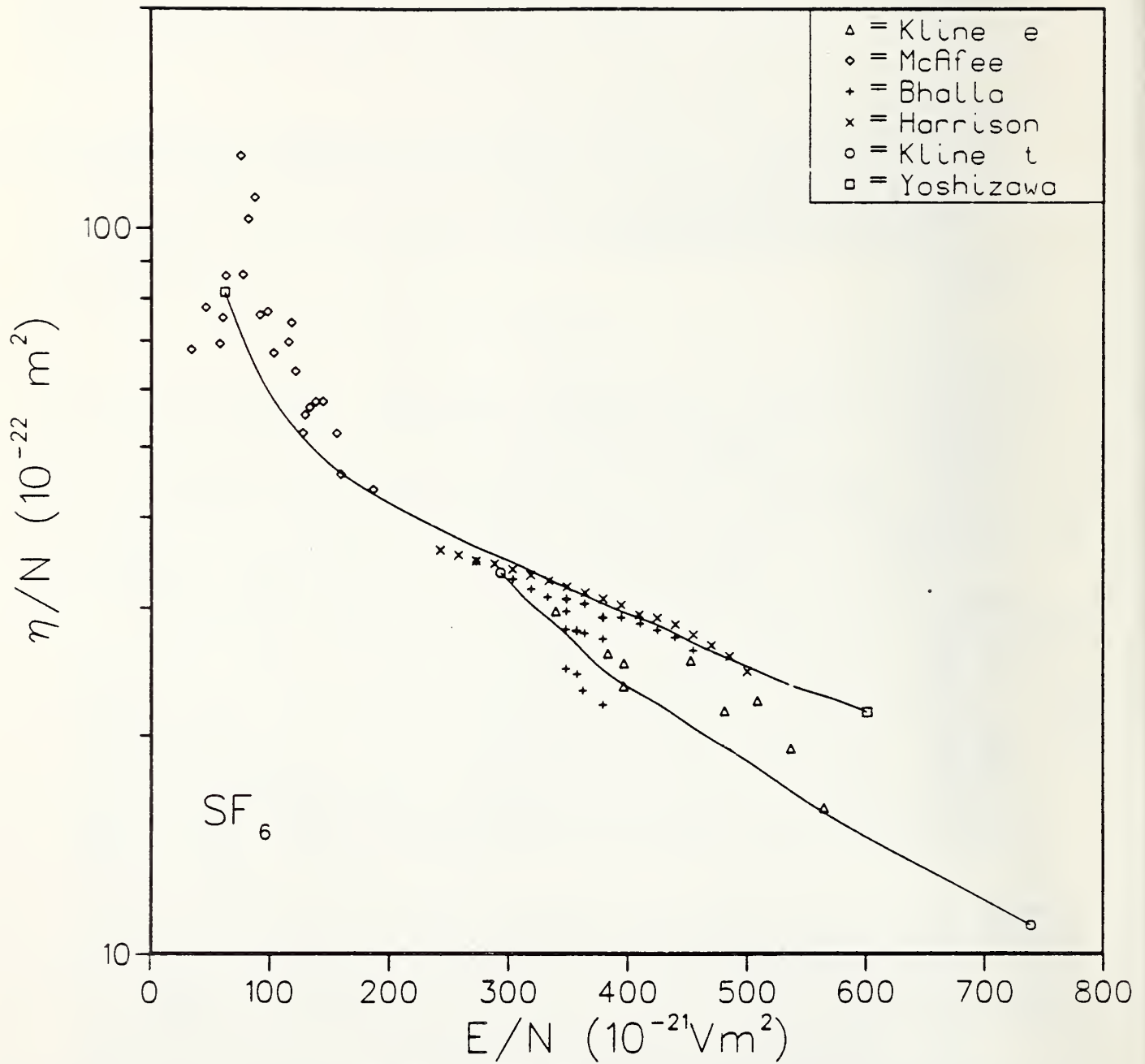


Figure 41. Attachment coefficient for electrons in SF_6 as a function of E/N .

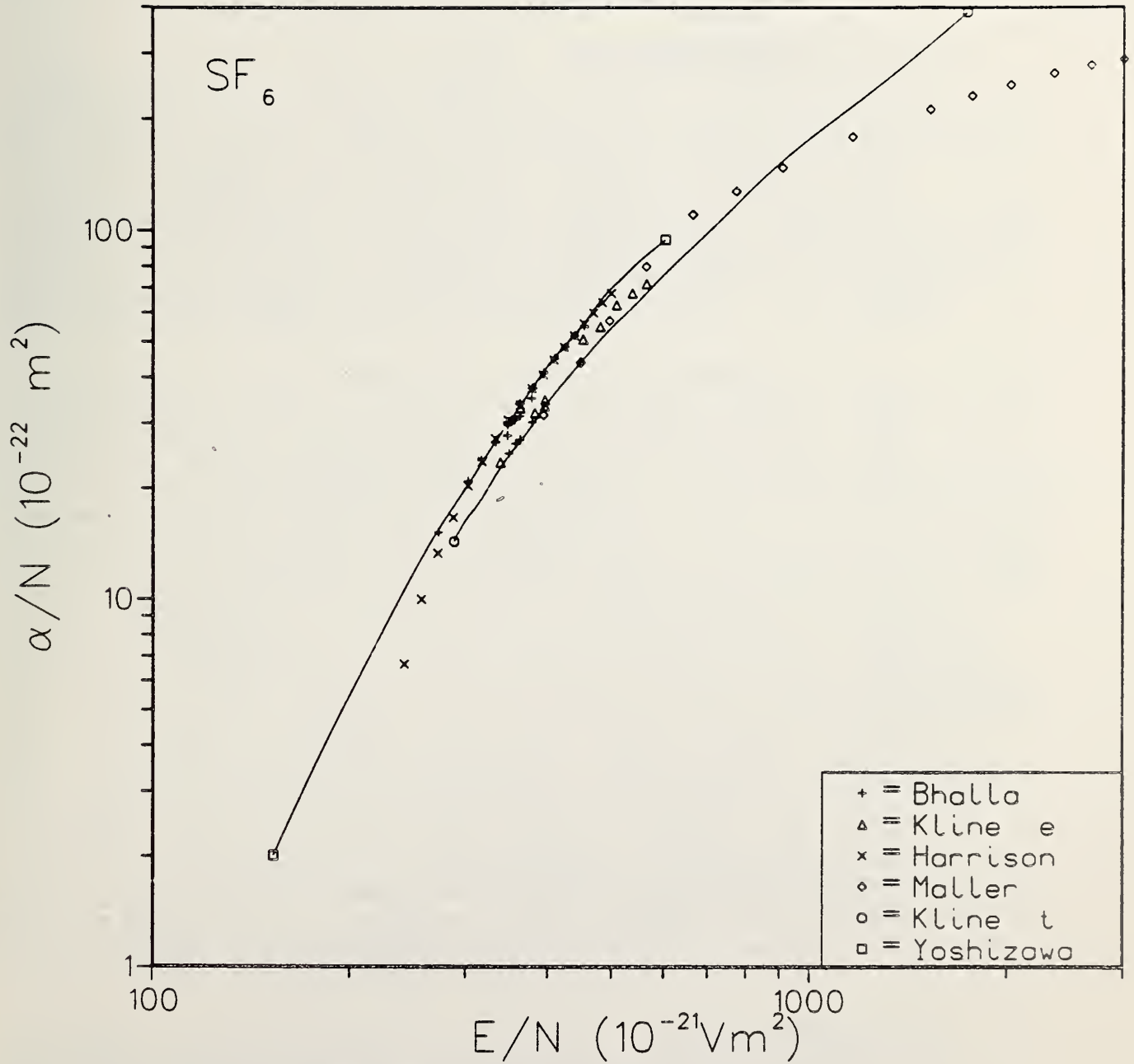


Figure 42. Ionization coefficient for electrons in SF₆ as a function of E/N.

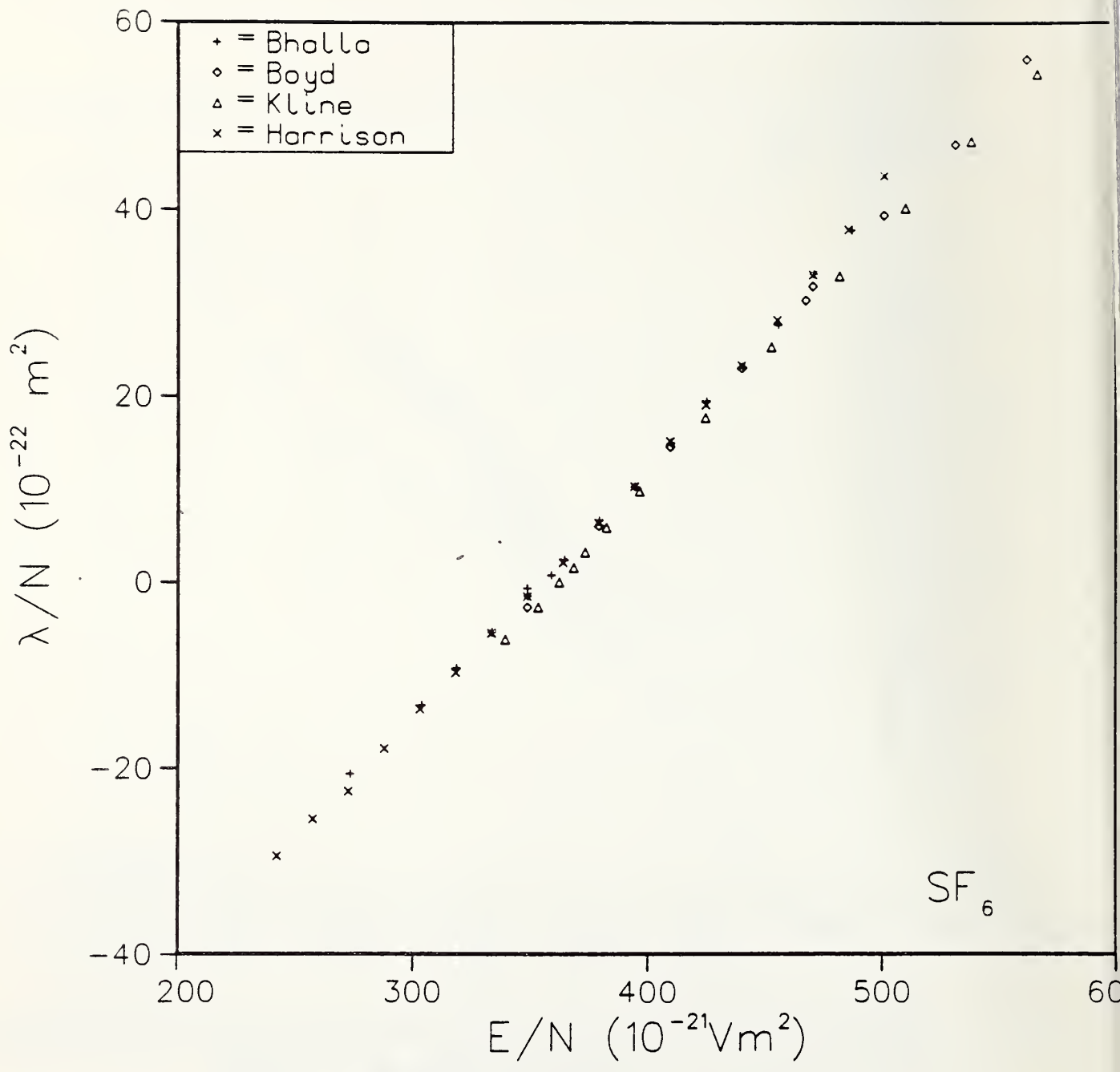


Figure 43. Electron growth constant (net ionization coefficient) for electrons in SF₆ as a function of E/N.

pattern of other results. These are distinguishable from the other data because of experimental circumstances and are considered as inferior and rejected. We include them because they illustrate a problem with the method. While the cathode current is not a directly desired result of the measurements, it is needed as part of the data analysis. Cathode current is normally assumed to be constant as the electrode separation is changed, and indirect measurements are used to infer its value. For some of their data, Bhalla and Craggs determined the cathode current as part of the data-fitting procedure with the result that low values of η_a were derived.

Kline and co-workers [64] also reported values of α_j , η_a , and λ derived from an analysis of a Townsend discharge. Here η_a is the "effective attachment coefficient" which includes the effect of detachment. These data were obtained using the methods of Davies [75], in which the possibility of collisional detachment is considered, and probably the most reliable available in the E/N range 200 to 600 x 10⁻²¹ Vm². Special consideration was given to determination of the E/N value which yielded $\lambda = 0$, because for this case it is only necessary to distinguish whether the net electron growth is positive or negative, and a complete quantitative analysis is unnecessary. The reported zero-growth value of E/N is 362 x 10²¹ Vm². These data for η_a/N , α_j/N , and λ/N are displayed in figures 41-43.

In 1955 McAfee [76] reported results on electron attachment in SF₆ which involved examining the transient currents following a pulse of light in a Townsend discharge. These data were described as preliminary, and as later results from the same experimental group are significantly different, we assume that the 1955 data have been superseded. In 1963 McAfee and Edelson [77] reported attachment coefficient data in SF₆ derived from a pulsed Townsend discharge, but with no description of experimental or data analysis techniques. In 1964 Edelson and McAfee [78] reported a detailed description of their data analysis techniques and used the 1963 SF₆ attachment data as an illustration. In this technique it is relatively easy to distinguish the electron and negative ion components of the total current, and unlike the steady-state situation, attachment produces an observable effect even without ionization. More generally, the transient currents provide much more detailed information about a variety of processes. By doing an extensive statistical analysis of their data, Edelson and McAfee were able to provide direct evidence that their derived coefficients are statistically significant. These attachment data, displayed in figure 41, are the only data available at low E/N. The maximum in η_a/N must be treated with caution. Although from the point of view of the data analysis it is statistically significant, a systematic error which varies with E/N is possible. As E/N tends to zero the drift velocity tends to zero, but the reaction rate constant remains non-zero. The result is that η_a/N tends to infinity as E/N tends to zero. A local maximum such as found by Edelson and McAfee must reflect an unusual behavior in either k_2 or W .

Samples of some of the other data available from steady-state Townsend discharges are also displayed in the figures. Boyd and Crichton [79] repeated the steady-state Townsend measurements with careful attention to detail and report data for α_j , η_a , and λ . Their measurements covered a wide range of gas density and lead to the conclusion that the swarm coefficients are proportional to gas density, a conclusion which is no longer contested. Their reported data are not significantly different from those of Harrison and Geballe. Their values for λ/N are included in figure 43.

Maller and Naidu [38] also extended the steady-state Townsend technique. In 1975 they reported values of α_i and η_a for mixtures of SF₆ with other gases. In 1976 data on pure SF₆ were reported which are extended to higher values of E/N than previous data. Their data on α_i/N are included in figure 42. Figures 41 and 42 also show values calculated by Kline and co-workers [64] and by Yoshizawa and co-workers [65]. These calculations assume that a consistent set of cross sections can be found which give agreement between measured and calculated swarm parameters, rather than providing an independent theoretical confirmation of experimental values.

Some other data have been reported but not included in figures 41-43. Bortnik and Panoff [43] reported Townsend discharge measurements, the results of which are shown in figure 33, and seen to be similar to those displayed here in figure 42. Dutton, Harris, and Jones [80] also reported studies of current growth in a Townsend discharge but with a tentative conclusion that the swarm coefficients were not linear in the gas density, a conclusion which is not supported by other data. Many investigations have been carried out on steady-state Townsend discharges in SF₆ and, in general, the data are remarkably consistent. There may be, however, difficulties at large values of E/N. As was already shown in figure 33, results for λ obtained by Sangi [41] depart significantly from the results implied by the data of Maller and Naidu [38] at high E/N. Moreover, the calculated results of Yoshizawa and co-workers [65] appear in figure 42 to show poorer agreement with the Maller and Naidu data for $E/N > 1 \times 10^{-18} \text{ Vm}^2$.

Application of the pulsed Townsend technique at high E/N requires a very rapid light pulse. Teich and Branston [81] used this technique in SF₆ with a laser as a light source, but were unable to account for all the phenomena contributing to their transient currents. They reached a general conclusion that detachment is an important process in SF₆ at pressures above about 5 torr (0.67 kPa), but did not report detachment data. In some special circumstances the observations could be interpreted adequately to yield values of λ in the range $108-130 \times 10^{-21} \text{ Vm}^2$. The results of this measurement are not significantly different from those obtained from the steady-state Townsend method.

Eccles et al. [52] reported detachment data, but with no identification of the detaching ion species. The relative ion concentrations change with N and E/N. Their principal conclusion is that for sufficiently low E/N the detachment coefficient is so small that it is negligible in the analysis of steady-state Townsend currents. As previously noted, however, (see Sec. II.C.6), more recent determinations of the detachment coefficient for SF₆⁻ in SF₆ by O'Neill and Craggs [53] indicate that the assumption $\delta_d/N \ll \eta_a/N$ cannot be assured once $E/N > 1.4 (E/N)_c$, where $(E/N)_c$ corresponds to the point where $\eta_a = \alpha_i$. To obtain detachment data, O'Neill and Craggs [53] used a double-gas drift tube arrangement in which negative ions were formed by attachment in the first chamber and detached in the second. Negative ions reaching the anode were identified by mass analysis. The density dependence of the anode current implied that either the detachment was not a two-body process or that the detaching species were involved in some other competing process, the rate of which depended on N. The detachment coefficient for SF₆⁻ was determined from the analysis of the negative-ion current and the current growth curves utilizing a reaction scheme including attachment, ionization, detachment, and charge transfer and ion-conversion reactions involving SF₅⁻ and F⁻ as well as SF₆⁻. It was estimated to be $0.8 \times 10^{-22} \text{ m}^2$ for $E/N = 233 \times 10^{-21} \text{ Vm}^2$ and $N = 16 \times 10^{22} \text{ m}^{-3}$.

Except for the work of Kline et al., analyses of steady-state Townsend data have included the assumption that electron detachment does not occur. In SF₆ it is quite likely that more than one negative ion species is created, and some of these may be in excited states. Following attachment, any excitation can be expected to decay and ion-molecule reactions will produce other ion species. Additional data on the detachment coefficients which include specification of the ion species and the state of excitation are needed in SF₆.

II.E. Chemical Diagnostics Development

II.E.1 Motivation

It has been the purpose of this activity to examine and evaluate sensitive chemical diagnostic techniques that can be applied to study the degradation of gaseous dielectrics under conditions of high electrical stress. Of concern here are conditions under which the rates of gaseous decomposition are relatively slow such as might occur in the presence of a low-level corona discharge. Excluded from this study are the effects associated with sudden, extraordinary stresses such as correspond to an arc discharge. A number of studies of arc-induced decomposition of SF₆ have already been reported in the literature [2]. It is the intent of this work to provide information that might prove useful in the design of tests to evaluate long-term chemical stability of gaseous dielectrics. The focus has been on SF₆ since this serves as a kind of reference gas.

In this report we examine the feasibility of using a highly sensitive measurement of the dielectric constant as a means of monitoring the content of polar contaminants such as H₂O and HF in gaseous SF₆. We also report on the results of measuring the discharge power dependence of the rates of H₂O and oxyfluoride production from corona in SF₆. A gas chromatograph-mass spectrometer (GC/MS) was used to perform the chemical analysis in these experiments. This latter activity is an extension of work previously reported [13-15].

II.E.2 Effects of Polar Contaminants on the SF₆ Dielectric Constant

There exists within NBS the capability of measuring the low frequency (static) dielectric constants and dielectric losses in insulating materials subjected to high voltages to an accuracy of 1 ppm [82]. The technique has been applied to measurements of dielectric properties of insulating materials at cryogenic temperatures [83]. In the case of gaseous dielectrics, one is motivated to consider the technique of accurate dielectric constant measurement as a way of detecting the buildup of polar gaseous contaminants which might result, for example, from corona-induced decomposition of the gas [1,15]. It may also serve as a convenient method for calibrating, or checking on the calibration of the measurement of H₂O content using a gas chromatograph-mass spectrometer for cases where this contaminant is introduced to study its effects on corona characteristics, electrical breakdown, etc.

Calculations are performed here to determine the sensitivity of the method. The question to be addressed is: given that one can detect a 1 ppm change in the dielectric constant of the gas, what would that indicate about the

change in polar contaminant concentrations, e.g., the amount of H₂O present? Would a precision measurement of the dielectric constant be an accurate indicator of polar contaminants?

We begin by considering the Debye expression for molar polarizability \underline{P} of a pure gas, namely [84],

$$\underline{P} = \frac{\epsilon - 1}{\epsilon + 2} V = \frac{4\pi N\alpha}{3} + \frac{4\pi N\mu^2}{9kT}, \quad (50)$$

where in this expression

ϵ = dielectric constant

V = molar volume = 22.414×10^3 cm³

α = molecular polarizability

μ = permanent molecular dipole moment

N = Avogadro's number = 6.02217×10^{23}

k = Boltzmann's constant = 1.3805×10^{-16} erg (K⁻¹)

T = temperature in K.

For a gas mixture consisting of several molecular species, each with a specified number density n_i , we can write

$$\begin{aligned} \frac{\epsilon - 1}{\epsilon + 2} &= \frac{4\pi}{3} \sum_i (n_i \alpha_i + \frac{n_i \mu_i^2}{3kT}) \\ &= \frac{4\pi}{3} \sum_i n_i g_i(T), \end{aligned} \quad (51)$$

where $g_i(T) \equiv \alpha_i + \mu_i^2/3kT$.

Solving for the dielectric constant ϵ gives

$$\epsilon = (1 + \frac{8\pi}{3} \sum_i n_i g_i) / (1 - \frac{4\pi}{3} \sum_i n_i g_i). \quad (52)$$

Now consider a variation δn_i in the molecular number density of the i th species. By taking the partial derivative of eq (52) with respect to n_i , we can find the fractional change in the dielectric constant resulting from δn_i . Thus,

$$\delta\epsilon/\epsilon = 4\pi g_i \delta n_i / \left\{ \left(1 + \frac{8\pi}{3} \sum_i g_i n_i \right) \left(1 - \frac{4\pi}{3} \sum_i g_i n_i \right) \right\}. \quad (53)$$

This is a general expression relating changes in dielectric constant to changes in the concentration of a particular component in a gas mixture. For most gases this expression can be greatly simplified by noting that $(\epsilon - 1) \ll 1$, e.g., for gaseous SF_6 at a pressure of 100 kPa (~ 1 atm) and at a temperature of 24°C , $\epsilon - 1 = 0.00205$ (see [85] and [86]). In this approximation eq (51) reduces to

$$\epsilon - 1 = 4\pi \sum_i n_i g_i(T), \quad (54)$$

and eq (53) is replaced by

$$\frac{\delta\epsilon}{\epsilon} = 4\pi g_i(T) \delta n_i, \quad (55)$$

where again only the i th component is assumed to change.

Now if we let ϵ_i be the known reduced dielectric constant of the i th component of the gas at $T = 300^\circ\text{K}$ and at atmospheric pressure (100 kPa), then another more convenient expression employing the above approximation is

$$\frac{\delta P_i}{P} = \frac{P'/P}{(\epsilon_i - 1)} \frac{\delta\epsilon}{\epsilon}, \quad (56)$$

where $P' = 100$ kPa, P is the total gas pressure given by $P = \sum_i P_i$, and the ideal gas law has been assumed, i.e.,

$$n_i = P_i/kT. \quad (57)$$

From eq (56) above we can find the change in partial pressure δP_i of the i th species that would correspond to a measured fractional change $\delta\epsilon/\epsilon$ in the dielectric constant. Assuming now that existing instrumentation allows for a sensitivity of 1 ppm, we have $\delta\epsilon/\epsilon = 10^{-6}$. It should next be noted that the sensitivity for detection of a particular species is proportional to the factor $1/(\epsilon_i - 1)$. Therefore, the sensitivity for detection increases as the amount by which the reduced dielectric constant of the species differs from unity increases. As shown in table III, species with relatively large permanent dipole moments μ_i tend to have larger values for ϵ_i ; thus, they can be detected with greater sensitivity than species having low values for μ_i . Also shown in table I are the predicted sensitivities in ppm for detection of various species derived from the ratio of partial pressure to an assumed total pressure of 100 kPa found using eq (56) with $\delta\epsilon/\epsilon = 10^{-6}$. It is seen that the highly polar species such as H_2O , HF , and SO_2 can be detected at the level of $\sim 0.1\%$ concentration by partial pressure, whereas, nonpolar species like CF_4 and CO_2 can only be detected at roughly the 1% level.

Table III

Dipole moments, calculated dielectric constants at 20°C and 100 kPa, and calculated detection sensitivities for SF₆ and contaminants commonly observed in SF₆ after electric discharges.

<u>Gas</u>	<u>Dipole Moment (μ) in debyes</u>	<u>Reduced Dielectric Constant(ϵ)</u>	<u>Calculated Detection Sensitivity (ppm)</u>
SF ₆	0.1	1.00205	490
H ₂ O	1.85	1.00984	102
SO ₂ F ₂	0.23	1.0002 ^a	5000
SO ₂	1.63	1.00864	116
CF ₄	0.0	1.00130	768
COS	0.67	1.0031	318
HF	1.91	1.0120 ^a	83
CO ₂	0.00	1.00092	1087

^aPossible large uncertainties due to lack of reliable data on molecular polarizability.

The predicted sensitivity is thus considerably below that of a gas chromatograph-mass spectrometer, but it is comparable, for example, to infrared absorption spectroscopy. The other disadvantage of the technique considered here is that it does not identify the contaminant species. It merely indicates the change in polar gas content. Moreover, to achieve even a 0.1% sensitivity, it would be necessary to construct a highly stable gas capacitor. The estimates made here suggest that the technique is perhaps most useful as a supplementary way of checking on the calibration of other analytical devices for polar gases like H₂O and HF for which there may be special problems in achieving the desired accuracy even at relatively high concentration levels. No specific plans exist at present to apply this method in our laboratory, although further consideration will be given to its use in monitoring H₂O for experiments in which the effects of this gas on discharge characteristics are studied.

II.E.3 Production of Oxyfluorides and Water Vapor From Corona Discharges in SF₆

The rates of production of the by-products generated in a corona discharge were measured for SF₆ at an absolute pressure of 200 kPa (~2 atm) for average discharge power levels in the range of 50 to 670 mW with polished stainless steel, point-plane electrodes. The volume of the test cell was 4.0 liters and the corona was operated at constant current for a positive dc-voltage applied to the plane electrode. The currents used were within the range of 1.5 to 16.0 μ A. A gas chromatograph-mass spectrometer (GC/MS), details of which have previously been discussed [15], was used to monitor the concentrations of H₂O, SOF₂ (thionylfluoride) and SO₂F₂ (sulfurylfluoride) as a function of time. The concentrations of the latter two compounds could be determined quantitatively with a sensitivity of about 1 ppm. During this year, improvements were made in the analytical procedure which enabled us to obtain data on trace gas concentrations in SF₆. These more recent data are considered to be more reliable than those we previously reported [15]. Nevertheless, more work is required before we can confidently assign uncertainties to the results reported here which must, therefore, be considered preliminary. As might be expected, the uncertainties are greatest at the lowest concentrations but in no case do we believe they are greater than \pm 50% of the measured value. To assure reliability in the quantitative analysis, the GC/MS was calibrated before and after each corona degradation experiment using several individually prepared standard samples of SOF₂ and SO₂F₂ in SF₆.

Thus far we have not succeeded in preparing reliable standard samples having known amounts of H₂O in SF₆. Therefore, only relative concentrations of H₂O could be determined with the present system. It is believed that H₂O is produced by discharge-induced desorption from the electrode surface. Its concentration builds up rapidly with time at first and then levels off, reaching roughly a constant value independent of discharge power. This is illustrated by the data shown in figure 44 which shows relative concentrations of H₂O as a function of total energy dissipated in the discharge at the indicated power levels. There is some indication from these data that the H₂O concentration initially builds up more rapidly at the higher discharge power levels. The accumulated time that the discharge was maintained is, in each case, given by the product of the energy dissipated and the reciprocal of the power.

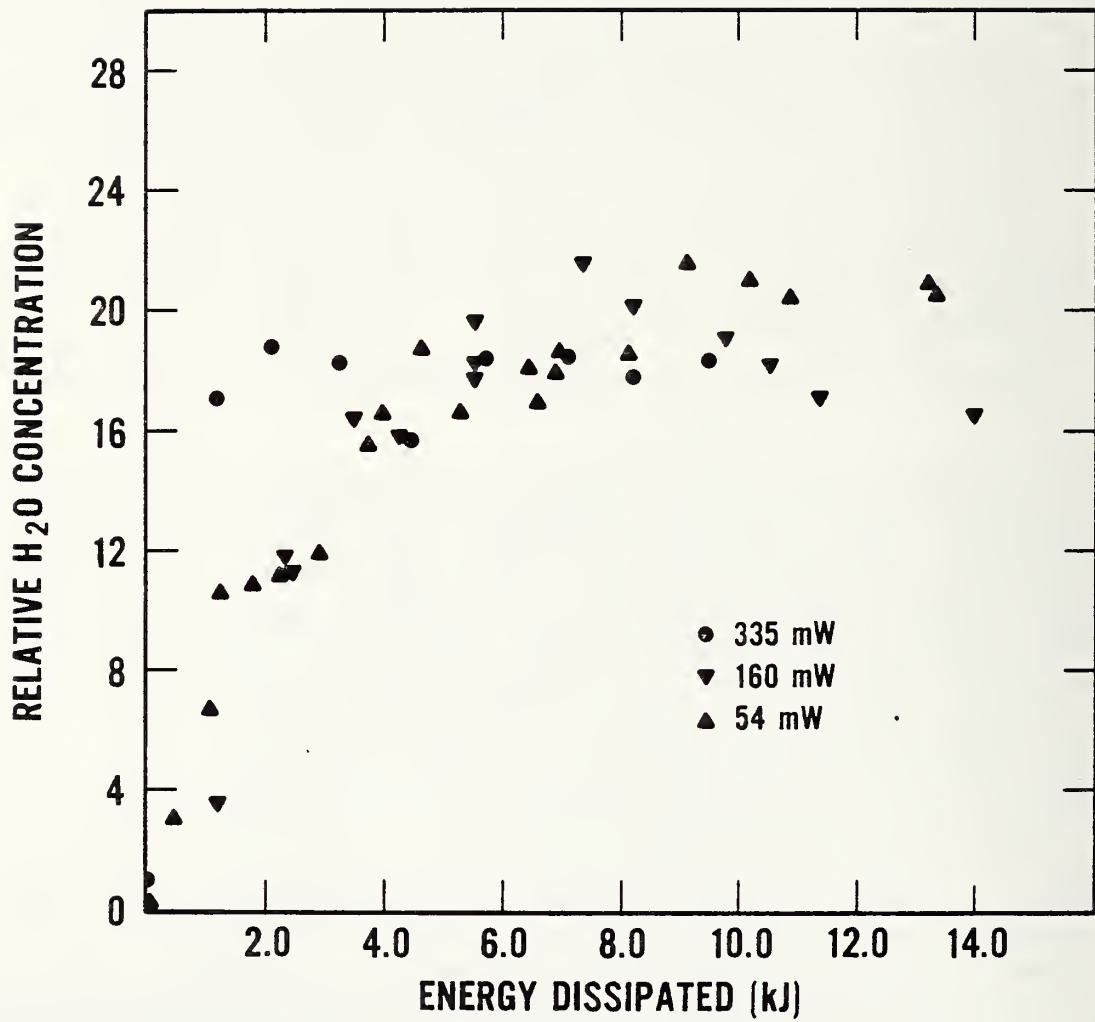


Figure 44. Relative concentration of H₂O in SF₆ as a function of energy dissipated by a positive dc corona discharge for the indicated discharge power levels.

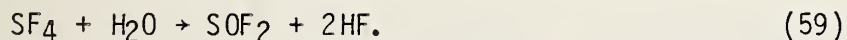
It has been hypothesized [2,14,15,87] that SOF_2 results primarily from hydrolysis of the primary decomposition product SF_4 , whereas, SO_2F_2 is generated within the discharge via reactions of sulfurylfluorides with free oxygen and H_2O . After arc discharges have occurred in SF_6 , the species SO_2F_2 has been observed [1,87] to be absent, or of very low concentration compared to SOF_2 .

The results of our measurements of SOF_2 and SO_2F_2 concentrations as a function of the net energy dissipated for three different power levels are shown in figure 45. The net energy $U(t)$ dissipated in the discharge at time t was found using the relationship

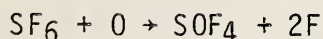
$$U(t) = I \int_0^t V(t') dt', \quad (58)$$

where I is the discharge current and $V(t')$ is the voltage across the cell.

The significant conclusions from these results are: a) the production rates of SOF_2 and SO_2F_2 are nearly constant, at least up to concentrations of 200 ppm, and roughly proportional to the power dissipated, and b) SOF_2 and SO_2F_2 appear with nearly equal concentrations. The fact that SO_2F_2 is produced with much more relative abundance in a corona discharge than in an arc is interesting, and possible reasons for this important observation need to be explored. It has been suggested, for example, by Becher and Massonne [1] that in an arc the predominant reactions are with vaporized electrode metal which always yield metal fluorides, SF_4 , and subsequently SOF_2 via the reaction



In a low power discharge like corona, on the other hand, free oxygen radicals are presumed to be present to a higher degree and thus give rise to SO_2F_2 production through reactions like



In the present work, the presence of SOF_4 could be detected, although its absolute concentration could not be determined due to lack of a reliable standard sample. Methods of indirectly calibrating the GC/MS for SOF_4 are being explored. It should also be noted that no attempt was made in the present experiments to monitor the HF concentration. It can presumably be estimated from data on SOF_2 , SO_2F_2 , and SOF_4 concentrations assuming the above reactions dominate.

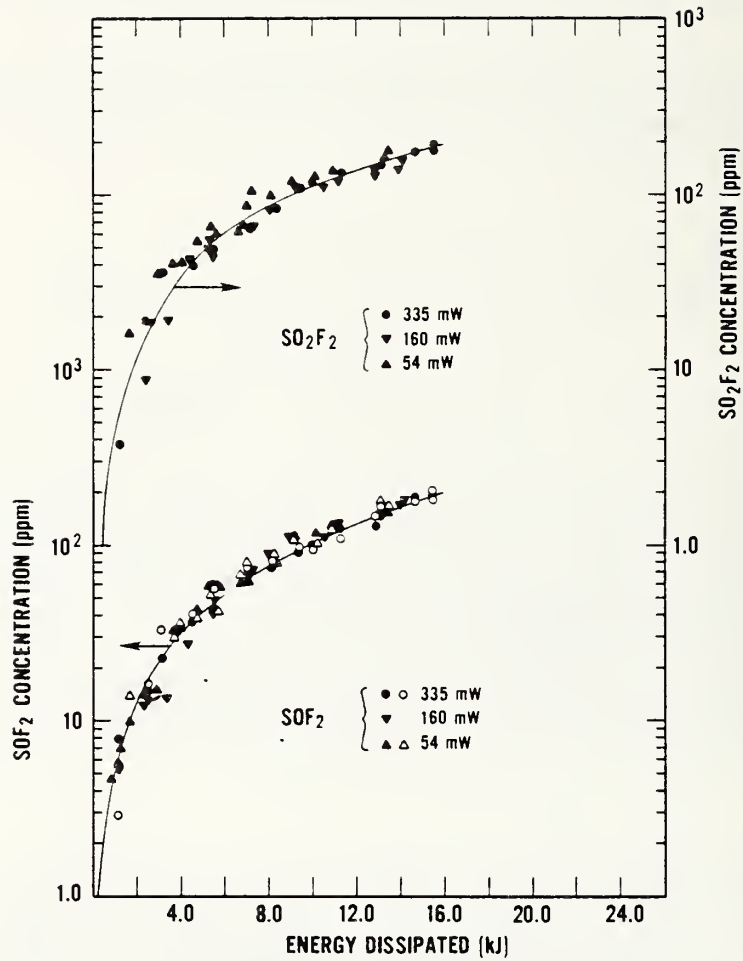


Figure 45. Measured concentrations of SOF₂ and SO₂F₂ as a function of net energy dissipated in corona discharges operated at the indicated power levels.

$A^* + h\nu \rightarrow A^{**} \rightarrow A + h\nu'$ - optical pumping

$A^* + B \rightarrow A + B + (h\nu \text{ or kinetic energy})$ - collisional quenching.

In the above reactions, A is assumed to be an atomic species in the ground state, and A^* is the same species in a metastable excited state. Additional mechanisms are possible particularly if A and B are taken to be molecular species.

Although one must consider all of these processes in attempting to predict equilibrium concentrations of metastables in a discharge, it is clear that some are likely to be much more important than others. In the absence of external radiation, for example, the production of metastables is most likely dominated by processes involving collisions of electrons with ground state atoms (or molecules). When an external radiation source is introduced, the populations of metastables can be significantly affected by the optical pumping processes.

Monitoring the resultant change in discharge voltage as a function of an external radiation source forms the basis of optogalvanic spectroscopy. Earlier NBS reports [15] have described our efforts to evaluate optogalvanic spectroscopy as a diagnostic technique for better understanding the physics of corona discharges. Attempts were made to observe the optogalvanic effect in a steady corona discharge in N_2 using coaxial electrodes and in SF_6 using point-plane electrodes. Consistent with the lack of evidence for the existence of SF_6 metastables (see [49]), no optogalvanic signals were observed in the measurements using pure SF_6 . A change in corona current due to the presence of the incident laser light was detected in N_2 , but an optogalvanic signal in the form of discrete lines corresponding to electronic transitions in N_2 [94] was not observed.

During the past year we have used optogalvanic spectroscopy of glow discharges to make a preliminary examination of the possible quenching of metastable Ne atoms and N_2 molecules in the presence of SF_6 . We have also used this technique to determine if neon metastable atoms survive in high pressure glow discharges ($P \sim 100$ kPa). Both measurements are relevant to gaseous dielectric studies because they provide information about the influence of metastables on the level of ionization in gas discharges. The effect of metastable atoms has been shown to be important in model calculations of breakdown in SF_6/He mixtures [64] and metastable molecules appear to influence the development of streamers in air [89,91].

II.F.2 Apparatus and Experimental Results

The dye laser system for obtaining optogalvanic spectra is shown schematically in figure 46. The external light source was a tunable dye laser pumped by an argon-ion laser. The laser beam was chopped with a mechanical chopper wheel and directed into the discharge cell. A phase sensitive detector employing a lock-in amplifier was used to observe changes in the discharge voltage which occurred as the wavelength of the laser was varied. The output of the phase sensitive detector was plotted on an X-Y recorder. For the measurements reported here, the wavelength was scanned from 580 nm to 620 nm. The measurements were performed with a hollow cathode lamp which was fitted with a valve in order to change gases and vary the gas pressure. Thus,

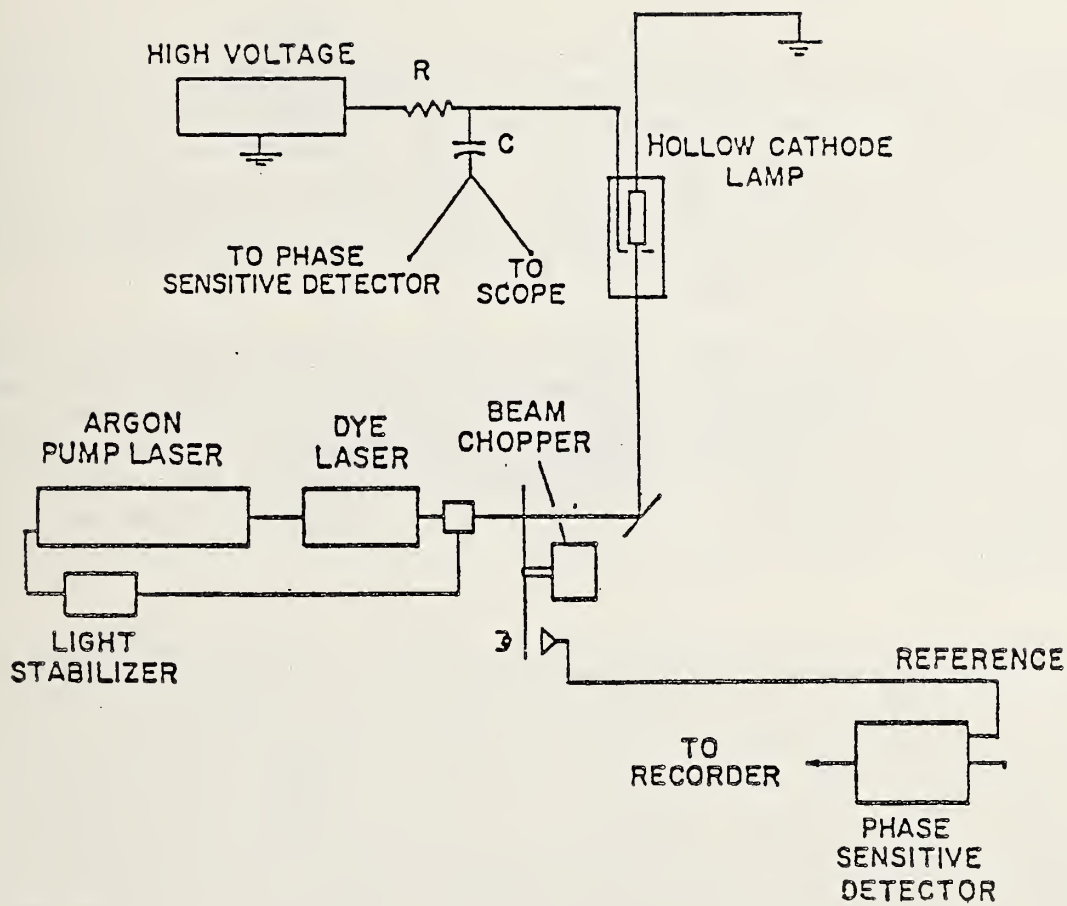


Figure 46. Schematic view of apparatus for performing optogalvanic measurements in a hollow cathode lamp.

all the data were obtained with static gases. Prior to the introduction of any gas, the hollow cathode lamp and associated gas lines were evacuated to a pressure of approximately 1.3×10^5 Pa ($\sim 1 \times 10^{-7}$ torr).

II.F.3 Low Pressure Measurements

II.F.3.1 Ne and Ne + SF₆

An optogalvanic spectrum obtained with research grade neon (99.999% cylinder purity) in a hollow cathode discharge is shown in figure 47. These measurements were performed in part to verify proper performance of the measuring system. The discharge current, laser power, and gas pressure are ~ 2.5 mA, 30 mW, and 677 Pa (5.1 torr), respectively. Spectroscopic lines which reveal the presence of the 3P_2 and 3P_0 metastable states in the discharge are indicated in figure 47. Lines which show the presence of the radiative 1P_1 and 3P_1 states are also shown [95].

Spectra obtained with small amounts of SF₆ (1 to 5%) mixtures with neon show no dramatic changes. For comparison, an optogalvanic spectrum of neon with 5% SF₆ is also presented in figure 47 for approximately the same current, laser power, and total gas pressure. The difference in line heights for the two spectra is not considered significant because some changes in line heights are observed to occur normally as a function of time due to changes in gas and electrode conditions which can happen during operation of the discharge.

The fact that the neon optogalvanic spectrum is largely unaffected by SF₆ is of some interest. Both metastable states of neon (3P_2 , 16.62 eV and 3P_0 , 16.72 eV) have electronic energies which overlap with the band of photoionization energies for the $3t_{1g}$ orbital of SF₆ centered near 16.96 eV and exceed the ionization energy of the $3t_{1u}$ orbital centered near 15.96 eV [96]. Penning ionization of either orbital is thus energetically possible. In addition, there are many states in SF₆ with excitation energies near those of the neon metastable atoms [49,97] and presumably some of these states could be excited via collisions with the metastable atoms. Our measurements suggest that both processes, as well as others [98] which could deplete the population of metastable atoms and affect the discharge and associated optogalvanic spectrum, do not appear to have sufficiently large cross sections to have a measurable effect at the concentrations studied.

While the presence of SF₆ does not markedly affect the appearance of the spectra, the glow discharge was less stable and became noisier with time. Higher voltages were also required to obtain the same discharge current when SF₆ was added to the neon. A higher voltage is expected when an electronegative gas such as SF₆ is added to neon because the electron drift velocity is reduced due to temporary electron attachment to SF₆. This is equivalent to having electrons make more collisions with the non-attaching gas at some higher pressure [99]. Attempts to obtain optogalvanic spectra with 10% SF₆ were not successful because of excessive noise levels associated in part with oscillations in the discharge intensity. The cause of the noise was not investigated.

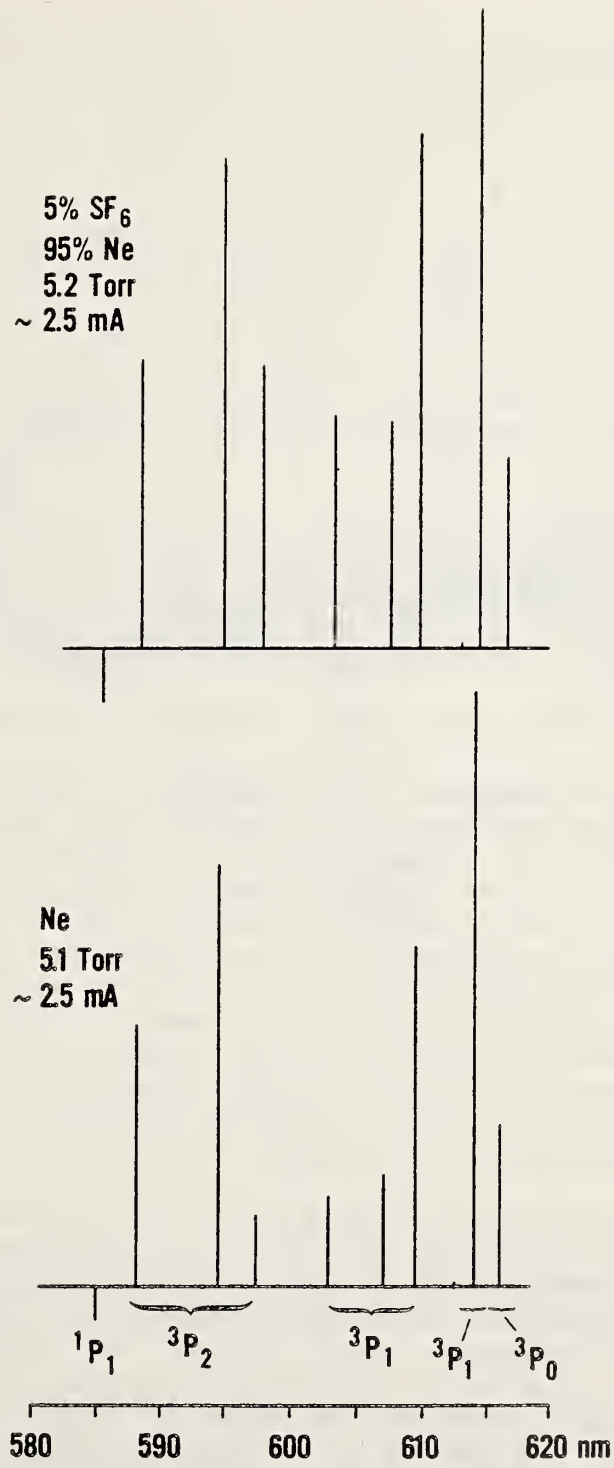


Figure 47. Optogalvanic spectra of neon and a mixture of neon with 5% SF₆ for comparable discharge current and gas pressure.

II.F.3.2 N₂ and N₂ + SF₆

Measurements of optogalvanic spectra in nitrogen (99.9995% cylinder purity) were more difficult than for neon. As has been noted previously in the literature [94], the nitrogen optogalvanic spectral lines are several orders of magnitude weaker than the neon metastable lines. Figure 48 shows a tracing of a portion of the N₂ spectra for a gas pressure of 320 Pa (2.4 Torr), discharge current of ~ 2.5 mA, and dye laser power near 400 mW. The results are complicated by the overlapping of the first positive band (B³Π_g ← A³Σ_u⁺) and the Ledbetter system (c₄¹Π_u ← ¹Σ_g⁺) [94,100]. Indicated in figure 48 are the (8,4) band head at 595.9 nm from the first positive system and the Q branch of the Ledbetter system at 597.7 nm. The structure to the left and right of the Q branch is due in part to the rotational lines of the R and P branches. The two states, A³Σ_u⁺ and ¹Σ_g⁺, which are optically pumped with the dye laser are metastable and lie 6.4 eV and 12.3 eV, respectively, above the ground state of N₂ [100,101].

Attempts to see the effects of SF₆ on the optogalvanic spectrum of N₂ were not very successful. While some indication of the Q branch of the Ledbetter system could be observed with a 1% mixture of SF₆ for a discharge current of ~ 1 mA, spectra at higher currents (e.g., ~ 2.5 mA, figure 48) could not be obtained because of electrical noise in the discharge.

II.F.4 Detection of Metastable Neon at Atmospheric Pressure

As noted earlier, the presence of electronically excited metastable atoms or molecules has been considered in calculations of the dielectric strength of gaseous insulators and the development of streamer formation in air. Because gas pressures of 100 kPa or more are normally considered in such problems, it is reasonable to examine whether metastable atoms or molecules, which are readily detected experimentally at low pressures, can survive quenching processes which are pressure dependent. With this question in mind, an effort was made to obtain optogalvanic spectra of neon at atmospheric pressure. Optical absorption measurements have revealed the presence of the ³P₂ metastable state of neon at pressures of ~ 40 kPa (~ 300 torr) and 53 kPa (400 torr) [102,103], and the vacuum-uv-emission data of Leichner [104,105] have implied the existence of the same state at pressures as high as 133 kPa (~ 1000 torr).

Figure 49 shows an optogalvanic spectrum of neon obtained with the hollow cathode lamp at a discharge current of 3.6 mA and pressure of 100 kPa. These results represent the first observation of the optogalvanic effect in a neon glow discharge at atmospheric pressure and directly indicate the presence of both Ne metastable atomic states. At such high pressures the appearance of the discharge is significantly modified from that at low pressure. A miniature negative glow region and a positive column of small diameter extend from the cathode to anode as sketched in the left inset of figure 49. The discharge was electrically very noisy and intermittent periods of high-frequency oscillations could be observed with an oscilloscope. The physical location of the negative glow-positive column combination would occasionally move, disrupting the measurements. Optogalvanic spectra were measurable only when the dye laser beam was incident on the negative-glow region. The data in figure 49 were obtained with a dye laser power of 150 mW for the first two lines (585.2 nm, 588.2 nm) and 110 mW for the remaining lines. The three strongest ³P₂ lines were truncated by the X-Y recorder.

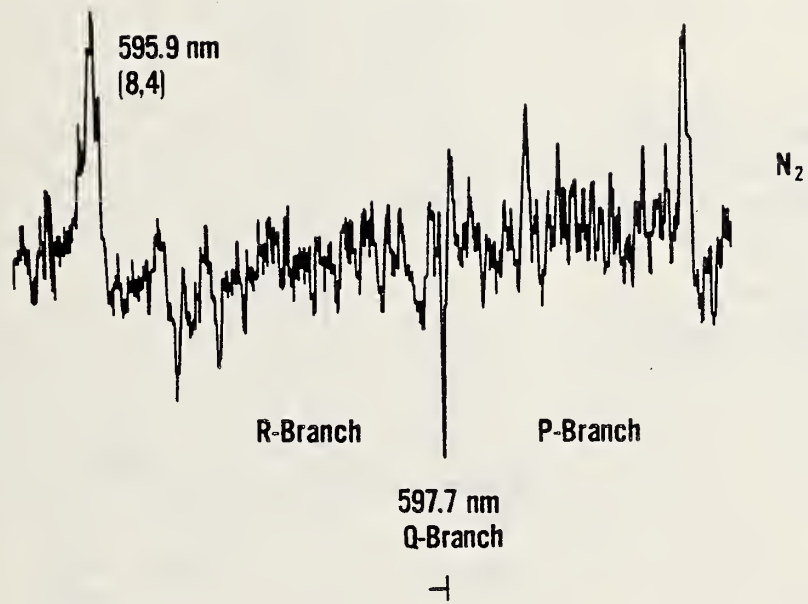


Figure 48. Optogalvanic spectrum for N₂ showing lines from the Ledbetter system and the (8,4) bandhead for the first positive system.

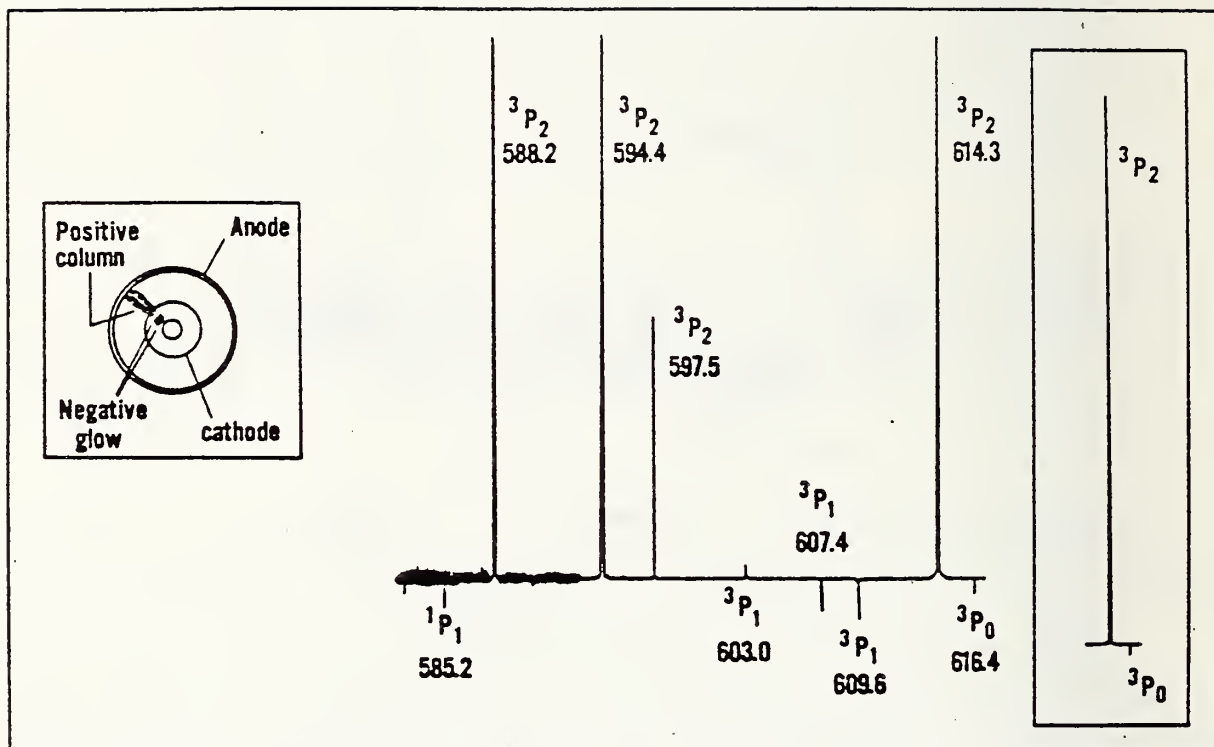


Figure 49. Measurement of neon optogalvanic spectrum at atmospheric pressure (100 kPa) and 3.6 mA discharge current. Optogalvanic transitions could be observed only in the negative glow region of the discharge.

Shown in the right inset of figure 49 are the relative line heights at 614.3 nm (3P_2) and 616.4 nm (3P_0). The initially noisy signal suddenly changed to one with high-frequency oscillations. Phase-sensitive detection permitted extraction of a relatively noise-free signal during this period of high-frequency oscillation.

Considerable information has been published in the literature regarding collisional destruction and creation processes in neon following pulsed discharges [102-108], but little appears to be known about why certain states are excited by a glow discharge and not others [93,107]. What figure 49 directly shows is that one of the metastable states of neon continues to be produced at atmospheric pressure (100 kPa) and significantly influences the degree of ionization in the discharge.

Specifically, as the number of 3P_2 metastable atoms are depleted by optical pumping, the level of ionization in the discharge is reduced leading to an increase in the discharge cell impedance. The voltage drop across the electrodes of the hollow cathode lamp increases and a positive optogalvanic signal is observed [92,93].

Care must be exercised in estimating the relative equilibrium densities of the various excited states from the optogalvanic spectra in figure 49. If the low pressure results of Zalewski, et al. [93] regarding abundances of the 1P_1 and 3P_2 excited states and corresponding line heights can be carried over to the present high pressure measurements, comparison of figures 47 and 49 suggests that at 100 kPa, a reduction in the number of atoms in the 1P_1 state has occurred relative to the 3P_2 state. This extrapolation is not without risk [109] and ignores, for example, the likely change in electron energy distribution that occurs at higher gas pressures and the resultant change in efficiency of ionization of the final states (i.e., $2p^53p$ configuration discussed below) excited by the dye laser.

The relative line heights of the 3P_1 (607.4 nm and 609.6 nm) and 3P_0 (616.4 nm) lines are also smaller when compared with the 3P_2 lines, but the change in sign at high pressure further complicates any interpretation regarding relative abundances of these excited states. Low pressure hollow cathode discharge measurements [95] indicate that sign changes occur for the noted lines but at higher discharge currents (e.g., ~ 15 mA for the 3P_0 line versus 3.6 mA at atmospheric pressure). The apparent discrepancy may be explained by the possible equivalence in current density for the high and low pressure measurements. As noted earlier, a constriction in the size of the discharge occurs at high pressure.

A model has been proposed which suggests that the gradual reduction in spectral line height and eventual sign change as the discharge current is increased is due to two types of competing processes following dye laser excitation [95]. The model is briefly explained for the 3P_2 state with the aid of a simplified energy level diagram for neon shown in figure 50. Optical pumping of the 3P_2 level produces transitions to states with the $1s^22s^22p^53p$ electron configuration. At low discharge currents these laser excited states radiate back to the $1s^22s^22p^53s$ levels with known branching ratios (optical transitions to the ground state are forbidden). Because some of the laser excited states decay to the 1P_1 and 3P_1 states, which in turn can radiate to the ground state, the net effect is a

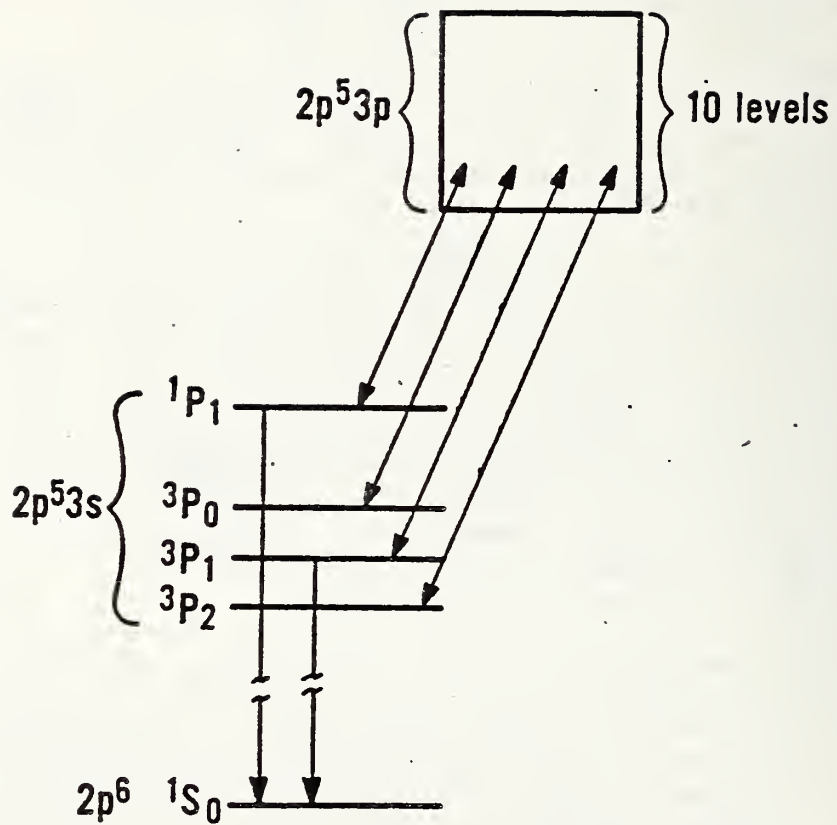


Figure 50. Simplified energy level diagram for neon. Optogalvanic signals are obtained when laser-induced transitions occur from the $2p^5 3s$ states to the $2p^5 3p$ manifold of excited states.

loss in the number of metastable atoms. As noted earlier, this reduces the level of ionization and produces a positive optogalvanic signal; i.e., it increases the impedance of the discharge cell with a resulting increase in voltage drop (see fig. 46). Again, a reduction in the ionization level is expected if the metastable population declines, since not only is ionization of metastables via electron collisions likely to be more probable than for ground state species, but additional processes such as Penning ionization and super elastic collisions can also enhance ionization. If ionization of metastables by electron collisions dominates, then a decline in the metastable population can be interpreted as giving a lower ionization coefficient for the gas (see Sec. II.B).

At higher discharge currents, a second competing process occurs after the $1s^2s^2p^53p$ states are excited. If the current is allowed to increase, there will be a resulting increase in the collision frequency of electrons with atoms in these states excited by the laser. Thus the likelihood will increase that ionization from these states will take place before they have an opportunity to radiatively decay to lower states. The resulting increase in ionization level reduces the voltage difference across the hollow cathode lamp electrodes and yields a negative optogalvanic signal.

Although the change in size of the signal associated with the 3P_0 state can be understood by this model, it is not clear that it can explain the observed sign reversal for transitions involving the 3P_1 state (see fig. 49). As shown in figure 50, this state is not considered to be metastable. In this case collisional processes that couple the 3P_1 state to the 3P_0 and 3P_2 states may also play a role [95]. Through coupling, population of the 3P_1 state will indirectly affect the population of the 3P_0 and 3P_2 states.

Consistent with the above model, sign reversal requires successively higher currents for the 609.6 nm, 607.4 nm, and 603.0 nm lines [95]. The data indicate that sign reversal occurred for the first two lines and the third line approached a near zero magnitude. Because, as shown in [95], the 3P_2 lines require greater discharge currents than the 3P_1 lines before sign reversal occurs, the 3P_2 positive lines shown in figure 49 are also compatible with the model, i.e., sufficient current was not achieved to give reversal in the present experiments.

A very preliminary comparison of the optogalvanic linewidths for one of the 3P_2 transitions has been made for pressures of 1.2 kPa (9 torr) and 100 kPa (750 torr). The increase in linewidth due to pressure broadening is readily observed. Because information regarding the lifetime of excited states can be learned from linewidth measurements, possibilities of obtaining more refined data should be explored.

III. OTHER ACTIVITIES

During this reporting period there were several other activities and accomplishments that deserve mention. Using a photomultiplier, preliminary measurements were made of correlation between optical emission pulses and electrical current pulses from positive-dc-corona discharges in SF_6 . The temporal resolution of the measurement system was 2 ns. The results indicate a high degree of correlation in time, i.e., no measurable average delay

between the optical and electrical signals. Because the results are still considered preliminary and in need of verification, they have not been presented in this report. More work on this is in progress.

A discussion [110] was prepared on a paper by J. M. Pelletier, et al. [111]. In this discussion, a connection was drawn between Paschen's law and Olivier's equation [112], which was used to fit data on electrical breakdown for gas mixtures.

In the past year the project supported the completion of one thesis [9] and three major archival papers [8,11,58] which have been submitted for publication. Presentations were given at the 33rd Gaseous Electronics Conference [13], the 1980 Conference on Electrical Insulation and Dielectric Phenomena [9,10], and the 1981 NATO Advanced Study Institute on Electrical Breakdown and Discharges in Gases. Talks and seminars were also given at the General Electric Research and Development Center and at the Massachusetts Institute of Technology. Visitors to NBS who were consulted concerning technical aspects of the project included Dr. Diethard Hansen of the Hahn-Meitner Institute, Dr. David W. Tong of the General Electric Research Laboratory, Dr. A. H. Qureshi of the University of Windsor, Dr. John Moore of the University of Maryland, and Dr. Andreas Kelen of ASEA. Dr. Kelen presented a seminar at NBS entitled "Detection of Aging in Dielectric Materials." The project also supported a seminar at the MIT High Voltage Laboratory, by Dr. Eric E. Kunhardt of Texas Tech University. Special assistance in preparing standard samples for gas analysis was provided by Dr. George Lockyer of the Allied Chemical Corporation.

IV. CONCLUSION AND SUMMARY

We outline here some of the more significant conclusions that can be derived from the work described in this report. First concerning the measurement of corona characteristics for SF₆, a new measurement scheme employing pulse counting and pulse-height analysis has been demonstrated and shown to yield interesting quantitative information about the statistics of electron avalanches and streamers not obtainable by other means [8]. During the past year new data were acquired on the pulse characteristics of positive-dc, point-plane corona in SF₆ which confirm tentative conclusions previously offered [16]. Further studies were carried out on the behavior of negative corona in SF₆ which showed that the nature of the phenomenon near inception depends critically on the point electrode conditions if no external radiation is present. For clean, polished stainless steel electrodes, the negative corona will, in the absence of radiation, appear initially as relatively large Trichel-like pulses at voltages significantly above the theoretical onset. If radiation is introduced, or if the electrodes are conditioned by operating a discharge for a short time at currents above a microampere, then the corona will appear at onset predominantly in the form of low level electron avalanches of high repetition rate with only an occasional "large" pulse.

Measurements of higher sensitivity carried out at the MIT High Voltage Laboratory in connection with this project also showed that negative corona in irradiated gaps for SF₆ initially appears in the form of electron avalanches which follow a modified Furry-type size distribution [9]. At voltages above avalanche inception, significant deviations from the Furry distribution become evident and there is often an abrupt appearance of

large pulses having amplitudes noticeably in excess of those of the main body of electron avalanches. Current stochastic models of electron avalanche formation cannot predict this behavior, and an entirely new theoretical approach is needed which includes possible effects of electrohydrodynamic instabilities. This sudden transition to large pulses is similar to the behavior observed in the NBS laboratory for positive corona in SF₆, and an understanding of this transition is perhaps the key to understanding the fundamental breakdown process in SF₆ and other highly electronegative gases.

A set of preferred mechanisms for initiation of corona discharges in SF₆ were proposed [11]. For negative corona the predominant mechanisms appear to be field emission of electrons from the stressed electrode surface in the absence of radiation, and field enhanced photo-electric emission in the presence of radiation. For positive corona the mechanisms are field-enhanced collisional detachment of negative ions in the absence of radiation, and photodetachment in the presence of radiation, assuming of course that the energy of the radiation exceeds that for the electron affinity of the negative ions. It is shown [11] that this set of mechanisms is consistent with observed polarity, geometry, and pressure effects, and with differences between ac and dc corona [10]. Comparisons of calculated and measured corona inception for highly nonuniform fields show agreement only for negative corona. This is expected on the basis of the assumed initiation mechanisms. No conclusions could be drawn from this comparison about the critical avalanche size to be used in the streamer criteria. This is due to large uncertainties arising from lack of precise knowledge about the electric field variation near the tip of a sharp point electrode. Pulse height distribution data [8,9] suggest a critical avalanche size which is considerably below the commonly accepted value of 1×10^8 electrons.

Additional possible difficulties were uncovered in the modeling of corona inception for highly nonuniform electric fields. One is the questionable validity of swarm parameters, particularly the ionization coefficient, for E/N in highly nonuniform situations where electrons are unable to attain equilibrium. The other, made evident in part from the survey of electron swarm data, is the possibility of large uncertainties in measured values for ionization coefficients in electronegative gases at high E/N where contributions from electron detachment processes might become important.

The survey of swarm data [58] revealed a number of gaps in the data needed for modeling discharges in electronegative gases, and in some cases raised questions about the reliability of the existing data. For example, in the case of SF₆ there is a serious lack of information about detachment of negative ions in this gas; whereas, in the case of O₂, the available detachment data display enormous disagreement. This survey points to areas where more measurements, or new measurement techniques, and calculations are needed.

Concerning the measurement of discharge-generated contaminants in SF₆, the results of calculations reported here indicate that a measurement of the low-frequency dielectric constant for SF₆ at a sensitivity of 1 ppm will reveal the presence of polar contaminants such as H₂O at a level of about 100 ppm. This technique is thus seen to lack sensitivity, but might prove useful for calibration purposes. In the use of the GC/MS to monitor buildup

of corona-generated stable by-products in SF_6 , it was found that the oxyfluorides SOF_2 and SO_2F_2 are produced at rates directly proportional to the discharge power for power levels between 50 and 600 mW. The production rates are also constant, at least up to concentrations of 200 ppm. The compounds SOF_2 and SO_2F_2 are produced in corona at nearly equal rates, which is contrary to the results from arc decomposition studies that show almost no production of SO_2F_2 . The reason for this difference is not yet completely understood.

The results of optogalvanic measurements in glow discharges showed that the presence of SF_6 in neon (at least up to the 5% level) had little or no effect on the relative strengths of the observed signals associated with transitions from metastable states. It can be inferred from this that SF_6 has no dramatic effect on modifying the metastable populations in the discharge. Optogalvanic spectra were also observed for the first time in a high pressure (100 kPa) neon discharge.

V. REFERENCES

- [1] W. Becher and J. Massonne, "Contribution to the Decomposition of Sulfur Hexafluoride in Electric Arcs and Sparks," *Elektrotech. Z.*, Vol. A91, pp. 605-610, 1970.
- [2] C. C. Boudene, J. Cluet, G. Keib, and G. Wind, "Identification and Study of Some Properties of Compounds Resulting from the Decomposition of SF₆ Under the Effect of Electrical Arcing in Circuit-Breakers," *Revue Generale De L' Electricite (RGE)* - Numero Special, pp. 45-78, 1974.
- [3] T. Suyzuki, S. Nakayama, and T. Yoshimitsu, "Degradation of Insulating Materials, Due to SF₆ Gas Dissociation Products," *IEEE Trans. Elec. Insul.*, Vol. EI-15, No. 1, pp. 53-58, 1980.
- [4] L. B. Loeb, "Electrical Coronas - Their Basic Physical Mechanisms," University of California Press, pp. 26-40, 1965.
- [5] R. S. Sigmond, "Corona Discharges," Electrical Breakdown of Gases, Ed. by J. M. Meek and J. D. Craggs, John Wiley and Sons, pp. 319-384, 1978.
- [6] R. Hazel and E. Kuffel, "Static Field Anode Corona Characteristics in Sulphur Hexafluoride," *IEEE Trans. on Power App. Syst.*, Vol. PAS-95, pp. 178-186, 1976.
- [7] O. Farish, O. E. Ibrahim, and A. Kurimoto, "Prebreakdown Corona Processes in SF₆ and SF₆/N₂ Mixtures," *Proc. 3rd Int'l. Symp. on High Voltage Eng.*, Milan, 1979. Q. E. Ibrahim, "Corona Stabilization and Breakdown in SF₆ and SF₆/N₂ Mixtures," Thesis, University of Strathclyde, March 1980.
- [8] R. J. Van Brunt and D. A. Leep, "Characterization of Point-Plane Corona Pulses in SF₆," *J. Appl. Phys.*, Vol. 52, pp. 6588-6600, 1981.
- [9] R. G. Gels and C. M. Cooke, "Distribution of Electron Avalanches in SF₆," *Proc. Conf. on Electrical Insulation and Dielectric Phenomena*, National Academy Press, pp. 470-476, 1980; R. G. Gels, "Electron Avalanches and Inception in Compressed Electron - Attaching Gases," Thesis, Massachusetts Institute of Technology, 1981.
- [10] R. J. Van Brunt and M. Misakian, "Comparison of DC and 60-Hz AC Positive and Negative Discharge Inceptions in SF₆," *Proc. Conf. on Electrical Insulation and Dielectric Phenomena*, National Academy Press, pp. 461-469, 1980.
- [11] R. J. Van Brunt and M. Misakian, "Mechanisms for Inception of DC and 60-Hz AC Corona in SF₆," *IEEE Trans. Elec. Insul.* Vol. EI-17, No. 2, pp. 106-120, 1982.

- [12] J. Dutton, "A Survey of Electron Swarm Data," J. Phys. Chem. Ref. Data, Vol. 4, No. 3, pp. 577-856, 1975.
- [13] D. A. Leep and R. J. Van Brunt, "Pulse Characteristics of Positive DC Corona in SF₆: Effects of Trace Decomposition Products," Proc. 33rd Gaseous Electronics Conf., Bull. Am. Phys. Soc., Vol. 26, No. 5, pp. 716, 1981.
- [14] R. J. Van Brunt and D. A. Leep, "Partial Discharge Induced Degradation of Compressed SF₆," Proc. Workshop on Arc By-Products in Gas-Insulated Equipment, Electric Power Research Institute, Final Report EPRI EL-80-8-LD, pp. 13-14, 1980.
- [15] R. J. Van Brunt, M. Misakian, D. A. Leep, K. J. Moy, and E. C. Beaty, Annual Report: Technical Assistance for Future Insulation Systems Research, Task Order A053-EES, DoE Contract EA-77-01-6010 (1980).
- [16] R. J. Van Brunt, J. S. Hilten, and D. P. Silver, "Partial Discharge Pulse Height Distributions and Frequencies for Positive and Negative DC Corona in SF₆ and SF₆-N₂ Mixtures," Gaseous Dielectrics II, Proc. of the Second Int'l. Symposium on Gaseous Dielectrics, Pergamon Press, pp. 303-311, (1980).
- [17] D. T. A. Blair, B. H. Crichton, and I. C. Somerville, "Avalanche Statistics and the Streamer Criterion," Proc. of the Int'l. Symp. on Gaseous Dielectrics, Knoxville, pp. 360-365, 1978.
- [18] V. H. Dibeler and F. L. Mohler, "Dissociation of SF₆, CF₄ and SiF₄ by Electron Impact," J. Res., Nat. Bur. Stand. (U.S.), Vol. 40, pp. 25-29, 1948.
- [19] A. P. Hitchcock and M. J. Van der Wiel, "Absolute Oscillator Strengths (5-63 eV) for Photoabsorption and Ionic Fragmentation of SF₆," J. Phys. B: Atom. Molec. Phys., Vol. 12, No. 13, pp. 2153-2169, 1979.
- [20] R. K. Asundi and J. D. Craggs, "Electron Capture and Ionization Phenomena in SF₆ and C₇F₁₄," Proc. Phys. Soc., Vol. 83, pp. 611-618, 1964.
- [21] M. G. Stock, P. C. H. Strachan, R. H. Parker, R. J. Donovan, and J. H. Knox, "Negative Ion Formation in Sulfur Hexafluoride and Other Group VI Fluorides," Dynamic Mass Spectrometry, Ed. by D. Price and J. F. J. Todd, Vol. 4, pp. 197-210, 1975.
- [22] H. Raether, "Untersuchung der Elektronenlawine mit der Nebelkammer," Zeitschrift fur Physik, Vol. 107, pp. 91, 1937.
- [23] M. S. Naidu and A. N. Prasad, "Diffusion and Drift of Electrons in SF₆," J. Phys. Vol. D 5, pp. 1090-1095, 1972.

- [24] H. Raether, "The Development of the Electron Avalanche in a Spark Channel (from Observations in a Cloud Chamber)," *Zeitschrift fur Physik*, Vol. 112, pp. 464, 1939.
- [25] H. Raether, "The Development of Kanal Discharges," *Archiv fur Electrotechnik*, Vol. 34, pp. 49, 1940.
- [26] R. A. Wijsman, "Breakdown Probability of a Low Pressure Gas Discharge," *Phys. Rev.*, Vol. 75, pp. 833, 1949.
- [27] W. H. Furry, "On Fluctuation Phenomena in the Passage of High Energy Electrons through Lead," *Phys. Rev.*, Vol. 52, pp. 569, 1937.
- [28] Von Werner Legler, "Die Statistik der Elektronenlawinen in Elektronegativen Gasen bei hohen Feldstarken und bei grosser Gasverstarkung," *Zeitschrift fur Naturforschung*, Vol. 16A, pp. 253-261, 1961.
- [29] J. Byrne, "Statistics of the Electron-Multiplication Process in Proportional Counters," *Proc. Roy. Soc. Edinburgh, Sec. A*, Vol. 66, pp. 33, 1962.
- [30] D. G. Kendall, "On the Generalized 'Birth-and-Death' Process," *Annal. Math. Stat.*, Vol. 19, pp. 1-50, 1948.
- [31] R. Bartnikas and E. J. McMahon, "Engineering Dielectrics - Corona Measurements and Interpretation," *ASTM*, Vol. 1, 1979.
- [32] M. Goldman and A. Goldman, "Corona Discharges," *Gaseous Electronics - Electrical Discharges*, Vol. 1, Ed. by M. N. Hirsh and H. J. Oskam, Academic Press, pp. 219-290, 1978.
- [33] M. Menes and L. H. Fisher, "Positive Point-to-Plane Corona Studies in Air," *Phys. Rev.* Vol. 94, No. 1, pp. 1-6, 1954.
- [34] J. M. Meek, "A Theory of Spark Discharge," *Phys. Rev.* Vol. 57, pp. 722-728, 1940.
- [35] L. Frommhold, "Uber Verzogerte Elektronen in Elektronenlawinen, insbesondere in Sauerstoff und Luft, durch Bildung und Zerfall Negativer Ionen (O^-)," *Fortschritte der Physik*, Vol. 12, pp. 597-643, 1964.
- [36] E. Weber, "Electromagnetic Theory," Dover, pp. 609-610, 1965.
- [37] T. L. Ferrell, J. K. Baird, D. R. James, M. O. Pace, and L. G. Christophorou, "A Solution to Laplace's Equation for Hyperboloidal Electrodes with Application to Dielectric Testing in Nonuniform Electric Fields," *Gaseous Dielectric II, Proc. of the Second International Symposium on Gaseous Dielectrics*, Ed. by L. G. Christophorou, Pergamon Press, pp. 383-388, 1980.

- [38] V. N. Maller and M. S. Naidu, "Sparking Potentials and Ionization Coefficients in SF₆," Proc. IEE, Vol. 123, pp. 107-108, 1976. The data reported in this reference were selected because they correspond to the highest values of E/N reported in the literature.
- [39] H. Raether, "Zum Aufbau von Gasentladungen," Naturwissenschaften, Vol. 28, pp. 749-750, 1940; H. Raether, "Electron Avalanches and Breakdown in Gases," Butterworths, London, 1964.
- [40] S. Sangkasaad, "Breakdown Characteristics of Compressed SF₆ in Concentric Spheres Field," 4th Intl. Conf. Gas Discharges, IEE Conf. Publ. No. 143, pp. 145-148 (1976).
- [41] B. Sangi, "Basic Discharge Parameters in Electronegative Gases," Thesis, University of Manchester, Institute of Science and Technology, 1971; T. H. Teich and B. Sangi, "Discharge Parameters for Some Electronegative Gases and Emission of Radiation from Electron Avalanches," Proc. Symp. on High Voltage Technology, Ed. by F. Heilbronner, Vol. 1, pp. 391-395, 1972. Data are presented here for $(\alpha_i - \eta_a)/P$ which disagree significantly with the results in Ref. 22 for E/N > 500 V/cm torr.
- [42] M. S. Bhalla and J. D. Craggs, "Measurement of Ionization and Attachment Coefficients in Sulphur Hexafluoride in Uniform Fields," Proc. Phys. Soc. London, Vol. 80, pp. 151-160, 1962.
- [43] I. M. Bortnik and A. A. Panov, "Discharge Ignition Characteristics and the Ionization and Electron-Attachment Coefficients of CF₄, C₂F₆, and SF₆," Sov. Phys. Tech. Phys., Vol. 16, pp. 571-575, 1971.
- [44] C. M. Cooke, High Voltage Research Laboratory, Massachusetts Institute of Technology, (private communication).
- [45] M. Goldman, "Corona Discharges and Their Applications," Proc. IEE, Vol. 128, No. 4, pp. 298-302, 1981.
- [46] E. Nasser and M. Heizler, "The Propagation of Streamers in Air," J. Appl. Phys. Vol. 45, pp. 3396-3401, 1974.
- [47] E. H. Holt and R. E. Haskell, "Foundations of Plasma Dynamics," MacMillan, pp. 454-455, 1965.
- [48] O. E. Ibrahim and O. Farish, "Negative-Point Breakdown and Pre-breakdown Corona Processes in SF₆ and SF₆/N₂ Mixtures," Proc. 6th Int'l. Conf. on Gas Discharges and Their Applications, Part 1, IEE Publ. No. 189, pp. 161-164, 1980.
- [49] S. Trajmar and A. Chutjian, "Electron Impact Excitation of SF₆," J. Phys. B: Atom. Molec. Phys. Vol. 10, No. 14, pp. 2943-2949, 1977. Evidence is provided in this work of optically forbidden excitations by electron collisions to triplet states that lie above 9.6 eV in energy. However, nothing is known about the lifetimes of those states, and it would appear that the lowest in this series is too low in energy to allow ionization by 4.2 eV photons.

- [50] G. Berger and R. Hahn, "Collisional Detachment Lifetime Measurements of Negative Ions in Atmospheric Air from the Statistical Time-Lag Distribution of an Electrical Discharge," Proc. 6th Int'l. Conf. on Gas Discharges and Their Applications, Part 2, IEE publ. No. 189, pp. 195-197, 1980.
- [51] L.D. Doverspike, B. T. Smith, and R. L. Champion, "Total Electron Detachment Cross Sections for Collisions of Negative Halogen Ions with Various Molecules for Energies Around Threshold," Phys. Rev. A, Vol. 22, No. 2, pp. 393-398, 1980, S. E. Haywood, D. J. Bowen, R. L. Champion, and L. D. Doverspike, "Electron Detachment in I⁻-Rare-Gas Collisions," J. Phys. B: Atom Molec. Phys., Vol. 14 pp. 261-266, 1981; M. H. Hug, D. S. Fraedrich, R. L. Champion, and L. D. Doverspike, "Total Cross Section Measurements for Collisions of F⁻ with H₂ and D₂," Proc. XII Int'l. Conf. on the Physics of Electronic and Atomic Collisions, Gatlinburg, pp. 533-534, 1981.
- [52] M. Eccles, A. N. Prasad, and J. D. Craggs, "Electron Detachment in Sulfur Hexafluoride," Electronics Letters, Vol. 3, No. 9, pp. 410-411, 1967.
- [53] B. C. O'Neill and J. D. Craggs, "Collisional Detachment of Electrons in Sulphur Hexafluoride," J. Phys. B: Atom. Molec. Phys., Vol. 6, pp. 2634-2640, 1973.
- [54] J. A. Rees, "Fundamental Processes in the Electrical Breakdown of Gases," Electrical Breakdown of Gases, Ed. by J. M. Meek and J. D. Craggs, John Wiley and Sons, pp. 1-128, 1978.
- [55] D. W. Goodson, R. J. Corbin, and L. Frommhold, "Electron Avalanches in Oxygen: Detachment from the Diatomic Ion O₂⁻," Phys. Rev. A, Vol. 9, No. 5, pp. 2049-2059, 1974.
- [56] J. Comer and G. J. Schulz, "Measurement of Electron Detachment Cross Sections from O⁻," J. Phys. B: Atom. Molec. Phys., Vol. 7, No. 8, pp. L249-L253, 1974.
- [57] H. C. Schweinler and L. G. Christophorou, "Calculation of Electric Field-Induced Detachment Rates of Electrons from Mononegative Ions; Relevance to Gaseous Dielectrics," Gaseous Dielectrics II, Proc. of the Second International Symposium on Gaseous Dielectrics, Ed. by L. G. Christophorou, Pergamon Press, pp. 12-24, 1980.
- [58] J. W. Gallagher, E. C. Beaty, J. Dutton, and L. C. Pitchford, "A Survey of Electron Swarm Data for Electro-Negative Gases," (submitted for publication in J. Phys. Chem. Ref. Data).
- [59] L. G. H. Huxley and R. W. Crompton, "The Diffusion and Drift of Electrons in Gases," John Wiley and Sons, New York, 1974.

- [60] J. S. Townsend, "The Conductivity Produced in Gases by the Motion of Negatively-Charged Ions," *Nature*, Vol. 62, pp. 340-341, 1900.
- [61] L. G. H. Huxley and F. W. Bennett, "The Lateral Diffusion of a Stream of Ions in a Gas," *Phil. Mag.*, Vol. 30, pp. 396-413, 1940.
- [62] J. C. Bowe, "Drift Velocity of Electrons in Nitrogen, Helium, Neon, Argon, Krypton, and Xenon," *Phys. Rev.*, Vol. 117, pp. 1411-1415, 1960.
- [63] R. R. Newton, "Transients in Townsend Discharges," *Phys. Rev.*, Vol. 73, pp. 570-583, 1948.
- [64] L. E. Kline, D. K. Davies, C. L. Chen, and P. J. Chantry, "Dielectric Properties for SF₆ and SF₆ Mixtures Predicted from Basic Data," *J. Appl. Phys.*, Vol. 50, pp. 6789-6796, 1979.
- [65] T. Yoshizawa, Y. Sakai, H. Tagashira, and S. Sakamoto, "Boltzmann Equation Analysis of the Electron Swarm Development in SF₆," *J. Phys. D.*, Vol. 12, pp. 1839-1852, 1979.
- [66] F. M. Harris and G. J. Jones, "Drift Velocities of Electrons in Sulphur Hexafluoride," *J. Phys. B*, Vol. 4, pp. 1536-1540, 1971.
- [67] J. Dutton, F. M. Harris, and G. J. Jones, "Drift Velocities of Electrons in Sulphur Hexafluoride," 10th Int'l. Conf. on Phenomena in Ionized Gases, Contributed Papers (Oxford, England, 13-18 September 1971), R. N. Franklin, Editor, Donald Parsons & Co., 1971.
- [68] V. N. Maller and M. S. Naidu, "Ratio of Diffusion Coefficient to Mobility for Electrons in SF₆-Air and Freon-Nitrogen Mixtures," *IEEE Trans. Plasma Sci.*, Vol. 3, pp. 205-208, 1975.
- [69] A. Chutjian, "Experimental SF₆⁻/SF₆ and Cl⁻/CFCl₃ Electron Attachment Cross Sections in the Energy Range 0-200 meV," *Phys. Rev. Lett.*, Vol. 46, pp. 1511-1514, 1981.
- [70] Y. V. Veldre, A. V. Lyash, L. L. Rabik, and L. A. Fridkin, "Total Effective Cross Sections of Excitation of Atoms by Electron Impact, Using a Classical Approximation," *Latv. PSR Zinat. Akad. Vestis Fiz. Teh. Zinat. Ser.*, Vol. 4, pp. 3-12, 1965.
- [71] R. W. Crompton, A. G. Robertson, K. Nygaard, and R. Hegerberg, "Measurements of the Rate Coefficient for Attachment of Thermal Electrons to SF₆," *Proc. 33rd Gaseous Electronics Conf.*; *Bull. Am. Phys. Soc.*, Vol. 26, No. 5, pp. 726, 1981.
- [72] M. S. Foster and J. L. Beauchamp, "Electron Attachment to Sulfur Hexafluoride: Formation of Stable SF₆⁻ at Low Pressure," *Chem. Phys. Lett.*, Vol. 31, pp. 482-486, 1975.

- [73] B. M. Hochberg and E. Sandberg, "A Study of the Dielectric Strength of Gases," *Zh. Tekh. Fiz.*, Vol. 12, pp. 65-77, 1942; "Ionization of Gases and Their Breakdown Strength," *Compt. Rend. Acad. Sci. URSS*, Vol. 53, pp. 511-514, 1946.
- [74] L.B. Loeb, "The Formation of Negative Ions," Basic Processes of Gaseous Electronics, University of California Press, Berkeley, pp. 375-476, 1965.
- [75] D. K. Davies, "Analysis of Current Growth Measurements in Attaching Gases," *J. Appl. Phys.*, Vol. 47, pp. 1916-1919, 1976.
- [76] K. B. McAfee, "Pulse Technique for Measurement of the Probability of Formation and Mobility of Negative Ions," *J. Chem. Phys.*, Vol. 23, pp. 1435-1440, 1955.
- [77] K. B. McAfee and D. Edelson, "Identification and Mobility of Ions in a Townsend Discharge by Time-Resolved Mass Spectrometry," *Proc. Phys. Soc., London*, Vol. 81, pp. 382-384, 1963.
- [78] D. Edelson and K. B. McAfee, "Improved Pulsed Townsend Discharge Experiment," *Rev. Sci. Instrum.*, Vol. 35, pp. 187-194, 1964.
- [79] H. A. Boyd and G. C. Crichton, "Measurement of Ionization and Attachment Coefficients in SF₆," *Proc. IEE*, Vol. 118, pp. 1872-1877, 1971.
- [80] J. Dutton, F. M. Harris, and G. J. Jones, "Ionization, Attachment and Breakdown in SF₆," *Nature*, Vol. 227, pp. 702-703, 1970.
- [81] T. H. Teich and D. W. Branston, "Time Resolved Observation of Ionization and Electron Detachment in SF₆," 3rd Int'l. Conf. Gas Discharges, IEE Conf. Publ. No. 118, pp. 109-113, 1974.
- [82] O. Petersons and W. E. Anderson, "A Wide Range High-Voltage Capacitance Bridge with One PPM Accuracy," *IEEE Trans. on Instru. and Meas.*, Vol. IM-24, No. 4, pp. 336-344, 1975.
- [83] W. E. Anderson and R. S. Davis, "Measurement of Insulating Materials at Cryogenic Temperatures," Final Report for DoE Contract EA-77-A-01-6010, National Bureau of Standards Internal Report, NBSIR 79-1950, 1980.
- [84] H. Frohlich, "Theory of Dielectrics," Oxford University Press, London, 1958.
- [85] A. A. Maryott and F. Buckley, "Table of Dielectric Constants and Electric Dipole Moments of Substances in the Gaseous State," NBS Circular 537, 1953.
- [86] R. D. Nelson, D. R. Lide, and A. A. Maryott, "Selected Values of Electric Dipole Moments for Molecules in the Gas Phase," National Bureau of Standards Report, NSRDS-NBS 10, 1967.

- [87] A. Baker, R. Dethlefsen, J. Dodds, N. Oswalt, and P. Vouros, "Study of Arc By-Products in Gas-Insulated Equipment," EPRI Final Report, EL-1646, 1980.
- [88] K. W. Meissner and W. F. Miller, "Influence of Irradiation on the Characteristic of a Glow Discharge in Pure Rare Gases," *Phys. Rev.*, Vol. 92, pp. 896-898, 1953.
- [89] F. E. Acker and G. W. Penney, "Influence of Previous Positive Streamers on Streamer Propagation and Breakdown in a Positive Point-to-Plane Gap," *J. Appl. Phys.*, Vol. 39, pp. 2363-2369, 1968.
- [90] E. Kuffel and M. Abdullah, High Voltage Engineering, Pergamon Press, New York, 1970.
- [91] G. Hartman and I. Gallimberti, "The Influence of Metastable Molecules on the Streamer Progression," *J. Phys. D: Appl. Phys.*, Vol. 8, pp. 670-680, 1975.
- [92] K. C. Smyth, R. A. Keller, and F. F. Crim, "Photon-Induced Ionization Changes in a Neon Discharge," *Chem. Phys. Lett.*, Vol. 55, pp. 473-477, 1978.
- [93] E. F. Zalewski, R. A. Keller, and R. Engleman, Jr., "Laser Induced Impedance Changes in a Neon Hollow Cathode Discharge. A Mechanistic Study," *J. Chem. Phys.*, Vol. 70, pp. 1015-1026, 1979.
- [94] D. Feldmann, "Opto-Galvanic Spectroscopy of Some Molecules in Discharges: NH_2 , NO_2 , H_2 , and N_2 ," *Opt. Comm.*, Vol. 24, pp. 67-72 (1979).
- [95] K. C. Smyth and P. K. Schenck, "Opto-Galvanic Spectroscopy of a Neon Discharge: Mechanism Studies," *Chem. Phys. Lett.*, Vol. 55, pp. 466-472, 1978.
- [96] A. W. Potts, H. J. Lempka, D. G. Streets, and W. C. Price, "Photoelectron Spectra of the Halides of Elements in Groups III, IV, V, and VI," *Phil. Trans. Roy. Soc. London*, Vol. A. 268, pp. 59-76, 1970. The identities of the orbitals are those of Potts, et al. Alternative assignments of the orbitals are given by Hay in Ref. 97.
- [97] P. J. Hay, "Excited States and Positive Ions of SF_6 ," *J. Am. Chem. Soc.*, Vol. 99:4, pp. 1013-1019, 1977.
- [98] Other processes such as neutral dissociation and neutral dissociative excitation should also be considered. For example, Hay's calculations (Ref. 97) predict an anti-bonding orbital ($6a_{1g}$) which is energetically accessible. For a further discussion of processes which can lead to destruction of metastable atoms in gas mixtures, see D. H. Stedman and D. W. Stetser in "Prog. Reaction Kinetics," Vol. 6, p. 75ff, 1971.

- [99] G. Francis, "The Glow Discharge at Low Pressure" in *Encyclopedia of Physics*, Vol. XXII, Springer-Verlag, Berlin, 1956, p 177ff.
- [100] J. W. Ledbetter, Jr., "New Rydberg Bands in the Visible Region and Identification of the Lowest $^1\Sigma_g^+$ Rydberg State of the N_2 Molecule," *J. Molec. Spectr.*, Vol. 42, pp. 100-111, 1972.
- [101] A. Lofthus and P. H. Krupenie, "The Spectrum of Molecular Nitrogen," *J. Phys. Chem. Ref. Data*, Vol. 6, pp. 113-307, 1977.
- [102] A. V. Phelps, "Diffusion, De-Excitation, and Three-Body Collision Coefficients for Excited Neon Atoms," *Phys. Rev.*, Vol. 114, pp. 1011-1025, 1959.
- [103] R. A. Sierra, J. D. Clark, and A. J. Cunningham, "An Experimental Study of the Reactions of Excited Neon Atoms in Pure Afterglow Plasmas Using Resonance Absorption Spectroscopy," *J. Phys. B: Atom. Molec. Phys.*, Vol. 12, pp. 4113-4129, 1979.
- [104] P. K. Leichner, "Time and Pressure Dependence of the Vacuum-Ultraviolet Radiation in Neon," *Phys. Rev. A*, Vol. 8, pp. 815-822, 1973.
- [105] P. K. Leichner, J. D. Cook, and S. J. Luerman, "Time Dependence of the Vacuum-UV Emissions from Neon, and Energy Transfers to the Resonance States $Ne(^1P_1)$ and $Ne(^3P_1)$ in Helium-Neon Mixtures," *Phys. Rev. A*, Vol. 12, pp. 2501-2513, 1975.
- [106] J. R. Dixon and F. A. Grant, "Decay of the Triplet P Levels of Neon," *Phys. Rev.*, Vol. 107, pp. 118-124, 1957.
- [107] C. S. Willett, "Introduction to Gas Lasers: Population Inversion Mechanics," Pergamon Press, New York, 1974, Chapt. 3.4.
- [108] J. S. Cohen, L.A. Collins, and N. F. Lane, "Theory of Inelastic Collisions Between Low-Lying Excited and Ground-State Ne Atoms," *Phys. Rev. A*, Vol. 17, pp. 1343-1356, 1978.
- [109] The complexities of modeling the neon discharge are discussed in Ref. 95.
- [110] R. J. Van Brunt, "Discussion on paper 81 WM 014-0 by J. M. Pelletier, Y. Gervais, and D. Mukhedkar," *IEEE Trans. on Power App. Syst.*, Vol. PAS-100, pp. 3867-3868, 1981.
- [111] J. M. Pelletier, Y. Gervais, and D. Mukhedkar, "Dielectric Strength of N_2 -He Mixtures and Comparison with N_2 - SF_6 and CO_2 - SF_6 Mixtures," *IEEE Trans. on Power App. Syst.*, Vol. PAS-100, pp. 3861-3869, 1981.
- [112] G. Olivier, Y. Gervais, and D. Mukhedkar, "A New Approach to Compute Uniform Field Breakdown of Gases," *IEEE Trans. Power App. Syst.*, Vol. PAS-97, pp. 969-976, 1978.

- [113] K. T. Compton, "On the Motions of Electrons in Gases,"
Phys. Rev. Vol. 22, pp. 333-346, 1923.
- [114] L. Loeb, Basic Processes of Gaseous Electronics, U. of
California Press, Berkeley, pp. 211-373, 1961.

APPENDIX I.

Equilibrium Conditions - Estimation of Swarm Parameter Applicability

In applying electron swarm parameters, such as the ionization coefficients, to calculation of current growth, or discharge inception in gases, one needs some assurances that these parameters are meaningfully defined over the range of conditions to be encountered. The issue is especially significant at high E/N where electron velocities must necessarily become greater. The swarm parameter values are typically measured and used when the electrons are in "equilibrium" with the driving force from the electric field. By "equilibrium" it is meant that the average energy of the electrons has reached the value it would have if the electrons had been traveling a long distance; thus, also, the ionization rate which is influenced by electron energy is in equilibrium.

We propose here a useful, simple calculation for estimating the conditions under which the use of swarm parameters should be permissible. The technique, which is an adaption of methods introduced by Compton [113] with extensions suggested by Loeb [114], is believed to be applicable to regions of high E/N and also for nonuniform fields where average electron motion might not keep up with the rate of change of the field. While Monte Carlo methods provide one means of determining equilibrium conditions, the technique is proposed as an alternative and more easily used estimator. The validity of the simplified expression given here, however, should be checked by comparison with results of Monte Carlo calculations. Thus far this has not been done. The expression given below is a first-order nonlinear differential equation which can be solved by simple iteration techniques.

For convenience, the electrons in the gas are subjected to a z-directed electric field. Their motion in one dimension is defined in accordance with an energy balance constraint. This method equates the energy change to energy input less energy loss, all on a per-unit-path basis. The result is given here without proof:

$$\frac{e dU}{dz} = eE - ef(U - \Omega)U/(0.44 \lambda^2 E), \quad (\text{A.I.1})$$

where

- e = electronic charge
- U = average electron energy/coulomb (in eV)
- E = electric field in the z-direction (in V/cm)
- f = fractional energy lost/collision by an electron
- λ = mean free path (in cm)
- Ω = limiting thermal electron energy/coulomb.

If $E = 0$, then $U = \Omega$, corresponding to the limiting thermal energy. Generally, f and λ are U-dependent. Yet it can be shown that both f and λ may be approximated on the basis of experimental data and/or theoretical determinations of D/μ (the diffusion-mobility ratio) and W (the electron drift speed).

By derivation and curve fitting of published data to obtain specific values for SF₆, the following expressions were obtained for λ (electron mean free path) and for f; they apply for E/N in the range:

$$1 \times 10^{-20} < \frac{E}{N} < 3.3 \times 10^{-18} \text{ Vm}^2.$$

Mean Free Path:

$$\begin{aligned} \lambda &= 2.125 \frac{W}{E} \sqrt{\frac{m D}{e \mu}} \\ &= 5.07 \times 10^{-6} \frac{W}{E} \sqrt{\frac{D}{\mu}} \\ &= 1.43 \times 10^{18} \left(\frac{E}{N}\right)^{-0.043}, \end{aligned} \quad (\text{A.I.2})$$

where (from [64]),

$$\frac{D}{\mu} = 1.226 \times 10^{10} \left(\frac{E}{N}\right)^{0.05024} \quad (\text{A.I.3})$$

Fractional Energy Loss:

$$\begin{aligned} f &= \left(\frac{\sqrt{1.77}}{3} \frac{E \lambda}{D/\mu}\right)^2 \\ &= 2.676 \times 10^{15} \left(\frac{E}{N}\right)^{0.9092} \end{aligned} \quad (\text{A.I.4})$$

Equation (A.I.1) has been numerically solved for the CIZ configuration of interest in this study. The electric field, E, was chosen as the z-component of the Laplacian cathode tip field (see fig. A.I.1). For SF₆, values of D/μ and W_e were taken from the results of Kline et al. [64]. The results for various tip radii are shown in figures A.I.2 and A.I.3. For each figure, the abscissa quantity is the normalized distance from the cathode surface:

$$X \equiv \frac{Z}{R} - 1, \quad (\text{A.I.5})$$

where R is the tip radius and where Z/R = 1 at the very tip of the cathode.

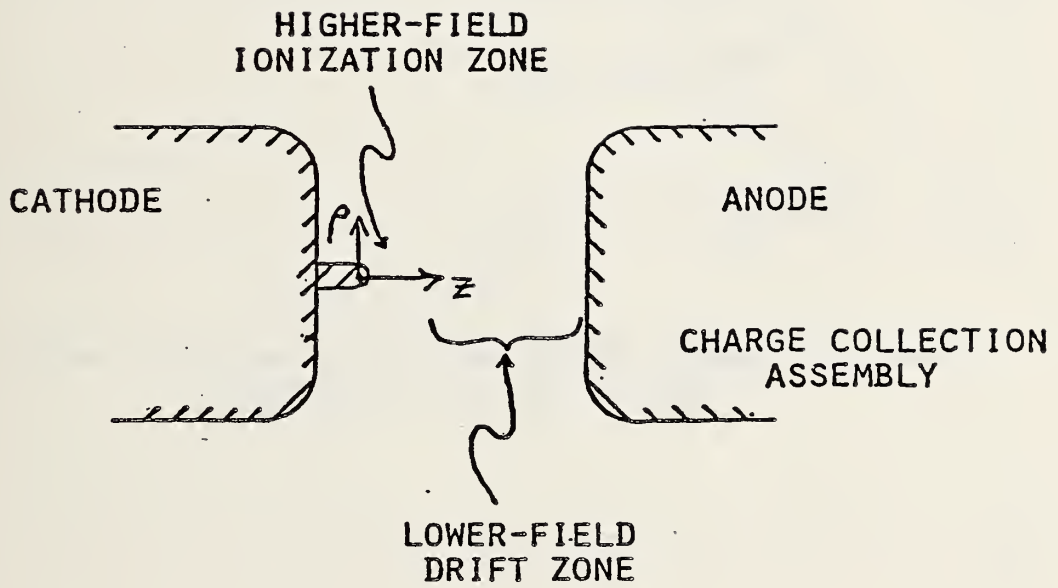


Figure A.I.1 Coordinates for Swarm Equilibrium Calculations in the CIZ test cell arrangement.

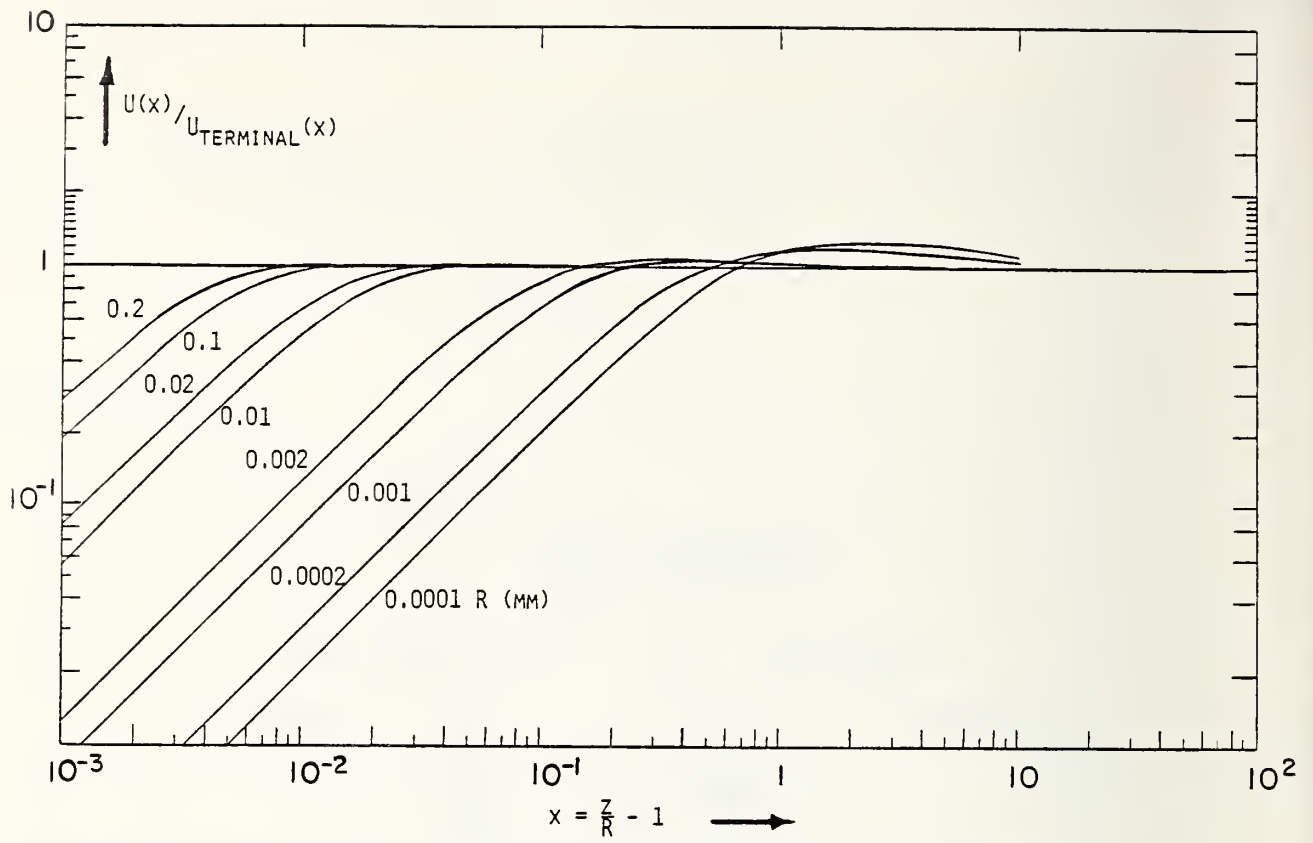


Figure A.I.2 Normalized average electron energy for swarms in the CIZ test cell arrangement.

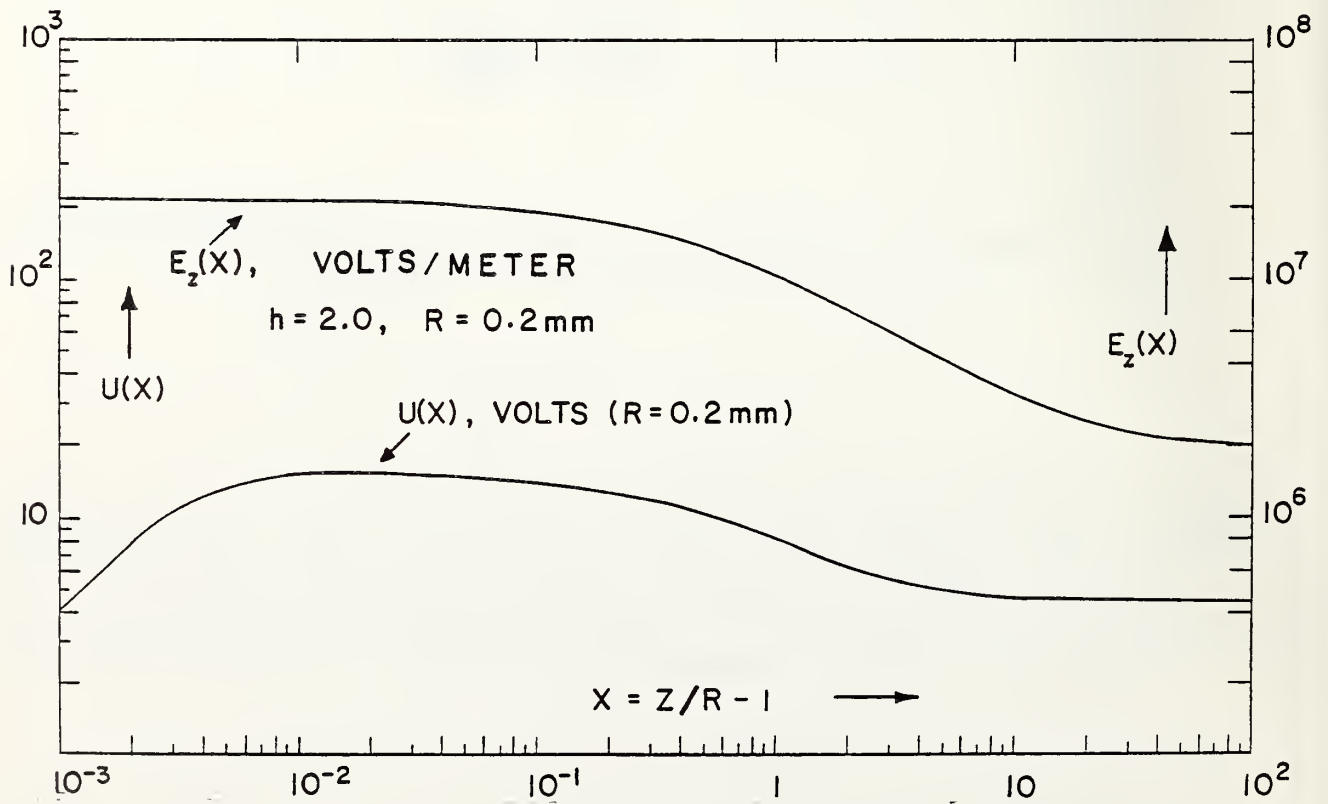


Figure A.I.3 Average electron energies in the CIZ test cell arrangement.

From figure A.I.2 the electrons are seen to remain within better than 95% of their terminal energy values after traveling less than a micron from the cathode tip (see the $R = 0.2$ mm curve). In figure A.I.3, the average electron energy $U(X)$ is shown as a function of X , for $R = 0.2$ mm, $h = 2$ mm, and $P = 100$ kPa, and compared with a plot of the field $E_z(X)$. For $X > 0.01$, $U(X)$ follows $E_z(X)$ as expected once thermal equilibrium is attained. These results are interpreted to provide adequate justification for the use of swarm parameters throughout more than 99% of the ionization region of the controlled-ionization-zone electrode configuration. This means that the avalanche calculations and studies of development of ionization discussed in Sec. II.B. have a reasonable basis for their validity.

APPENDIX II.

Inception as an Instability (Electrohydrodynamic Approach)

Electron avalanche growth in and of itself does not account for the sudden transition to discharge inception and breakdown. Additional processes which regenerate a continuing supply of avalanches or means to enhance greatly the gas ionization are needed. In this section, the discharge inception process is first discussed from a classic streamer point of view and then from a new approach in which general conditions of electrohydrodynamic events are considered.

The so-called "Raether streamer criterion" evolved from low-pressure measurements and simple space-charge field analysis. The criterion states that an avalanche which grows to a size of about 10^8 electrons will cause the formation of a streamer. While this has proven to be a good guide to estimating discharge inception, it does not provide information about conditions or gases which would alter the discharge inception values, information about expected variation, time dependence of the process, etc.

A more general description of the electron avalanche considers the transient electric field and pressure disturbance as a traveling electrohydrodynamic (EHD) phenomenon. The formulation describes the time and space evolution of the avalanche. It allows the study of possible uneven growth and hence for instabilities in the avalanche process. If such instabilities correspond to rapid enhanced ionization, they may also correspond to the detailed conditions of discharge inception. Hence, EHD techniques offer an ability to probe and search for inhomogeneous phenomena and for conditions and mechanisms of the sudden, violent, avalanche-streamer transition.

The formalism is to produce the coupled and, in general, nonlinear differential equations which adequately describe the avalanche. Determining which terms are needed and which may be neglected allows important simplifications to these equations. The stability of the process is probed by introducing small variations on desired terms, called "perturbations," then examining the system of equations to see whether the system is unstable or stable. The mathematical formalism is rigorous and powerful, but considerable algebra is usually involved.

A further complication arises because the discharge inception which is sought occurs as a superimposed event on an avalanche which is already dynamic in space and time. In this new approach, then, the Townsend avalanche prior to the appearance of a streamer is taken as the background equilibrium state upon which a fast instability develops.

Several relationships are useful in the definition of the problem. They include:

- ° Charged particle conservation,
- ° Gauss' law and Maxwell's equations,
- ° Conservation of momentum,
- ° Conservation of mass.

The first two concern the electrodynamics while the latter two concern the pressure (i.e., density) dynamics of the neutral gas. In general, the time scale for pressure waves to move is much longer than the expected avalanche time scales, so that pressure waves cannot be expected to move in front of an avalanche. However, pressure variations within and in the wake of the avalanche front may occur. It would be necessary to evaluate pressure effects in some examples in order to assess their influence. This is similar to the problem associated with including the effects of space-charge on avalanche development.

Typical expressions for the various relations are presented in order to gain a better appreciation for the problem. The following quantities are used:

ρ_m	= neutral mass density	\bar{w}_p	= positive ion drift velocity
\bar{v}	= neutral velocity vector	K_e	= electron diffusion coefficient
P	= gas pressure	K_p	= positive ion diffusion coefficient
β	= first coefficient of viscosity		
Λ	= second coefficient of viscosity		
ρ_p	= positive ion charge density		
ρ_e	= electron charge density		
\bar{E}	= electric field		
\bar{w}_e	= electron drift velocity		

Considering the case in which the only charged particles are electrons and single-species positive ions and where electron impact ionization (with coefficient α_i) is the significant charge generation mechanism, the relating equations become:

Charged particle conservation:

$$\frac{\partial}{\partial t} \rho_e = K_e \nabla^2 \rho_e - \nabla \cdot [\rho_e (\bar{v} - \bar{w}_e)] + \alpha_i |w_e| \rho_e \quad \text{A. II.1}$$

$$\frac{\partial}{\partial t} \rho_p = K_p \nabla^2 \rho_p + \nabla \cdot [\rho_p (\bar{v} - \bar{w}_p)] + \alpha_i |w_e| \rho_e \quad \text{A. II.2}$$

Gauss and Maxwell:

$$\nabla \cdot \epsilon_0 \vec{E} = \rho_p - \rho_e \quad \text{A. II.3}$$

$$\nabla \times \vec{E} = 0. \quad \text{A. II.4}$$

Conservation of momentum (Navier-Stokes equation):

$$\rho_m \left(\frac{d\vec{v}}{dt} + \vec{v} \cdot \nabla \vec{v} \right) + \nabla P = \beta \nabla^2 \vec{v} + \left(\Lambda + \frac{1}{3} \beta \right) \nabla (\nabla \cdot \vec{v}) + (\rho_p - \rho_e) \vec{E} . \quad \text{A.II.5}$$

Note that here the momentum change is driven by the force of the moving charged particles.

Conservation of Mass:

$$\frac{\partial \rho_m}{\partial t} + \nabla \cdot (\rho_m \vec{v}) = 0. \quad \text{A.II.6}$$

A perturbation analysis is employed to probe these equations for an instability. Specifically, the variable quantities such as charge density, ionization coefficient, and electric field are considered to be composed of two terms: a base-line or zero-order term which is the regular avalanche growth, and a small variation or perturbation term, a first-order change.

The motivation for this is to see if the variation will grow faster than the base avalanche or decay. This technique is very analogous to the method used to study the well-known Rayleigh-Taylor instability in fluid systems.

The perturbation thus results in the following form for electron density:

$$\rho_e(x,y,z,t) = \rho_{e_0}(x,y,z,t) + \rho'_e(x,y,z,t) \quad \text{A.II.7}$$

and similar forms for the other variables of interest. The prime notation indicates the small perturbation quantity.

By substitution of the two component variables into the governing relations and by elimination as negligible terms with the product of two or more primed quantities and/or their derivatives, first-order equations for the perturbation variables can be obtained. The perturbation dynamics can then be studied by first seeing if the perturbation grows or decays in time or space. If growth can take place, there is a possibility for instability and the equations are further solved for the conditions to obtain the instability. A useful technique is to assume the perturbation quantity is a complex exponential in form. While this means that the perturbation is of single wavelength, it can be varied and by Fourier series, in principle, any shape can be constructed if necessary. As an example, when perturbations are created in the y-direction for a system which has only zero-order x-directed variations, the electron density would take the form:

$$\begin{aligned} \rho_e(x,y,z,t) &= \rho_{e_0}(x,t) + \rho'_e(x,y,t) \\ &= \rho_{e_0}(x,t) + \text{Re} \{ \tilde{\rho}_e(x) e^{(st-jky)} \} \end{aligned} \quad \text{A.II.8}$$

where $\tilde{\rho}_e$ is the complex amplitude of the ρ_e perturbation.

The above substitution produces an n^{th} -order differential equation in s called the "characteristic" equation. The value of n depends on what processes are kept in the avalanche equations. If the equation has positive real roots, the perturbation is an expanding instability. Thus, the problem has been reduced to the study of the characteristic equation.

While stability analysis is not unique to avalanching, what is proposed here is significant for two reasons:

- 1) Stability analysis can be applied to a non-stationary system where normal avalanche growth is taken as the background;
- 2) The avalanche is treated in general as an EHD event, and relevant terms may be kept as needed, according to the situation.

This new approach to the study of discharge inception could be very powerful. In principle, it could show not only that instabilities can occur, but also give the specific conditions required for onset. It is proposed that studies using this approach be continued and that typical examples be worked out. One- or two-dimensional problems could be investigated first because they should be simpler and would allow examination of a wider range of effects. Then, with the experience of the simpler system, 3-D problems can be undertaken.

APPENDIX III.

The computer program used to calculate average maximum avalanche sizes in terms of number of electrons for one starting electron in SF₆ is listed here, together with a sample of the output printout. The program is written in BASIC. It applies in its present form only to SF₆ in a point-plane gap in which the point has the shape of a hyperboloid of revolution. In order to apply this to another gas, one has to insert an analytical expression for the difference between the ionization and attachment coefficients ($\alpha_i - \eta_a$) into lines 411-425 and lines 232-235. Use of the program requires the following input: 1) the critical field-to-pressure ratio where $\eta_a = \alpha_i$ in units of V cm⁻¹ torr⁻¹, 2) the absolute gas pressure in kPa, 3) the starting gap voltage, 4) the voltage increment, 5) the number of points (voltages) desired, 6) the characteristic angle (η_0) of the hyperboloid in radians, 7) the focal length of the hyperboloid in centimeters, and 8) the point-to-plane gap spacing in centimeters.

The output as indicated in the sample printout gives the value of the integral given in eq (27) of the text and the corresponding value of \bar{n}_e (called EXP in the printout) for each voltage requested. From a plot of \bar{n}_e versus voltages one can determine the voltage at which \bar{n}_e attains some critical value corresponding to corona inception.

In the program listing that follows, the © sign means exponentiation (**).

```

LIST
10 DIM US(1)
12 N7=0
15 Y=0
20 ;"CRITICAL E/P"
30 INPUT E1
40 ;"PRESSURE IN KPA"
41 INPUT P
42 P=P*7.6
43 E1=E1*P
50 ;"INITIAL VOLTAGE IN KV"
51 INPUT VO
52 VO=VO*1000
60 ;"VOLTAGE INCREMENT IN VOLTS"
61 INPUT D
62 ;"NUMBER OF PTS"
63 INPUT M5
64 IF N7=0 GOTO 70
65 ;"IS ELECTRODE GAP UNCHANGED ?(Y OR N)"
66 INPUT US$
67 IF US$="Y" GOTO 120
70 ;"INFORMATION ON ELECTRODE GEOMETRY"
71 ;"FOR HYPERBOLOID PT. ELECTRODE"
72 ;"ANGLE IN RADIANS"
73 INPUT EO
74 ;"FOCAL LENGTH IN CM."
75 INPUT F
80 ;"GAP SPACING IN CM."
81 INPUT DO
82 IF F>DO GOTO 90
83 DO=DO-.1E-4*F
90 A=COS(EO)
95 M=10
98 N1=1
100 U=(A+1)/(1-A)
110 T=.5*LOG(U)
111 ;"EXAMINE FIELD AND FUNC. (Y OR N)"
112 INPUT US$
115 IF US$="Y" GOTO 700
120 Q=F*T*(1-(DO/F)2)
130 E=VO/Q
143 ;"PRINT DIAGNOSTICS ? (Y OR N)"
144 INPUT US$
145 IF US$="N" GOTO 150
146 PRINT E/P,N1
150 IF E>E1 GOTO 210
160 VO=VO+D
170 N1=N1+1

```

```

180 IF N1>500 GOTO 635
200 GOTO 130
210 B=DO
215 N2=1
220 C=1-V0/(E1*F*T)
225 IF C<0 GOTO 637
230 A=F*SQR(C)
232 E5=P*250
233 C=1-V0/(E5*F*T)
234 IF C<0 GOTO 637
235 A1=F*SQR(C)
236 IF U$="N" GOTO 240
237 PRINT DO-B,DO-A,DO-A1
240 T5=F*T
250 U5=V0/P
251 IF N2>1 GOTO 310
300 ;"FOR SF6 ONLY"
301 ;"FOR NEW GAS CHANGE LINES 411-425"
302 ;"    ALSO CHANGE EXPRESSION FOR LIMIT A1, LINES 232-235"
305 K9=0
310 Y1=0
320 ;"NUMERICAL INTEGRATION"
370 N=40
375 IF U$="N" GOTO 381
380 PRINT Y,N
381 K=1
382 IF K9=1 GOTO 391
383 IF A1>DO GOTO 386
384 B9=A1
385 GOTO 387
386 B9=DO
387 A9=A
389 N9=N
390 GOTO 398
391 IF A1>DO GOTO 619
392 B9=DO
393 A9=A1
394 N9=2*N
398 Z=0
399 H=(B9-A9)/N9
400 X=A9
405 M=N9+1
410 FOR J=1 TO M
411 Q6=T5*(1-(X/F)2)
412 U=U5/Q6
414 IF X>A1 GOTO 421
415 Y=1.66508-.621827E-1*U
416 U1=U2

```

```

417 Y=Y+.530589E-3*U1
418 U1=U*U1
419 Y=Y-.100829E-5*U1
420 GOTO 426
421 Y=-1.74312+.269375E-1*U
422 U1=U*U
423 Y=Y-.249789E-4*U1
424 U1=U1*U
425 Y=Y+.913096E-8*U1
426 IF Y>0 GOTO 430
427 ;"*****"
428 Y=0
430 IF J=1 OR J=M GOTO 500
440 IF K=0 GOTO 530
450 K=0
460 Z=4*Y+Z
470 GOTO 600
500 Z=Z+Y
520 GOTO 600
530 Z=Z+2*Y
540 K=1
600 X=X+H
610 NEXT J
611 Y=(Z*H)/3
612 IF A1>D0 GOTO 619
614 IF K9=1 GOTO 618
615 K9=1
616 Y9=Y
617 GOTO 381
618 Y=Y+Y9
619 Y7=Y*P
620 Z=(Y-Y1)/Y
621 Y1=Y
622 Z1=ABS(Z)
623 N=N+2
624 IF Z1<.5E-2 GOTO 628
625 IF N>42 GOTO 627
626 GOTO 375
627 ;" ERROR > 0.5%"
628 ;"INTEGRAL =",Y7,"EXP =",EXP(Y7)
629 ;"VOLTAGE =",VO
630 IF N2=M5 GOTO 640
631 N2=N2+1
632 VO=VO+D
634 GOTO 220
635 ;"ERROR 2"
636 GOTO 640
637 ;"ERROR 3"

```

```

640 GOTO 900
700 ;"FUNC ? (Y OR N)"
701 INPUT US
702 IF US="N" GOTO 806
703 ;"INITIAL E/P"
710 INPUT U1
720 ;"FINAL E/P"
730 INPUT U2
740 U7=(U2-U1)/50
750 ;"FUNC. OUTPUT,E/P,FUNC"
755 U=U1
760 FOR J=1 TO 50
770 IF U>250 GOTO 790
771 Y=1.66508-.621827E-1*U
772 U3=U2
773 Y=Y+.530589E-3*U3
774 U3=U3*U
775 Y=Y-.100829E-5*U3
776 GOTO 800
790 Y=-1.74312+.269375E-1*U
791 U3=U2
792 Y=Y-.249789E-4*U3
793 U3=U3*U
794 Y=Y+.913096E-8*U3
800 PRINT U,Y
801 U=U+U7
805 NEXT J
806 ;"FIELD ? (Y OR N)"
807 INPUT US
808 IF US="N" GOTO 880
810 ;"INITIAL DISTANCE"
812 INPUT X0
815 ;"FINAL DISTANCE"
817 INPUT X1
818 X2=(X1-X0)/50
820 ;"OUTPUT - E/P, E, X"
830 X=X0
835 FOR J=1 TO 50
840 E=V0/(F*T*(1-(X/F)2))
845 U=E/P
850 PRINT U,E,X
855 X=X+X2
860 NEXT J
870 ;"TERMINATE RUN ? (Y OR N)"
871 INPUT US
872 IF US="Y" GOTO 950
880 GOTO 111
900 ;"MORE DATA ?(Y OR N)"

```

```
910 INPUT US
920 IF US="N" GOTO 950
930 N7=1
940 GOTO 15
950 END
BASIC 03-04
```

```

RUN
CRITICAL E/P
117
PRESSURE IN KPA
100
INITIAL VOLTAGE IN KV
8.2
VOLTAGE INCREMENT IN VOLTS
200
NUMBER OF PTS
5
INFORMATION ON ELECTRODE GEOMETRY
FOR HYPERBOLOID PT. ELECTRODE
ANGLE IN RADIAN
.0269
FOCAL LENGTH IN CM.
2.28007
GAP SPACING IN CM.
2.278
EXAMINE FIELD AND FUNC. (Y OR N)
N
PRINT DIAGNOSTICS ? (Y OR N)
N
FOR SF6 ONLY
FOR NEW GAS CHANGE LINES 411-425
    ALSO CHANGE EXPRESSION FOR LIMIT A1, LINES 232-235
NUMERICAL INTEGRATION
INTEGRAL = 17.538          EXP = .413663E8
VOLTAGE = 8200
NUMERICAL INTEGRATION
INTEGRAL = 18.1719        EXP = .77979E8
VOLTAGE = 8400
NUMERICAL INTEGRATION
INTEGRAL = 18.6725        EXP = .12864E9
VOLTAGE = 8600
NUMERICAL INTEGRATION
INTEGRAL = 19.3159        EXP = .244776E9
VOLTAGE = 8800
NUMERICAL INTEGRATION
INTEGRAL = 19.8195        EXP = .405048E9
VOLTAGE = 9000
MORE DATA ?(Y OR N)
N
BASIC 03-04

```

APPENDIX IV.

Given here is a listing of the BASIC computer program used to calculate corona initiation volumes according to the prescription given in the text by Eq. (33). The restrictions that apply are the same as for the program described in Appendix III. The input information requested is also nearly the same, with the exception that the critical value for E/p is here assumed to be that for SF_6 and one must indicate a critical electron avalanche size, e.g., 1×10^8 electrons.

The output, an example of which is shown, gives the x-y coordinates in centimeters of the boundaries of a cross section of the initiation volume in a plane containing the electrode axis, and also gives the calculated volume in cubic centimeters for each voltage requested.

```

LIST
10 DIM US(1)
20 DIM X(100),C(100),S(100),U(100)
25 DIM Y(100),A(100),B(100)
26 DIM A1(3,3),B1(3,1),C1(3,1),D1(3,3),E1(3,1),F1(3,1)
27 ;"PRINT DIAGNOSTICS ?(Y OR N)"
28 INPUT US$
30 E1=117
40 ;"PRESSURE IN KPA"
41 INPUT P
42 P=P*7.6
43 E1=E1*P
50 ;"INITIAL VOLTAGE IN KV"
51 INPUT VO
52 VO=VO*1000
60 ;"VOLTAGE INCREMENT IN VOLTS"
61 INPUT D
62 ;"NUMBER OF PTS"
63 INPUT M5
70 ;"INFORMATION ON ELECTRODE GEOMETRY"
71 ;"FOR HYPERBOLOID PT. ELECTRODE"
72 ;"ANGLE IN RADIANS"
73 INPUT EO
74 ;"FOCAL LENGTH IN CM."
75 INPUT F
80 ;"MIN. AVALANCHE SIZE (NO. OF ELECTRONS)"
90 INPUT N
91 K=LOG(N)
100 REM          - ANGLE INCREMENT = D1
120 N4=1
190 A=COS(EO)
191 U=(A+1)/(1-A)
192 T=.5*LOG(U)
200 C(1)=1
210 S(1)=0
215 D1=.2E-1
220 X2=F*A
230 Q=1-VO/(E1*F*T)
240 IF Q<0 GOTO 1060
250 X1=F*SQR(Q)
252 IF X1<X2 GOTO 260
253 VO=VO+D
254 GOTO 230
260 E5=P*250
270 Q=1-VO/(E5*F*T)
280 IF Q<0 GOTO 1060
290 X3=F*SQR(Q)
292 U(1)=X3

```

```

295 C6=C(1)
300 GOSUB 1100
301 IF U$="N" GOTO 310
302 PRINT "K=",K1
310 IF K1>K GOTO 340
320 V0=V0+D
330 GOTO 230
340 PRINT "VOLTAGE = ",V0
350 X(1)=X1
360 Y(1)=0
365 IF U$="N" GOTO 370
366 PRINT "X1=",X1,"X2=",X2,"X3=",X3
370 PRINT "    X1    -    Y1    X2    -    Y2"
385 Z=0
390 N1=2
394 M8=0
395 M7=0
400 Z=Z+D1
410 E=EXP(Z)
420 E9=EXP(-Z)
430 C(N1)=(E+E9)/2
440 S(N1)=(E-E9)/2
441 IF U$="N" GOTO 450
445 PRINT "ANGLE=",Z,"COSH=",C(N1)
450 E=(F*C(N1))2
460 A1=1/(E2)
470 B1=(C(N1)2+1)/E
480 C1=C(N1)2-(V0/(E1*T*F))2
490 E=B12-4*A1*C1
500 IF E<0 GOTO 1060
510 E9=SQR(E)
520 E=(B1-E9)/(2*A1)
530 IF E<0 GOTO 1060
540 X(N1)=SQR(E)
550 X1=X(N1)
560 X2=F*A*C(N1)
570 C1=C(N1)2-(V0/(E5*T*F))2
580 E=B12-4*A1*C1
590 IF E<0 GOTO 1060
600 E9=SQR(E)
610 E=(B1-E9)/(2*A1)
620 IF E<0 GOTO 1060
630 X3=SQR(E)
631 IF U$="N" GOTO 635
632 PRINT "X1=",X1,"X2=",X2,"X3=",X3
635 U(N1)=X3
640 C6=C(N1)
650 GOSUB 1100

```

```

651 IF U$="N" GOTO 658
652 PRINT "K=",K1
658 IF K1>K GOTO 667
660 M7=M7+1
661 M8=1
662 Z=Z-D1
663 D1=D1/2
664 N1=N1-1
665 IF M7>3 GOTO 705
666 GOTO 671
667 IF M8=0 GOTO 671
668 D1=D1/2
669 M7=M7+1
670 IF M7>3 GOTO 705
671 N1=N1+1
680 IF N1>100 GOTO 1040
690 GOTO 400
705 FOR N2=1 TO N1
710 N3=0
730 X2=F*A*C(N2)
740 X3=U(N2)
750 D5=(X2-X(N2))/2
760 X1=X(N2)+D5
770 C6=C(N2)
780 N3=N3+1
790 GOSUB 1100
795 IF U$="N" GOTO 800
796 PRINT N3,K1,X1
800 IF N3>20 GOTO 910
810 E9=K-K1
820 E=ABS(E9)
830 E9=E/K
840 IF E9<.1E-1 GOTO 920
850 D5=D5/2
860 IF K1>K GOTO 890
870 X1=X1-D5
880 GOTO 780
890 X1=X1+D5
900 GOTO 780
910 IF U$="N" GOTO 920
911 PRINT "ERROR>1%"
920 E=1-(X(N2)2)/(F*C(N2))2
930 IF E<0 GOTO 1060
940 Y1=F*S(N2)*SQR(E)
950 E=1-(X12)/(F*C(N2))2
960 IF E<0 GOTO 1060
970 Y2=F*S(N2)*SQR(E)
980 PRINT X(N2),Y1,X1,Y2

```

```

981 Y(N2)=Y1
982 A(N2)=X1
983 B(N2)=Y2
990 NEXT N2
995 GOSUB 1705
1000 N4=N4+1
1010 IF N4>M5 GOTO 1070
1020 V0=V0+D
1030 GOTO 200
1040 ;"ERROR-EXCEEDED ARRAY SIZE"
1050 GOTO 1070
1060 ;"SQR-NEG.ARG."
1070 GOTO 2300
1100 K9=0
1105 U5=V0/P
1110 U5=U5/(F*T)
1111 Q=F*C6
1115 N=30
1120 K4=1
1130 IF K9=1 GOTO 1210
1140 IF X3>X2 GOTO 1170
1150 B9=X3
1160 GOTO 1180
1170 B9=X2
1180 A9=X1
1190 N9=N
1200 GOTO 1250
1210 IF X3>X2 GOTO 1619
1220 B9=X2
1230 A9=X3
1240 N9=2*N
1250 Z1=0
1260 H=(B9-A9)/N9
1270 X=A9
1280 M=N9+1
1290 FOR J=1 TO M
1295 W=(X/Q)2
1300 E=C62-W
1310 IF E<0 GOTO 1640
1320 E9=SQR(E)
1330 E=1-W
1340 IF E<0 GOTO 1640
1350 E9=E9*SQR(E)
1360 U=U5/E9
1370 E=(C62-W)/(1-W)
1380 IF E<0 GOTO 1640
1390 L=SQR(E)/C6
1400 IF X>=X3 GOTO 1421

```

```

1415 Y=1.66508-.621827E-1*U
1416 U1=U2
1417 Y=Y+.530589E-3*U1
1418 U1=U*U1
1419 Y=Y-.100829E-5*U1
1420 GOTO 1426
1421 Y=-1.74312+.269375E-1*U
1422 U1=U*U
1423 Y=Y-.249789E-4*U1
1424 U1=U1*U
1425 Y=Y+.913096E-8*U1
1426 IF Y>0 GOTO 1430
1427 ;"*****"
1428 Y=0
1430 Y=Y*L
1431 IF J=1 OR J=M GOTO 1500
1440 IF K4=0 GOTO 1530
1450 K4=0
1460 Z1=4*Y+Z1
1470 GOTO 1600
1500 Z1=Z1+Y
1520 GOTO 1600
1530 Z1=Z1+2*Y
1540 K4=1
1600 X=X+H
1610 NEXT J
1611 Y=(Z1*H)/3
1612 IF X3>X2 GOTO 1619
1614 IF K9=1 GOTO 1618
1615 K9=1
1616 Y9=Y
1617 GOTO 1120
1618 Y=Y+Y9
1619 K1=Y*P
1630 GOTO 1650
1640 PRINT "ERROR-NEG SQR ARG"
1650 RETURN
1705 R1=0
1710 R2=0
1715 R3=0
1720 R4=0
1725 S1=0
1730 S2=0
1735 S3=0
1740 FOR W1=1 TO N1
1745 R1=R1+Y(W1)2
1750 NEXT W1
1755 A1(1,2)=R1

```

```

1760 A1(2,1)=R1
1765 FOR W2=1 TO N1
1770 R2=R2+Y(W2)④
1775 NEXT W2
1780 A1(1,3)=R2
1785 A1(2,2)=R2
1790 A1(3,1)=R2
1795 FOR W3=1 TO N1
1800 R3=R3+Y(W3)⑥
1805 NEXT W3
1810 A1(2,3)=R3
1815 A1(3,2)=R3
1820 FOR W4=1 TO N1
1825 R4=R4+Y(W4)⑧
1830 NEXT W4
1835 A1(3,3)=R4
1837 A1(1,1)=N1
1840 FOR W5=1 TO N1
1845 S1=S1+X(W5)
1850 NEXT W5
1855 C1(1,1)=S1
1860 FOR W6=1 TO N1
1865 S2=S2+(Y(W6)②)*X(W6)
1870 NEXT W6
1875 C1(2,1)=S2
1880 FOR W7=1 TO N1
1885 S3=S3+(Y(W7)④)*X(W7)
1890 NEXT W7
1895 C1(3,1)=S3
1900 MAT A1=INV(A1)
1901 IF U$="N" GOTO 1915
1905 ;"INVERSE MATRIX A1"
1910 MAT PRINT A1
1915 MAT B1=A1*C1
1920 IF U$="N" GOTO 1935
1925 ;"LEAST SQR FIT COEFF, OUTER BD"
1930 MAT PRINT B1
1935 R1=0
1940 R2=0
1945 R3=0
1950 R4=0
1955 S1=0
1960 S2=0
1965 S3=0
1970 FOR F1=1 TO N1
1975 R1=R1+B(F1)②
1980 NEXT F1
1985 D1(1,2)=R1

```

```

1990 D1(2,1)=R1
1995 FOR F2=1 TO N1
2000 R2=R2+B(F2)⊗4
2005 NEXT F2
2010 D1(1,3)=R2
2015 D1(2,2)=R2
2020 D1(3,1)=R2
2025 FOR F3=1 TO N1
2030 R3=R3+B(F3)⊗6
2035 NEXT F3
2040 D1(2,3)=R3
2045 D1(3,2)=R3
2050 FOR F4=1 TO N1
2055 R4=R4+B(F4)⊗8
2060 NEXT F4
2065 D1(3,3)=R4
2070 D1(1,1)=N1
2075 FOR F5=1 TO N1
2080 S1=S1+A(F5)
2085 NEXT F5
2090 F1(1,1)=S1
2091 FOR F6=1 TO N1
2092 S2=S2+(B(F6)⊗2)*A(F6)
2106 NEXT F6
2110 F1(2,1)=S2
2115 FOR F7=1 TO N1
2120 S3=S3+(B(F7)⊗4)*A(F7)
2125 NEXT F7
2130 F1(3,1)=S3
2135 MAT D1=INV(D1)
2136 IF U$="N" GOTO 2150
2140 ;"INVERSE MATRIX D1"
2145 MAT PRINT D1
2150 MAT E1=D1*F1
2151 IF U$="N" GOTO 2165
2152 ;"LEAST SQR FIT COEFF, INNER BD"
2155 MAT PRINT E1
2160 REM      - VOLUME DETERMINATION
2165 L5=(E1(1,1)-B1(1,1))*(Y(N1)⊗2)/2
2170 L6=(E1(2,1)-B1(2,1))*(Y(N1)⊗4)/4
2175 L7=(E1(3,1)-B1(3,1))*(Y(N1)⊗6)/6
2180 L8=6.283*(L5+L6+L7)
2185 ;"VOLUME =",L8
2190 RETURN
2300 END
BASIC 03-04

```

```

RUN
PRINT DIAGNOSTICS?(Y OR N)
N
PRESSURE IN KPA
100
INITIAL VOLTAGE IN KV
7
VOLTAGE INCREMENT IN VOLTS
1000
NUMBER OF PTS
2
INFORMATION ON ELECTRODE GEOMETRY
FOR HYPERBOLOID PT. ELECTRODE
ANGLE IN RADIANS
.0404044
FOCAL LENGTH IN CM.
1.251
MIN. AVALANCHE SIZE (NO. OF ELECTRONS)
1E+8
VOLTAGE = 7000
  X1      -      Y1          X2      -      Y2
1.24087      0          1.24571      0
1.24128      .315237E-2    1.24604      .228213E-2
1.24235      .620399E-2    1.24707      .443846E-2
1.24421      .900533E-2    1.24872      .638018E-2
1.24671      .115021E-1    1.25034      .862641E-2
1.24978      .136459E-1    1.2522      .112282E-1
1.25154      .145615E-1    1.25304      .129171E-1
1.25201      .147582E-1    1.25275      .139521E-1
VOLUME = .348314E-5
VOLTAGE = 8000
  X1      -      Y1          X2      -      Y2
1.23942      0          1.24635      0
1.2398      .337668E-2    1.24673      .212554E-2
1.2409      .665243E-2    1.24775      .412165E-2
1.24275      .970154E-2    1.24927      .598381E-2
1.24526      .124623E-1    1.25126      .773911E-2
1.24837      .148765E-1    1.25353      .964407E-2
1.25208      .168658E-1    1.25629      .115665E-1
1.25629      .18455E-1     1.25908      .143083E-1
1.25857      .191103E-1    1.26063      .158156E-1
1.25975      .194025E-1    1.26107      .172591E-1
1.26034      .195602E-1    1.26099      .18515E-1
VOLUME = .109686E-4
BASIC 03-04

```


U.S. DEPT. OF COMM. BIBLIOGRAPHIC DATA SHEET	1. PUBLICATION OR REPORT NO. NBSIR 82-2555	2. Gov't. Accession No.	3. Recipient's Accession No.
4. TITLE AND SUBTITLE 1981 ANNUAL REPORT: TECHNICAL ASSISTANCE FOR FUTURE INSULATION SYSTEMS RESEARCH		5. Publication Date November 1982	
		6. Performing Organization Code	
7. AUTHOR(S) R. J. Van Brunt, M. Misakian, D. A. Leep, E. C. Beaty, J. W. Gallagher, C. M. Cooke, K. Wyatt, R. G. Gels		8. Performing Organ. Report No.	
9. PERFORMING ORGANIZATION NAME AND ADDRESS NATIONAL BUREAU OF STANDARDS DEPARTMENT OF COMMERCE WASHINGTON, DC 20234		10. Project/Task/Work Unit No.	
		11. Contract/Grant No.	
12. SPONSORING ORGANIZATION NAME AND COMPLETE ADDRESS (Street, City, State, ZIP) U.S. Department of Energy Office of Electric Energy Systems Washington, D.C. 20585		13. Type of Report & Period Covered Annual Report FY81	
		14. Sponsoring Agency Code	
15. SUPPLEMENTARY NOTES <input type="checkbox"/> Document describes a computer program; SF-185, FIPS Software Summary, is attached.			
16. ABSTRACT (A 200-word or less factual summary of most significant information. If document includes a significant bibliography or literature survey, mention it here.)			
<p>A system for measuring the electrical properties of corona pulses has been characterized and is discussed. Additional data on the pulse height distributions of positive and negative corona pulses in pure SF₆ for point-plane electrode geometries are presented. Basic mechanisms for initiation of electric discharges in SF₆ for highly nonuniform fields have been investigated in a collaborative effort between NBS and the High Voltage Research Laboratory of the Massachusetts Institute of Technology. Effects of radiation, electrode geometry, and polarity on corona inception in SF₆ have been measured. Corona inception voltages and discharge initiation volumes have been calculated using the streamer criterion. Limitations of the streamer criterion as applied to SF₆ in highly nonuniform fields are discussed.</p>		<p>namely that for SF₆. Using a gas-chromatograph/mass spectrometer, absolute concentrations of SOF₂ and SO₂F₂ and relative concentrations of H₂O in SF₆ have been measured as a function of total energy dissipated in corona discharges operated at power levels between 50 and 700 mW. The observed production rates for SOF₂ and SO₂F₂ appear to be proportional to power level, and the ratio of SO₂F₂ to SOF₂ concentrations for corona is considerably higher than that typically observed for arc discharges in SF₆.</p>	
<p>The statistics of electron avalanche growth in SF₆ have been measured and compared with results of theory. While the avalanche pulses, on average, followed expected theoretical behavior, the distribution was not found to be regular or to follow a simple stochastic theory. A thorough compilation and survey of electron swarm data for electronegative gases used, and proposed for use, as components of gaseous dielectrics was completed. The parameters considered include: electron drift velocity, attachment coefficient, ionization coefficient, electron growth constant, diffusion coefficient, detachment coefficient, and characteristic energy. These are quantities needed for prediction of breakdown and modeling of gas discharges. Some of the important gases included in this study are: O₂, CO₂, SF₆, H₂O, air, nitrogen oxides, halogens, and various halogenated hydrocarbons, e.g., CF₄, C₂F₆, C₃F₈, C₄F₁₀, CCl₂F₂, CClF₃, c-C₄F₈, c-C₅F₈, CH₃Br, CH₂Cl₂, CHCl₃, etc. In this report we include only an example of the data collected.</p>		<p>Estimates have been performed to determine the sensitivity of a technique to detect polar gas contaminants in gaseous SF₆ using an accurate ppm measurement of changes in the low frequency (dc) dielectric constant of the gas. Measurements have been performed of optogalvanic spectra from glow discharges in Ne, N₂ and mixtures of these with SF₆. The effect of SF₆ in quenching metastables in these gases is discussed.</p>	
17. KEY WORDS (six to twelve entries; alphabetical order; capitalize only the first letter of the first key word unless a proper name; separated by semicolons) corona discharges; decomposition; electronegative gases; electron avalanches; electron swarm data; optogalvanic spectra; oxyfluorides; SF ₆ ; sulfur hexafluoride; water vapor.			
18. AVAILABILITY <input checked="" type="checkbox"/> Unlimited <input type="checkbox"/> For Official Distribution. Do Not Release to NTIS <input type="checkbox"/> Order From Sup. of Doc., U.S. Government Printing Office, Washington, DC 20402, SD Stock No. SN003-003- <input checked="" type="checkbox"/> Order From National Technical Information Service (NTIS), Springfield, VA. 22161		19. SECURITY CLASS (THIS REPORT) UNCLASSIFIED	21. NO. OF PRINTED PAGES 157
		20. SECURITY CLASS (THIS PAGE) UNCLASSIFIED	22. Price \$15.00



